



Search for $t\bar{t}$ resonances in fully hadronic final states in pp collisions at $\sqrt{s} = 13$ TeV with the ATLAS detector

The ATLAS Collaboration

This paper presents a search for new heavy particles decaying into a pair of top quarks using 139 fb^{-1} of proton–proton collision data recorded at a centre-of-mass energy of $\sqrt{s} = 13$ TeV with the ATLAS detector at the Large Hadron Collider. The search is performed using events consistent with pair production of high-transverse-momentum top quarks and their subsequent decays into the fully hadronic final states. The analysis is optimized for resonances decaying into a $t\bar{t}$ pair with mass above 1.4 TeV, exploiting a dedicated multivariate technique with jet substructure to identify hadronically decaying top quarks using large-radius jets and evaluating the background expectation from data. No significant deviation from the background prediction is observed. Limits are set on the production cross-section times branching fraction for the new Z' boson in a topcolor-assisted-technicolor model. The Z' boson masses below 3.9 and 4.7 TeV are excluded at 95% confidence level for the decay widths of 1% and 3%, respectively.

Contents

1	Introduction	3
2	ATLAS detector	4
3	Data and simulation samples	4
4	Event reconstruction and selection	6
4.1	Object reconstruction	6
4.2	Event selection and categorization	8
5	Background estimation	9
5.1	Background modelling using data and simulation	10
5.2	Determination of background parameterization	12
6	Systematic uncertainties	12
6.1	Signal modelling uncertainties	12
6.2	Background modelling uncertainties	14
7	Statistical analysis	15
8	Results	16
9	Conclusion	17

1 Introduction

Discovery of new phenomena beyond the Standard Model (SM) is of great importance for high-energy particle physics. Such discovery has the potential to shed light on unexplained observations in nature, e.g. the large difference between the scales of electroweak interactions at $\mathcal{O}(100)$ GeV and gravity at $\mathcal{O}(10^{19})$ GeV, the Planck scale. The top quark, the heaviest elementary particle in the SM, could provide a window to this new physics through its large coupling to the scalar sector with a Higgs field. Resonant production of top and anti-top quarks ($t\bar{t}$), if observed, strongly indicates the presence of new particles, such as those predicted by topcolor-assisted-technicolor (TC2) [1–3], the two-Higgs-doublet model (2HDM) [4] and Randall–Sundrum (RS) models of warped extra dimensions [5, 6]. These new particles could appear in the mass spectrum of the $t\bar{t}$ system ($m_{t\bar{t}}$) as a localized deviation from the SM prediction. This paper presents a search for $t\bar{t}$ resonances in the TeV mass range with subsequent decay into a fully hadronic final state ($t\bar{t} \rightarrow W^+bW^-\bar{b}$ with $W \rightarrow qq'$), performed using 139 fb^{-1} of proton-proton (pp) collision data recorded in 2015–2018 at $\sqrt{s} = 13$ TeV with the ATLAS detector at the Large Hadron Collider (LHC).

The fully hadronic final state benefits from the largest top-quark decay branching fraction. However, it poses challenges in reconstructing the $t\bar{t}$ system using hadronic jets, and in discriminating a new physics signal from SM production of multijet processes which have a high production cross-section. Exploiting dedicated top-quark identification techniques, both the ATLAS [7] and CMS [8] experiments demonstrated that the search in the fully hadronic final states can have comparable sensitivity at $m_{t\bar{t}}$ above ~ 1 TeV to the analysis in a lepton+jets final state (where one of the W -bosons decays into an electron or muon and a neutrino). This paper extends this further by adopting an advanced top-quark identification method based on a deep neural network. In this high-mass range, the top-quark decay products become close enough for the hadronically decaying top quark to be reconstructed as a single large-radius jet with a characteristic internal substructure. The search focuses on resonances with the intrinsic decay width comparable to or smaller than the detector resolution, by looking for a localized excess over the smoothly falling mass spectra of the reconstructed SM $t\bar{t}$ candidates. The background spectrum is derived from data by fitting a smoothly falling function to the $m_{t\bar{t}}$ distributions.

Searches for heavy particles decaying into a $t\bar{t}$ pair have been performed with the ATLAS and CMS experiments using pp collisions at $\sqrt{s} = 7$ TeV [9–13], 8 TeV [14–17] and 13 TeV [7, 8, 18, 19]. Both experiments performed the searches in the fully hadronic and lepton+jets final states using 13 TeV data collected in 2015–2016, while CMS included the dileptonic final states as well. The spin-1 colour-singlet boson in a topcolor-assisted-technicolor model [1, 2], used in the previous $t\bar{t}$ resonance search in the fully hadronic final state in ATLAS [7], continues to be used as a benchmark in the results presented in this paper. This leptophobic Z' boson (denoted by Z'_{TC2}), referred to as Model IV in Ref. [20], is mainly produced by $q\bar{q}$ annihilation and decays into first- and third-generation quarks. The model parameters are chosen to maximize the branching fraction of the $Z'_{\text{TC2}} \rightarrow t\bar{t}$ decay, which reaches 33%, and the intrinsic decay width of the Z'_{TC2} boson divided by its mass m is set to $\Gamma/m = 1\%$ or 3% .¹ The predicted $Z'_{\text{TC2}} \rightarrow t\bar{t}$ production cross section is about 2.0 (7.6) fb at the Z'_{TC2} mass of 4 TeV and $\Gamma/m = 1\%$ (3%). Among several benchmark signal models, the ATLAS searches excluded masses below 3.1 and 3.0 TeV in the fully hadronic and lepton+jets final states, respectively, for the new Z'_{TC2} boson with $\Gamma/m = 1\%$ [7, 18]. The CMS search excluded the Z'_{TC2} boson with $\Gamma/m = 1\%$ up to 3.8 TeV using the combination of all three final states including the dileptonic final state [8].

¹ In the rest of this paper, the decay width of a resonance divided by the resonance mass is referred to as the width.

2 ATLAS detector

The ATLAS experiment uses a multipurpose, forward–backward symmetric detector² with nearly 4π solid angle coverage, as described in Refs. [21–23]. It consists of an inner tracking detector (ID) surrounded by a thin superconducting solenoid, electromagnetic (EM) and hadronic calorimeters, and a muon spectrometer.

The ID consists of a silicon pixel tracker, a silicon microstrip tracker (SCT) and a transition radiation tracker, all immersed in a 2 T axial magnetic field, and provides charged-particle tracking in the range $|\eta| < 2.5$. The EM calorimeter is a lead/liquid-argon (LAr) sampling calorimeter, divided into a barrel section covering the range $|\eta| < 1.475$ and two endcap sections covering $1.375 < |\eta| < 3.2$. In the region $|\eta| < 1.8$, an additional thin LAr presampler layer is used to correct for energy losses in the material upstream of the calorimeters. The hadronic calorimetry is provided by a steel/scintillator tile sampling calorimeter in the central region ($|\eta| < 1.7$) and by a copper/LAr calorimeter in the endcap regions ($1.5 < |\eta| < 3.2$). The forward region ($3.1 < |\eta| < 4.9$) is instrumented with copper/LAr and tungsten/LAr calorimeter modules optimized for electromagnetic and hadronic measurements, respectively. Surrounding the calorimeters is a muon spectrometer that consists of three air-core superconducting toroidal magnets and tracking chambers, providing precision tracking for muons with $|\eta| < 2.7$ and trigger capability for $|\eta| < 2.4$.

A two-level trigger system is used to select events for offline analysis [24]. Events are first selected by the level-1 trigger implemented with custom electronics, which uses a subset of the detector information to reduce the event rate to approximately 100 kHz. This is followed by a software-based trigger that reduces the accepted event rate to an average of 1 kHz by refining the level-1 trigger selection.

3 Data and simulation samples

The search is performed using 139 fb^{-1} of data recorded from pp collisions at $\sqrt{s} = 13 \text{ TeV}$. The analysis uses data collected during stable beam conditions with the relevant detectors operational. Events are required to have at least one pp interaction vertex with two or more tracks with transverse momentum (p_T) greater than 500 MeV. If more than one vertex is found in an event, the one with the largest $\sum p_T^2$ of associated tracks is chosen as the primary vertex. Simulated signal and background event samples are used to optimize the event selection, to validate the background estimation technique and to perform hypothesis testing of the benchmark Z'_{TC2} signal model.

The main backgrounds after applying the event selection criteria (Section 4) are expected to be composed of events from SM $t\bar{t}$ and multijet production processes. The total number of background events, including events from other minor backgrounds, is estimated directly from data using functional fits to the $m_{t\bar{t}}$ spectra, as detailed in Section 5. However, simulated samples of SM $t\bar{t}$ and multijet events are used to establish the background estimation technique.

² ATLAS uses a right-handed coordinate system with its origin at the nominal interaction point (IP) in the centre of the detector and the z -axis along the beam pipe. The x -axis points from the IP to the centre of the LHC ring, and the y -axis points upwards. Cylindrical coordinates (r, ϕ) are used in the transverse plane, ϕ being the azimuthal angle around the z -axis. The pseudorapidity is defined in terms of the polar angle θ as $\eta = -\ln \tan(\theta/2)$. Angular distance is measured in units of $\Delta R \equiv \sqrt{(\Delta\eta)^2 + (\Delta\phi)^2}$.

For SM $t\bar{t}$ production, the next-to-leading-order (NLO) Monte Carlo (MC) generator POWHEG-Box v2 [25–27] was used with the NNPDF3.0 NLO [28] parton distribution function (PDF) set in the matrix element calculations. The $t\bar{t}$ production cross-section is scaled to a next-to-next-to-leading-order (NNLO) calculation in QCD including resummation of next-to-next-to-leading logarithmic soft gluon terms with Top++2.0 [29–35]. Parton showering, hadronization and the underlying event were simulated using PYTHIA v8.230 [36] with the leading-order (LO) NNPDF2.3 [37] PDF set and the A14 set of tuned parameters [38]. The h_{damp} parameter, which controls the transverse momentum of the first additional parton emission beyond the Born level, was set equal to the top-quark mass [39]. The top-quark kinematics in $t\bar{t}$ events were corrected to account for electroweak higher-order effects [40]. The generated events were weighted by this correction factor as a function of the flavour and centre-of-mass energy of the initial partons, and of the decay angle of the top quarks in the centre-of-mass frame of the initial partons. The value of the correction factor decreases with increasing $m_{t\bar{t}}$ from 0.98 at $m_{t\bar{t}} = 0.4$ TeV to 0.87 at $m_{t\bar{t}} = 3.5$ TeV. Multijet processes were simulated with PYTHIA v8.186 [36] using the NNPDF2.3 LO PDF set and the A14 set of tuned parameters for the underlying event.

Simulated signal samples of a spin-1 Z'_{TC2} boson decaying into a $t\bar{t}$ pair were generated using PYTHIA v8.165 with the NNPDF2.3 LO PDF set and the A14 set of tuned parameters. The production cross-section is scaled to a NLO prediction by multiplying by a factor 1.3 [41] and the coupling parameters of the Z'_{TC2} boson are chosen to be the same as those used in Ref. [7]. The signal samples were generated for Z'_{TC2} masses of 1750, 2000, 2250, 2500, 2750, 3000, 4000 and 5000 GeV. A sum of Crystal Ball³ and Gaussian functions (CB + Gauss) is used to model the signal $m_{t\bar{t}}$ distributions and create an interpolated signal $m_{t\bar{t}}$ template for masses where MC samples are not available. The fit function takes the form:

$$J(x; f, \mu, \sigma, \alpha_{\text{CB}}, n_{\text{CB}}, \mu_{\text{CB}}, \sigma_{\text{CB}}) = f \cdot g(x; \mu, \sigma) + (1 - f) h(x; \alpha_{\text{CB}}, n_{\text{CB}}, \mu_{\text{CB}}, \sigma_{\text{CB}})$$

where $g(x; \mu, \sigma)$ represents a Gaussian function with parameters μ and σ , $h(x; \alpha_{\text{CB}}, n_{\text{CB}}, \mu_{\text{CB}}, \sigma_{\text{CB}})$ represents a Crystal Ball function with parameters α_{CB} , n_{CB} , μ_{CB} and σ_{CB} and $0 < f < 1$ is a fractional coefficient. The parameters μ and σ represent the mean value and the width of the Gaussian function, and the α_{CB} and n_{CB} are the threshold and exponent parameters of the CB function, respectively. Thus there are seven shape parameters and an additional normalization parameter. The parameters for the interpolated signal templates are obtained by using either a linear or polynomial interpolation between the values of parameters estimated using a CB + Gauss fit to signal MC $m_{t\bar{t}}$ distributions. The interpolated signal $m_{t\bar{t}}$ templates are used at masses of 1875, 2125, 2375, 2625, 2875, 3250, 3500, 3750, 4250, 4500 and 4750 GeV. The signal MC samples are also used to evaluate the acceptance and selection efficiencies for the signals considered in the search.

The EVTGEN v1.2.0 program [42] was used in all simulated samples to model the properties of bottom and charm hadron decays. All simulated samples include the effects of multiple pp interactions in the same and neighbouring bunch crossings (pile-up) and were processed through the ATLAS detector simulation [43] based on GEANT4 [44]. Pile-up effects were emulated by overlaying simulated minimum-bias events generated with PYTHIA v8.186 using the MSTW2008LO PDF set [45] and the A2 set of tuned parameters [46]. The number of overlaid minimum-bias events was adjusted to match the observed data. Simulated events are processed through the same reconstruction software as the data, and corrections are applied so that the object identification efficiencies, energy scales and energy resolutions match those determined from control samples of data.

³ A Crystal Ball function is composed of a Gaussian distribution at the core, connected with a power-law distribution describing the lower tail.

4 Event reconstruction and selection

At high transverse momentum with p_T above approximately 350 GeV, the decay products of a hadronically decaying top quark can be reconstructed as a single large-radius ($R = 1$) jet. Such large- R jets are characterized by the presence of multiple cores associated with the ‘subjets’ from a b -hadron and a $W \rightarrow q\bar{q}'$ decay. One of the main backgrounds in this search, multijet production, is dominated by jets from light-flavour quarks and gluons. Typically, such jets have single cores, but would have enhanced contributions of multiple cores associated with large-angle emission when a conventional requirement of large jet mass is applied in the selection of top-quark candidate jets. Therefore, to discriminate genuine top-quark jets from multijet background with a mass around the top-quark mass, an improved analysis technique that takes advantage of more-detailed jet substructure information is desired. An additional challenge in high-mass $t\bar{t}$ resonance searches comes from the fact that the subjet containing a b -hadron (b -jet) in top-quark decays has, in close vicinity, hadronic activity from $W \rightarrow q\bar{q}'$ decays. Therefore, the identification of a b -jet inside a large- R jet will need to be optimized to reduce contributions from non- b -hadron decays. The analysis presented here addresses these challenges by adopting advanced top-quark tagging and b -jet identification techniques, as detailed below.

4.1 Object reconstruction

Large- R jets are built from three-dimensional topological clusters of energy deposits in the calorimeter, calibrated to the hadronic energy scale with the local cluster weighting (LCW) [47] procedure, using the anti- k_t algorithm [48] with a radius parameter $R = 1.0$. The non-compensating calorimeter response and the energy loss in dead material or due to out-of-cluster leakage of deposited energy are accounted for in the LCW procedure. The reconstructed jets are ‘trimmed’ [49] to reduce contributions from pile-up and soft interactions. This is performed by reclustering the jet constituents into subjets using the k_t algorithm [50–52] with a radius parameter $R = 0.2$ and discarding subjets with p_T less than 5% of the p_T of the parent jet [53]. The four-momenta of large- R jets are finally reconstructed from the momentum vectors of the remaining subjets and corrected using simulation [54, 55]. The mass of the large- R jet, m_J , is calculated by combining the calorimeter energy measurement with the track information from the ID to mitigate the effect on the mass resolution from the limited angular granularity of the calorimeter, as in Ref. [56]. The large- R jets considered in the analysis are selected by requiring $p_T > 200$ GeV, $|\eta| < 2.0$ and $m_J > 50$ GeV.

The identification of hadronically decaying top quarks that are reconstructed using large- R jets is performed using a multivariate classification algorithm employed in a deep neural network [57]. In the kinematic regime of interest in this search, a single large- R jet captures the top-quark decay products, resulting in a characteristic multi-core structure within the jet, in contrast to a typical single-core structure associated with jets in multijet background processes. In order to exploit this characteristic behaviour for the top-quark identification, a multivariate top-tagging classifier has been developed [57]. The tagger uses multiple jet-level discriminants as inputs, e.g. calibrated jet p_T and mass, information about the dispersion of the jet constituents such as N -subjettiness [58, 59], splitting scales [60] and energy correlation functions [61, 62].

The tagger used in this analysis is optimized for top-quark-initiated jets that satisfy the ‘contained’ criteria defined using the simulation as follows. First, particle-level large- R jets are built from all stable particles (with $c\tau > 10$ mm) at the generator level using a radius parameter $R = 1.0$ and trimmed in the same way as

for reconstructed jets in data. A trimmed particle-level jet is required to match a generator-level top quark within $\Delta R < 0.75$, have a mass above 140 GeV and at least one ghost-associated [63] b -hadron; hereafter the selected particle-level jet is referred to as a truth-contained jet. A reconstructed detector-level large- R jet is then required to satisfy the same ΔR requirement with respect to the matched particle-level jet to ensure that the jet contains the top-quark decay products. The top-tagger calibrated for such large- R jets turns out to be less sensitive to generator differences in the determination of top-quark decay products falling inside a jet, compared with the definition used in Ref. [57]. In this analysis the ‘top-tagged’ large- R jets are selected using requirements on the classifier corresponding to an efficiency of 80% over the range of generator-level top-quark p_T relevant for the considered Z'_{TC2} signal. With the requirement of 80% efficiency, the rejection factor for light-flavour quark and gluon jets is approximately 30 (12) at a top-quark p_T of 500 (3000) GeV.

Jets built from charged-particle tracks reconstructed in the ID (track-jets) are used to identify jets containing b -hadrons. The tracks are first selected by requiring them to be associated with the primary vertex and to contain a minimum number of hits in the pixel and SCT detectors, and then requiring them to have $p_T > 500$ MeV and $|\eta| < 2.5$. In the topology of highly boosted top quarks [57], the b -hadron decay product is surrounded by other hadronic activity from $W \rightarrow q\bar{q}'$ decays and this additional contribution from nearby particles degrades the identification of charged-particle tracks from the b -hadron decay. To overcome this, the track-jets are built from the selected tracks using the anti- k_t algorithm with R varying as a function of the jet p_T . This ‘variable-radius’ (VR) track-jet [64] has an effective jet radius, R_{eff} , proportional to the inverse of the p_T of the jet in the jet-finding procedure:

$$R \rightarrow R_{\text{eff}}(p_T) = \rho/p_T,$$

where the ρ -parameter that controls the effective radius is set to $\rho = 30$ GeV. There are two additional parameters, R_{min} and R_{max} , used to set the minimum and maximum bounds on the jet radius, and these are set to 0.02 and 0.4, respectively [65]. The values of these parameters are determined by examining the efficiency of identifying two b -jets within a large-radius jet associated with a high- p_T Higgs boson decaying into a b -quark pair [65].

The VR track-jets are composed of at least two constituent tracks and are required to have $p_T > 10$ GeV and $|\eta| < 2.5$. The VR track-jets containing b -hadrons are identified using the ‘DL1’ algorithm [66]. This algorithm is based on a multivariate classification technique with an artificial deep neural network to combine information from the impact parameters of displaced tracks, reconstructed muons in jets, and topological properties of secondary and tertiary decay vertices reconstructed within the jet. The b -jets are selected in the analysis using the requirement corresponding to an efficiency of 77% for identifying b -jets in simulated SM $t\bar{t}$ events. This requirement has corresponding rejection factors of 5 and 128 for jets containing c -hadrons and light-flavour jets, respectively. Efficiencies to identify b -jets, c -jets, and light-flavour jets are corrected in the simulation to account for deviations from the efficiencies observed in data [66].

Events containing charged leptons (electrons or muons) are removed in this analysis to avoid overlap with events selected by other $t\bar{t}$ resonance searches. Electrons are reconstructed from clusters of EM calorimeter energy deposits matched to an ID track [67] with $|\eta| < 2.47$, excluding the barrel and endcap transition region of $1.37 < |\eta| < 1.52$, and are calibrated in situ using $Z \rightarrow ee$ decays [68]. The electron candidates are required to have $E_T > 25$ GeV and to satisfy the ‘tight’ identification criteria defined in Ref. [69].

Muons are reconstructed by matching tracks reconstructed in the ID and the muon spectrometer. The muon candidates are required to have $p_T > 25$ GeV and $|\eta| < 2.5$, and satisfy the ‘medium’ quality requirements. The selected muons are calibrated in situ using $Z \rightarrow \mu\mu$ and $J/\psi \rightarrow \mu\mu$ decays [70].

Similarly to large- R jets, small- R jets are also built from three-dimensional topological clusters of energy deposits in the calorimeter, but reconstructed with a radius parameter of $R = 0.4$. Small- R jets from pile-up interactions are suppressed by applying the jet vertex tagger [71], which uses information from tracks associated with the hard-scatter and pile-up vertices. Electron and muon candidate tracks are required to be associated with the primary vertex using criteria based on the longitudinal and transverse impact parameters. To avoid the misidentification of jets as electrons and electrons from heavy-flavour hadron decays, the closest small- R jet within a cone of size $\Delta R_y = \sqrt{(\Delta y)^2 + (\Delta\phi)^2} = 0.2$ around a reconstructed electron is removed.⁴ If an electron is then found within $\Delta R_y = 0.4$ of a small- R jet, the electron is removed. If a muon is found within $\Delta R_y = 0.04 + 10 \text{ GeV}/p_T^\mu$ of a small- R jet (where p_T^μ is the muon transverse momentum), the muon is removed if the jet contains at least three tracks, otherwise the jet is removed.

4.2 Event selection and categorization

The analysis uses events selected by triggers that require at least one large- R jet with $p_T > 360\text{--}460$ GeV, depending on the data-taking period. The large- R jet with the highest p_T in the event (referred to as the leading jet) is required to have $p_T > 500$ GeV to ensure a nearly 100% trigger efficiency. Events are further required to contain at least one more large- R jet with $p_T > 350$ GeV to enhance the presence of two jets that can each fully contain the top-quark decay products. Events containing leptons (electrons or muons) are removed to ensure that there is no overlap with events selected by other lepton+jets or dilepton analyses. In addition, events containing small- R jets consistent with originating from detector noise or calorimeter energy deposits associated with non-collision processes are removed. The invariant mass, m_{JJ} , of the two highest- p_T large- R jets is required to be larger than 1.4 TeV to avoid a kinematic bias caused by the jet p_T requirements. The two leading jets are required to have a separation in azimuthal angle ($|\Delta\phi|$) larger than 1.6 to ensure a back-to-back topology of top-quark jets. In addition, the rapidity distance between the two leading jets, $|\Delta y_{JJ}|$, has to be less than 1.8. This requirement rejects multijet background events with large $|\Delta y_{JJ}|$ values, which are dominated by processes with t -channel gluon exchanges. Events selected after applying these cuts ('preselection') are further refined by the signal region (SR) selections described below.

In the analysis, the two leading large- R jets in the preselected events are required to be top-tagged. The selected events are further categorized into two orthogonal SRs by the number of b -tagged VR track-jets (n_b) associated with the top-tagged large- R jets by having a separation $\Delta R < 1.0$. Events satisfying $n_b = 1$, i.e. exactly one of the two top-tagged jets is associated with a b -tagged jet, are categorized into 'SR1 b '. Events satisfying $n_b = 2$, i.e. each of the two top-tagged jets is associated with a b -tagged jet, are categorized into 'SR2 b '. The normalized distributions of the reconstructed $m_{t\bar{t}}$ ($m_{t\bar{t}}^{\text{reco}}$) in the 1 b and 2 b signal events are shown in Figure 1 for different masses of the Z'_{TC2} boson. The $m_{t\bar{t}}^{\text{reco}}$ distribution has a tail towards masses lower than the generated mass due to off-shell production of the signal and the growth of low- x partons in the proton PDF (where x stands for Bjorken- x of the proton). The acceptance times efficiency as a function of the invariant mass of a top-quark pair at the generator level, $m_{t\bar{t}}^{\text{gen}}$, is shown separately for SR1 b and SR2 b in Figure 2. The acceptance is measured as the fraction of events with two leading truth-contained large- R jets, both satisfying the kinematical requirements on the p_T , η , $\Delta\phi$ and Δy described above, but not containing any generator-level leptons that satisfy certain kinematic selections.⁵ The acceptance \times efficiency is obtained with respect to the full analysis selections including

⁴ The rapidity is defined as $y = \frac{1}{2} \ln \frac{E+p_z}{E-p_z}$ where E is the energy and p_z is the longitudinal component of the momentum along the beam direction.

⁵ The generator-level leptons considered in the acceptance calculation are electrons or muons with $p_T > 25$ GeV and $|\eta| < 2.5$.

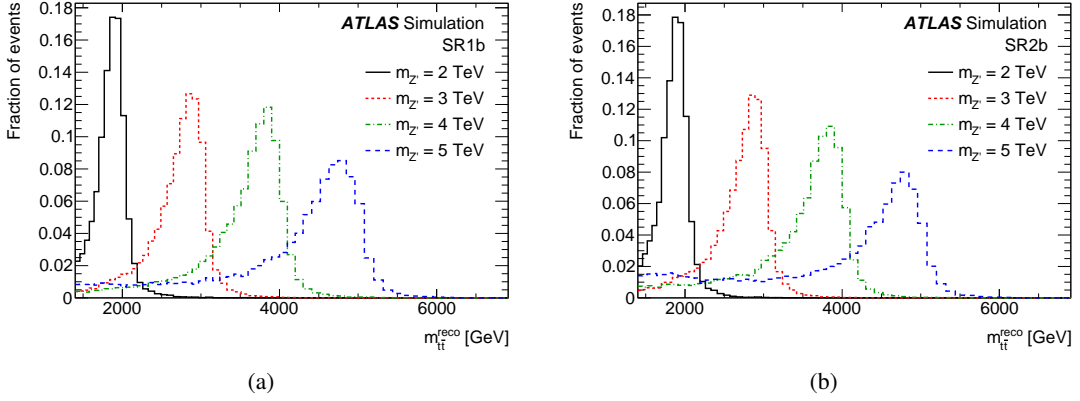


Figure 1: Normalized $m_{t\bar{t}}^{\text{reco}}$ distributions for simulated $Z'_{\text{TC}2} \rightarrow t\bar{t}$ signal events for $Z'_{\text{TC}2}$ masses of 2, 3, 4 and 5 TeV for (a) SR1b and (b) SR2b.

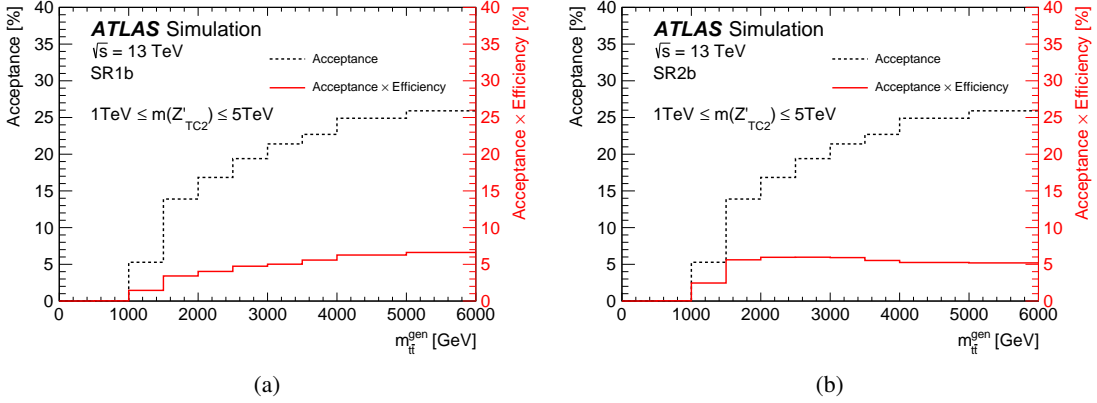


Figure 2: Acceptance (dashed histograms) and acceptance times selection efficiency (solid histograms) as a function of $m_{t\bar{t}}^{\text{gen}}$ in (a) SR1b and (b) SR2b. The acceptance is measured as the fraction of events with two leading truth-contained large- R jets, both satisfying the kinematic requirements, but not containing generator-level electrons or muons, as described in Section 4.2. The acceptance \times efficiency is calculated with respect to the full analysis selections including top- and b -tagging requirements on the two leading large- R jets. The $m_{t\bar{t}}^{\text{gen}}$ is calculated from the momenta of top and anti-top quarks at the generator level before final-state radiation. The branching fractions of the $t\bar{t}$ into all possible final states are included in the acceptance calculation.

top- and b -tagging requirements on the two leading large- R jets. The acceptance increases with increasing $m_{t\bar{t}}^{\text{gen}}$, largely due to the truth-contained requirements. The acceptance \times efficiencies have different $m_{t\bar{t}}^{\text{gen}}$ dependence for the two signal regions, mainly caused by the different b -tagging requirements.

5 Background estimation

The main backgrounds after applying the selection criteria described in Section 4 are expected to arise from SM production of $t\bar{t}$ pairs and multijet events. The background $m_{t\bar{t}}^{\text{reco}}$ distribution in the signal regions is estimated directly from data by performing a fit with a smoothly falling spectrum. The appropriate

functional form of the spectrum is determined using combinations of data and simulated events, as described below.

5.1 Background modelling using data and simulation

In order to ensure the correct functional modelling of the background, the functional form is determined using expected background spectra in the signal regions. These are obtained by summing the expected distributions of the SM $t\bar{t}$ and multijet events.

For the $t\bar{t}$ background, the simulation samples described in Section 3 are used. For the multijet background, in addition to the multijet simulation samples in Section 3, dedicated control regions (CRs) in data are used to extract the expected $m_{t\bar{t}}^{\text{reco}}$ distributions at low masses. The distributions extracted from the data are combined with those from the simulation sample, such that the combined multijet sample provides more events than expected for the data at high masses. Table 1 shows the CRs defined in data according to whether the leading and subleading large- R jets pass or fail the top- and/or b -tagging requirements. The SRs defined in Section 4.2 correspond to the regions $\text{SR}1b_{tbt\cancel{t}\cancel{b}}$, $\text{SR}1b_{t\cancel{t}tb}$ and $\text{SR}2b_{tbtb}$. The first (last) two subscripts correspond to the leading (subleading) large- R jet, and they indicate that the jet is tagged (k) or not (\cancel{k}) where $k = t$ (b) corresponding to top-tagging (b -tagging). The $\text{SR}1b$ signal region consists of the sum of the two regions, $\text{SR}1b_{tbt\cancel{t}\cancel{b}}$ and $\text{SR}1b_{t\cancel{t}tb}$. The ‘template region’ $\text{TR}_{t\cancel{t}\cancel{b}\cancel{b}}$ with two top-tags and zero b -tags is dominated by multijet events, with a purity of about 97%, and hence it is used to extract the shape of the multijet distribution. The multijet background contributions expected in the $\text{SR}i$ ($i = 1b_{tbt\cancel{t}\cancel{b}}$, $1b_{t\cancel{t}tb}$, $2b_{tbtb}$), $N_{\text{exp}}(\text{SR}i)$, is obtained by multiplying the observed events in the TR, $N(\text{TR}_{t\cancel{t}\cancel{b}\cancel{b}})$, by scale factors R for either one or both leading top-tagged jets to be b -tagged:

$$N_{\text{exp}}(\text{SR}i) = N(\text{TR}_{t\cancel{t}\cancel{b}\cancel{b}}) \times R(\text{TR}_{t\cancel{t}\cancel{b}\cancel{b}} \rightarrow \text{SR}i), \quad (1)$$

where

$$R(\text{TR}_{t\cancel{t}\cancel{b}\cancel{b}} \rightarrow \text{SR}1b_{t\cancel{t}tb}) = \kappa_{t_1b_2} \times \frac{N(\text{A}_{t\cancel{t}\cancel{b}\cancel{b}})}{N(\text{B}_{t\cancel{t}\cancel{b}\cancel{b}})}, \quad (2)$$

$$R(\text{TR}_{t\cancel{t}\cancel{b}\cancel{b}} \rightarrow \text{SR}1b_{tbt\cancel{t}\cancel{b}}) = \kappa_{t_2b_1} \times \frac{N(\text{I}_{tbt\cancel{t}\cancel{b}})}{N(\text{H}_{t\cancel{t}\cancel{b}\cancel{b}})} \quad (3)$$

and

$$R_1(\text{TR}_{t\cancel{t}\cancel{b}\cancel{b}} \rightarrow \text{SR}2b_{tbtb}) = R(\text{TR}_{t\cancel{t}\cancel{b}\cancel{b}} \rightarrow \text{SR}1b_{t\cancel{t}tb}) \times \kappa_{t_1b_1} \times \frac{N(\text{E}_{tbt\cancel{t}\cancel{b}})}{N(\text{B}_{t\cancel{t}\cancel{b}\cancel{b}})}, \quad (4)$$

$$R_2(\text{TR}_{t\cancel{t}\cancel{b}\cancel{b}} \rightarrow \text{SR}2b_{tbtb}) = R(\text{TR}_{t\cancel{t}\cancel{b}\cancel{b}} \rightarrow \text{SR}1b_{tbt\cancel{t}\cancel{b}}) \times \kappa_{t_2b_2} \times \frac{N(\text{G}_{tbt\cancel{t}\cancel{b}})}{N(\text{H}_{t\cancel{t}\cancel{b}\cancel{b}})}. \quad (5)$$

Here the N without subscript represents the observed number of events in the respective region.

The scale factors from $\text{TR}_{t\cancel{t}\cancel{b}\cancel{b}}$ to $\text{SR}2b_{tbtb}$ have two values, R_1 and R_2 , corresponding to the two possible paths: $\text{TR}_{t\cancel{t}\cancel{b}\cancel{b}} \rightarrow \text{SR}1b_{t\cancel{t}tb} \rightarrow \text{SR}2b_{tbtb}$ and $\text{TR}_{t\cancel{t}\cancel{b}\cancel{b}} \rightarrow \text{SR}1b_{tbt\cancel{t}\cancel{b}} \rightarrow \text{SR}2b_{tbtb}$, respectively. The two resulting $N_{\text{exp}}(\text{SR}2b_{tbtb})$ values agree within 10% with the average of the two, and the average is used as the final prediction for the region $\text{SR}2b_{tbtb}$. The $\kappa_{t_1b_2}$ ($\kappa_{t_2b_1}$) factor accounts for the correlation between

the top-tagging of the leading (subleading) large- R jet and the b -tagging of the subleading (leading) large- R jet and is obtained as follows:

$$\kappa_{t_1 b_2} = \left(\frac{N(G_{t\cancel{t}\cancel{b}})}{N(H_{t\cancel{t}\cancel{b}})} \right) / \left(\frac{N(C_{\cancel{t}\cancel{b}b})}{N(D_{\cancel{t}\cancel{b}\cancel{b}})} \right), \quad \kappa_{t_2 b_1} = \left(\frac{N(E_{\cancel{t}bt\cancel{b}})}{N(B_{\cancel{t}\cancel{b}t\cancel{b}})} \right) / \left(\frac{N(F_{\cancel{t}b\cancel{t}\cancel{b}})}{N(D_{\cancel{t}\cancel{b}\cancel{b}})} \right). \quad (6)$$

Similarly, the $\kappa_{t_1 b_1}$ ($\kappa_{t_2 b_2}$) factor accounts for the correlation between the top-tagging of the leading (subleading) large- R jet and the b -tagging of the leading (subleading) large- R jet, as follows:

$$\kappa_{t_1 b_1} = \left(\frac{N(I_{tb\cancel{t}\cancel{b}})}{N(H_{t\cancel{t}\cancel{b}\cancel{b}})} \right) / \left(\frac{N(F_{\cancel{t}bt\cancel{b}})}{N(D_{\cancel{t}\cancel{b}\cancel{b}})} \right), \quad \kappa_{t_2 b_2} = \left(\frac{N(A_{\cancel{t}\cancel{b}tb})}{N(B_{\cancel{t}\cancel{b}t\cancel{b}})} \right) / \left(\frac{N(C_{\cancel{t}\cancel{b}\cancel{t}\cancel{b}})}{N(D_{\cancel{t}\cancel{b}\cancel{b}})} \right). \quad (7)$$

These calculations in Eqs. (1)–(7) are performed bin-by-bin for the $m_{t\bar{t}}^{\text{reco}}$ distributions in all relevant CRs. The average values of the $\kappa_{t_1 b_2}$ and $\kappa_{t_2 b_1}$ factors range between 0.94 and 1.0 while those of $\kappa_{t_1 b_1}$ and $\kappa_{t_2 b_2}$ have larger values around 1.6–1.7 in the $m_{t\bar{t}}^{\text{reco}}$ region of 1.4–6.0 TeV. The large difference between the κ factors indicates that the variation of multijet event yields due to the top(b)-tagging depends on whether the same top(b)-tagged jet in the event is also b (top)-tagged or not.

The resulting multijet $m_{t\bar{t}}^{\text{reco}}$ distributions for the SRs are combined with the simulated sample of PYTHIA multijet events to reduce statistical fluctuation at high mass. This is carried out by using the simulated PYTHIA sample instead of the data-derived sample in the $m_{t\bar{t}}^{\text{reco}}$ region where the former has higher statistical power than the latter. It turns out that the simulated sample has different $m_{t\bar{t}}^{\text{reco}}$ shape than the data-derived sample and the difference is quantified as a linear fit to the ratio of data-derived to simulated event yields in $m_{t\bar{t}}^{\text{reco}}$. Therefore, the $m_{t\bar{t}}^{\text{reco}}$ shapes of the simulated sample are corrected in the SRs by applying the fit values in bins of the $m_{t\bar{t}}^{\text{reco}}$ distributions. In order to avoid a dependence on the choice of $m_{t\bar{t}}^{\text{reco}}$ value where the data-derived and simulated multijet samples are combined, the switching point is varied in steps of 140–200 GeV between 2260 and 3030 GeV when the background modelling uncertainty is considered (Section 6.2).

Table 1: Event categorization used to model the multijet background from data according to whether the leading and subleading large- R jets are top-tagged or b -tagged. If the large- R jet is top-tagged, it is denoted by t , and otherwise by \cancel{t} , as indicated in the left column or in the bottom row. Similarly, if the large- R jet is b -tagged, it is denoted by b , and otherwise by \cancel{b} . The percentages in parentheses show the expected fractions of SM $t\bar{t}$ events obtained using the $t\bar{t}$ and multijet simulation samples. Non- $t\bar{t}$ or non-multijet background events are negligible. The signal regions, SR1 b and SR2 b , are coloured in red, the template region (TR) in grey and the rest of the control regions A-I in light blue.

Subleading large- R jet	tb	A (6.1%)		SR1 b (23%)	SR2 b (90%)
	$t\cancel{b}$	B (0.5%)	E (1.8%)	TR (2.6%)	SR1 b (28%)
	$\cancel{t}b$	C (0.4%)		G (2.3%)	
	$\cancel{t}\cancel{b}$	D (< 0.1%)	F (0.3%)	H (0.4%)	I (6.7%)
		$\cancel{t}\cancel{b}$	$\cancel{t}b$	$t\cancel{b}$	tb
Leading large- R jet					

5.2 Determination of background parameterization

The expected background $m_{t\bar{t}}^{\text{reco}}$ distributions obtained in Section 5.1 are used, along with the simulated SM $t\bar{t}$ samples, to determine the functional forms of the fits to the SR data. To do this, a set of 1000 background distributions (referred to as S_{bkg} hereafter) is created for each SR by bin-wise variation of the nominal distribution assuming Poisson fluctuations. A typical bin width is chosen using the resolution of the reconstructed $m_{t\bar{t}}^{\text{reco}}$ distribution and is 60 GeV at $m_{t\bar{t}}^{\text{reco}} = 1.4$ TeV, increasing to 100 (130) GeV at $m_{t\bar{t}}^{\text{reco}} = 4$ (6) TeV. For each bin of the background $m_{t\bar{t}}^{\text{reco}}$ distribution, the square-root of the bin content is assigned as the uncertainty.

The following parameterized form [72] is used for the fit function:

$$F(x) = p_0(1-x)^{p_1}x^{p_2+p_3 \log(x)+p_4 \log(x)^2}, \quad (8)$$

where $x = m_{t\bar{t}}^{\text{reco}}/\sqrt{s}$, p_0 is a normalization factor and p_1 through p_4 are free parameters controlling the shape of the $m_{t\bar{t}}^{\text{reco}}$ distributions. The function can be used as a two- or three-parameter function by setting $p_3 = p_4 = 0$ or $p_4 = 0$, respectively. The number of shape parameters is then determined by performing fits with individual functions to the S_{bkg} set of background distributions and evaluating the goodness of the individual fits. The evaluation of the goodness of the fit is performed using χ^2 and BumpHunter [73] test statistics. The BumpHunter is a hypothesis-testing tool to look for local excesses or deficits in data relative to the background (obtained from fits in this analysis). After confirming that all the two-, three- and four-parameter functions are qualified, a Wilks' test [74] is repeated over the S_{bkg} set of background distributions to determine how many parameters are needed to describe them. Finally, the functional form with three shape parameters ($p_4 = 0$) is selected for both SR1*b* and SR2*b*. The fit with the three-shape-parameter function is performed to the data to estimate background in each of the SRs.

6 Systematic uncertainties

For uncertainties in the signal prediction, experimental uncertainties associated with the reconstruction and calibration techniques are considered in the analysis. In addition, an uncertainty associated with the interpolated signal templates and the statistical uncertainty of the simulated samples are taken into account as detailed below. Since the background is directly estimated from data using a functional fit, only the uncertainties associated with the fit method and the statistical uncertainty of the data are taken into account for the background modelling. Each source of experimental systematic uncertainty in the signal is treated as fully correlated across signal regions. The background uncertainties are considered to be uncorrelated as they are estimated from statistically independent samples.

6.1 Signal modelling uncertainties

The experimental systematic uncertainties considered for the signal prediction are dominated by uncertainties associated with the large- R jet energy scales (JES), jet mass scale (JMS), jet energy resolutions (JER), jet mass resolution (JMR), and the top-tagging and b -tagging efficiencies.

The uncertainty in the scale of large- R jet p_T and mass is evaluated by comparing the ratio of calorimeter-based to track-based measurements in multijet data and simulation [56, 75]. The uncertainty in the jet p_T resolution [76] is obtained by smearing the MC jet p_T using a Gaussian function with a relative width of

0.02 and calculating the resulting change from the unsmeared distribution. This is obtained as a one-sided systematic uncertainty and then symmetrized in the rest of the analysis. The jet mass resolution [56] uncertainty, derived specifically in the context of top-quark-initiated jets, is obtained by smearing the MC jet mass using a Gaussian function with a width corresponding to a 20% relative uncertainty on the jet mass resolution.

The top-tagging efficiency for hadronically decaying top quarks is measured using both data and simulation samples enriched in $t\bar{t}$ events with one-lepton final states [57]. The difference between the data and simulation efficiencies is taken as a correction factor to the simulated signal yield. The uncertainty in the correction factor, estimated to be 10–15% (per jet) depending on the top-quark jet p_T , is propagated through the signal yields in the SRs. An additional top-tagging systematic uncertainty is considered at high p_T , beyond a top-quark jet p_T of approximately 1 TeV, where the correction factor is not measured due to the limited number of one-lepton $t\bar{t}$ events in data. This uncertainty is evaluated as the variation of the efficiencies from simulated $t\bar{t}$ samples with different conditions applied to the GEANT4 calorimeter shower model and the detector material, and is 1–6% for the top-quark jet p_T between 1 and 3 TeV. This additional uncertainty is added in quadrature to the correction factor uncertainty at the highest available p_T bin to obtain the top-tagging systematic uncertainty beyond that p_T bin. The components of jet p_T scale and top-tagging uncertainties associated with the same sources of systematic uncertainties are varied together in the statistical analysis procedure.

The uncertainty in the b -tagging efficiency for b -quark-induced jets is accounted for in a way similar to that for the top-tagging uncertainty. The b -tagging efficiencies in data and simulated events are compared using $t\bar{t}$ events with final states containing two leptons, and the correction factor is derived as the difference between data and simulation efficiencies [77]. The b -tagging uncertainties in the correction factor are assessed in various kinematic regions, separately for b -jets, c -jets, and light-flavour jets. An additional b -tagging uncertainty at high p_T beyond the measured p_T range is also taken into account by an extrapolation technique. The uncertainties are then decomposed into various independent components for each of the flavour categories.

The uncertainty in the combined 2015–2018 integrated luminosity is 1.7% [78], obtained using the LUCID-2 detector [79] for the primary luminosity measurements. The pile-up modelling uncertainty including the uncertainty associated with the pile-up suppression by the jet vertex tagger is considered for simulated events. The uncertainties associated with lepton reconstruction and identification are negligible compared with other uncertainties. The uncertainty associated with the interpolated signal is taken into account by comparing expected limits obtained using the simulated and interpolated signal samples at the same masses. The uncertainty is estimated to be at most 5%, and therefore a 5% uncertainty is assigned to the signal event yield, along with the statistical uncertainty due to the limited number of simulated events.

A summary of the post-fit impacts on the 2 and 4 TeV Z'_{TC2} signal yields is given in Table 2. They are expressed as percentage deviations from the nominal yields due to the large- R jet related uncertainties, top- and b -tagging uncertainties as well as the luminosity and pile-up modelling uncertainties. The impacts on the signal yields are amplified from the per-jet p_T -scale and top-tagging uncertainties due to the presence of two top-quark jets in the events. The impact from the b -tagging uncertainty is larger in the SR1 b than the SR2 b at the same signal masses. This is understood as follows: signal events in both SR2 b and, to a lesser extent, SR1 b are dominated by events with two b -quarks, each associated with one of the two leading large- R jets. Both jets (exactly one jet) are required to be b -tagged in the SR2 b (SR1 b). This results in an increased impact from the b -tagging uncertainty for the SR1 b because, for the b -tagging criteria used in this analysis, the uncertainty in the inefficiency correction factor for the non- b -tagged jet is about a factor

Table 2: Summary of the post-fit impact of systematic uncertainties on the expected numbers of Z'_{TC2} signal events (expressed as percentage deviations from the nominal predictions) for masses of 2 and 4 TeV in each of the signal regions. The largest absolute value due to the $\pm 1\sigma$ variations is shown for each uncertainty source. The components of top-tagging uncertainties associated with the JES uncertainties are included in the numbers at the row labeled JES.

Source	2 TeV Z' [%]		4 TeV Z' [%]	
	SR1 <i>b</i>	SR2 <i>b</i>	SR1 <i>b</i>	SR2 <i>b</i>
JES	35	34	47	44
JMS	5.0	4.3	9.5	7.9
JER	0.1	0.1	0.1	< 0.1
JMR	3.9	4.0	8.0	8.0
<i>b</i> -tagging	14	5.0	23	5.3
Top-tagging	9.0	9.3	10	10
Luminosity	1.7	1.7	1.7	1.7
Pile-up modelling	0.2	0.2	0.2	0.2

of 3 larger than that in the efficiency correction factor for the *b*-tagged jet. The impact from the *b*-tagging uncertainty further increases for signals with mass of 4 TeV in the SR1*b* due to the additional contribution from the extrapolation to high p_T .

6.2 Background modelling uncertainties

The uncertainty in the background estimate is primarily associated with the choice of functional form and the fit range used to estimate the background. With a given fit function with a certain number of shape parameters and fit range, there is an ambiguity in the fit result due to intrinsic limitations associated with the chosen fit. Because of this, when a fit is performed to the background-only distribution, the fit creates a systematic difference between the estimated and real backgrounds, producing a ‘spurious’ signal. This systematic difference, referred to as the spurious-signal uncertainty, is evaluated in the statistical analysis as a bias in the signal estimate obtained from a signal-plus-background fit to the $m_{t\bar{t}}^{\text{reco}}$ distribution constructed under the background-only hypothesis. The signal model used in the signal-plus-background fit is extracted from the simulated Z'_{TC2} samples by performing fits to the reconstructed $m_{t\bar{t}}^{\text{reco}}$ spectra with the sum of a Gaussian function and a Crystal Ball function. The background model is the three-shape-parameter function of Eq. (8). The spurious-signal uncertainty is obtained from a signal-plus-background fit performed over the S_{bkg} set of background distributions used to determine the fit functions in Section 5.2. In the fit the switching point for the data-derived and simulated multijet samples is varied in each S_{bkg} set of background distributions (Section 5.1). The spurious signal uncertainty (taken from the average result of the fits) is estimated as a function of the generated signal mass and quantified relative to the statistical uncertainty of the background prediction within $\pm 20\%$ around the signal peak. It decreases monotonically from 80% to 2% between 1.75 and 5 TeV for the 1*b* signal region. For the 2*b* signal region, it is approximately constant within 30–40% up to 4 TeV, then increases significantly and reaches 200% at 5 TeV. The increase of the spurious-signal uncertainty at masses above 4 TeV in the 2*b* signal region is associated with the fact that the background distribution falls more rapidly than that in the 1*b* signal region, causing the function to be less constrained in the high-mass region and thus producing an increased amount of spurious signal. An additional uncertainty associated with the statistical uncertainty of the expected background in the signal

regions is also considered by propagating the impact of the uncertainties in the values of the fit parameters in Eq. (8) to the $m_{t\bar{t}}^{\text{reco}}$ spectra.⁶

7 Statistical analysis

The statistical interpretation of the data consists of two steps: a model-independent test for the presence of local deviations from smooth $m_{t\bar{t}}^{\text{reco}}$ spectra in data using BumpHunter, and hypothesis testing of data with the benchmark signal model using the profile likelihood ratio.

The BumpHunter test quantifies the significance of local excesses or deficits in the $m_{t\bar{t}}^{\text{reco}}$ distributions, taking into account the look-elsewhere effect [80, 81] associated with the scanned mass ranges.

The hypothesis testing with the benchmark signal is performed using a binned maximum-likelihood fit to the $m_{t\bar{t}}^{\text{reco}}$ distributions that is based on the expected signal and background yields. The likelihood model is defined as:

$$\mathcal{L} = \prod_i P_{\text{pois}}(n_i|\lambda_i) \times \mathcal{N}(\boldsymbol{\theta})$$

where $P_{\text{pois}}(n_i|\lambda_i)$ is the Poisson probability to observe n_i events when λ_i events are expected in bin i of the $m_{t\bar{t}}^{\text{reco}}$ distribution, and $\mathcal{N}(\boldsymbol{\theta})$ is a series of Gaussian or log-normal distributions for the nuisance parameters, $\boldsymbol{\theta}$, corresponding to the systematic uncertainties related to the signal and background yields in each bin. The λ_i is expressed as $\lambda_i = \mu s_i(\boldsymbol{\theta}) + b_i(\boldsymbol{\theta})$ with μ being the signal strength, defined as a signal cross-section in units of the theoretical prediction, determined by the fit, and $s_i(\boldsymbol{\theta})$ and $b_i(\boldsymbol{\theta})$ being the expected numbers of signal and background events, respectively. Nuisance parameters are allowed to float in the fit and thus vary the normalization and shape of the signal $m_{t\bar{t}}^{\text{reco}}$ distribution as well as the shape of the background $m_{t\bar{t}}^{\text{reco}}$ distribution.

The information about μ is extracted from a likelihood fit to data under the signal-plus-background hypothesis, using a test statistic based on the profile likelihood ratio. The distributions of the test statistic under the signal-plus-background and background-only hypotheses are obtained using the asymptotic formulae [82]. The systematic uncertainties with the largest post-fit impact on μ at $m = 2$ TeV and $m = 4$ TeV are the fit parameter uncertainty and the spurious-signal uncertainty for the background and the JES uncertainties for the signal. The level of agreement between the observed data and the background prediction is assessed by computing the local p_0 -value, defined as the probability to observe an excess at least as large as the one observed in data, under the background-only hypothesis. The global p_0 -value is computed by considering the look-elsewhere effect due to multiple testing on the signal mass points. Expected and observed upper limits are set at 95% confidence level (CL) on the cross-section times branching fraction ($\sigma \cdot B$) of new particles decaying into a $t\bar{t}$ pair using the CL_s prescription [83]. Cross-checks with the test statistic sampled using pseudo-experiments are performed to test the accuracy of the asymptotic formula in the high-mass region beyond 2 TeV. The $\sigma \cdot B$ limits from the asymptotic approximation are found to be stronger than those from the pseudo-experiments by at most 20% at masses above 4 TeV. The impact on the mass limit from this approximation is estimated to be below 100 GeV for the Z'_{TC2} signal considered in this analysis.

⁶ The fit parameter uncertainties are re-evaluated by using another set of background distributions obtained assuming Poisson uncertainties instead of the uncertainties from the square-root of bin contents. The impact on the fit parameter uncertainties from this change turns out to be negligible.

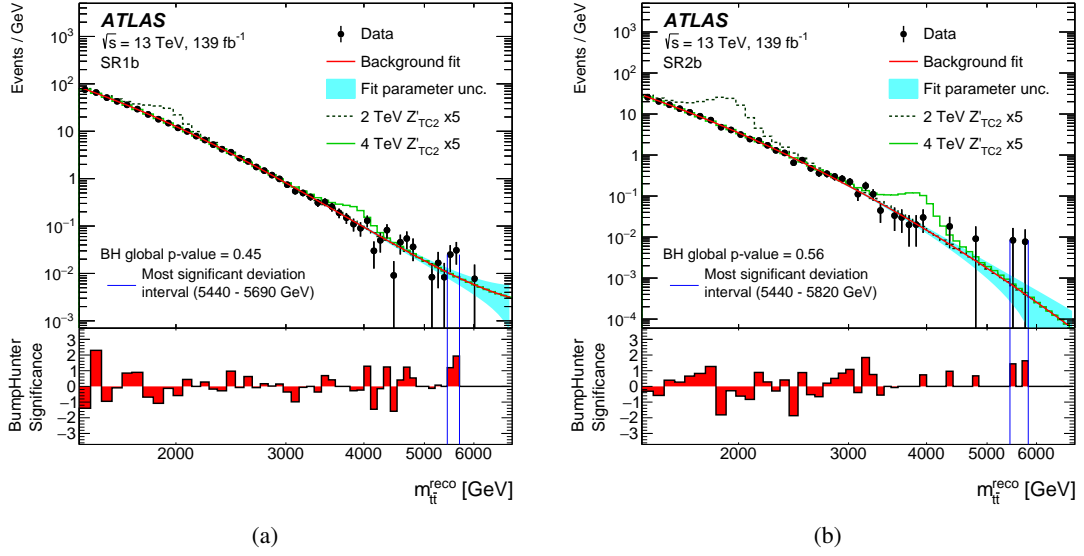


Figure 3: Observed $m_{i\bar{i}}^{\text{reco}}$ distributions in data for (a) SR1*b* and (b) SR2*b*, shown together with the result of the fit with the three-shape-parameter function. The shaded bands around the fits indicate the effect of the fit parameter uncertainty on the background prediction. The bin width of the distributions is chosen to be the same as that used in the background parameterization (Section 5.2). The predicted $Z'_{\text{TC}2}$ signal distributions with masses of 2 and 4 TeV (multiplied by a factor of 5) are superimposed on the background prediction. The lower panel shows the significance of data with respect to the background prediction from the fit, calculated in continuous mass intervals scanned over the binned $m_{i\bar{i}}^{\text{reco}}$ distributions. The two vertical lines extending between the upper and lower panel represent the most significant deviation interval. The global p -value of the interval is 0.45 (0.56) for SR1*b* (SR2*b*).

8 Results

The observed $m_{i\bar{i}}^{\text{reco}}$ distributions in the two SRs with fits using the three-shape-parameter function are shown in Figure 3. The observed number of data events is 26 964 (8160) in SR1*b* (SR2*b*). The BumpHunter tests for the compatibility of the data and the background prediction show that the fit describes the data well for both SRs. The interval with the most significant deviation is 5.44–5.69 TeV for SR1*b* and 5.44–5.82 TeV for SR2*b* with the corresponding global p -values of 0.45 and 0.56, respectively. The parameter values of the fit functions determined from the fits to the data are provided in HEPData [84]. The parameter values are consistent with those obtained from fits to the S_{bkg} set of expected background distributions, used in Section 5.2.

With the $Z'_{\text{TC}2}$ signal used in this analysis, the minimum local p_0 -value is found to be 0.06 (1.6σ) at $Z'_{\text{TC}2}$ mass of 1.88 TeV in the mass range between 1.75 and 5 TeV. In the absence of a significant excess above the background prediction, 95% CL upper limits on $\sigma \cdot B$ are calculated at each mass value of the $Z'_{\text{TC}2}$ signal model. The expected and observed upper limits on the $\sigma \cdot B$ of $Z'_{\text{TC}2} \rightarrow i\bar{i}$ are presented in Figure 4. The results from the two SRs are statistically combined to obtain these limits. From the comparison with the $\sigma \cdot B$ at NLO for the $Z'_{\text{TC}2}$ with $\Gamma/m = 1\%$ and 3% , the $Z'_{\text{TC}2}$ masses up to 3.9 and 4.7 TeV, respectively, are excluded at 95% CL. For the $Z'_{\text{TC}2}$ with $\Gamma/m = 1.2\%$ and the LO $\sigma \cdot B$ multiplied by 1.3 (scaled to NLO prediction), masses up to 4.1 TeV are excluded at 95% CL. The upper limits on $\sigma \cdot B$ are provided only up to 5 TeV for the $Z'_{\text{TC}2}$ signal mass because of the large spurious-signal uncertainty exceeding 200% at masses beyond 5 TeV, making the limit calculation unreliable at masses larger than ~ 5.2 TeV.

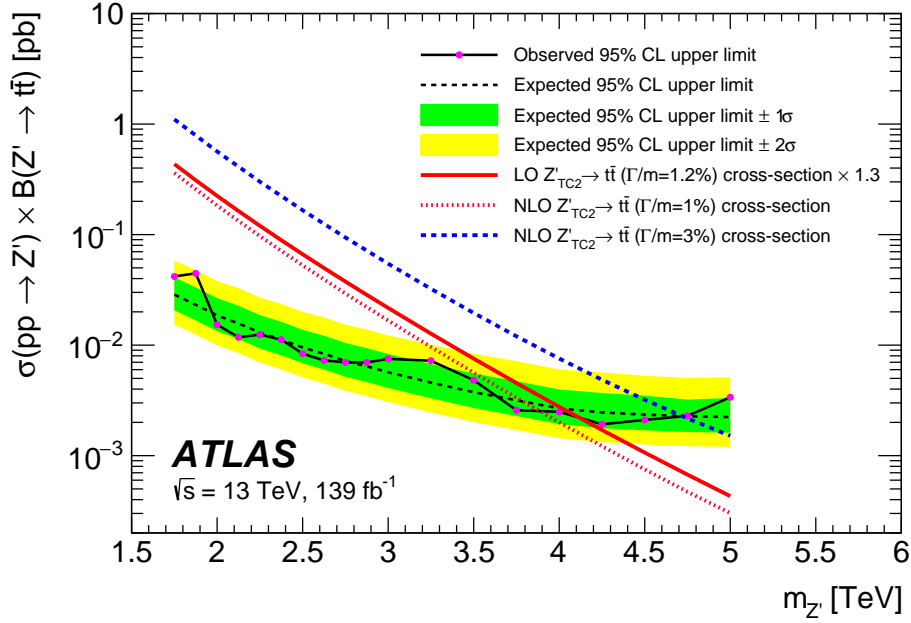


Figure 4: Observed and expected upper limits on the cross-section times branching fraction of the $Z'_{TC2} \rightarrow t\bar{t}$ as a function of the Z'_{TC2} mass. The NLO theory cross-sections times branching fraction for the Z'_{TC2} with $\Gamma/m = 1\%$ and 3% are shown by the red dotted and blue dashed lines, respectively. Shown by the red solid line is a NLO prediction, obtained by multiplying the LO theory cross-section times branching fraction by a factor 1.3 [41], for the Z'_{TC2} with $\Gamma/m = 1.2\%$.

The expected sensitivity of the present analysis is limited by the statistical uncertainty of the background prediction over the full mass range, except at high mass beyond 4.5 TeV where the systematic uncertainty due to the spurious signal dominates the statistical uncertainty.

9 Conclusion

This paper presents a search for new massive particles decaying into $t\bar{t}$ in the fully hadronic final state using 139 fb^{-1} of pp collision data recorded at $\sqrt{s} = 13 \text{ TeV}$ with the ATLAS detector at the LHC. The search focuses on the mass range above 1.4 TeV. It uses an improved top-quark tagging based on a multivariate classification algorithm with a deep neural network and b -hadron identification with variable-radius track-jets for highly boosted top quarks. The background is estimated from a fit to data. No significant deviation from the background expectation is observed over the search range. Upper limits are set on the production cross-section times branching fraction for the Z'_{TC2} boson in the topcolor-assisted-technicolor model, resulting in the exclusion of Z'_{TC2} masses up to 3.9 and 4.7 TeV for decay widths of 1% and 3%, respectively. Compared to the previous analysis with the 2015–2016 data set, the improved analysis techniques presented here provide a 65% improvement in the expected cross-section limit at 4 TeV when using the same data set.

Acknowledgements

We thank CERN for the very successful operation of the LHC, as well as the support staff from our institutions without whom ATLAS could not be operated efficiently.

We acknowledge the support of ANPCyT, Argentina; YerPhI, Armenia; ARC, Australia; BMWFW and FWF, Austria; ANAS, Azerbaijan; SSTC, Belarus; CNPq and FAPESP, Brazil; NSERC, NRC and CFI, Canada; CERN; ANID, Chile; CAS, MOST and NSFC, China; COLCIENCIAS, Colombia; MSMT CR, MPO CR and VSC CR, Czech Republic; DNRF and DNSRC, Denmark; IN2P3-CNRS and CEA-DRF/IRFU, France; SRNSFG, Georgia; BMBF, HGF and MPG, Germany; GSRT, Greece; RGC and Hong Kong SAR, China; ISF and Benozio Center, Israel; INFN, Italy; MEXT and JSPS, Japan; CNRST, Morocco; NWO, Netherlands; RCN, Norway; MNiSW and NCN, Poland; FCT, Portugal; MNE/IFA, Romania; JINR; MES of Russia and NRC KI, Russian Federation; MESTD, Serbia; MSSR, Slovakia; ARRS and MIZŠ, Slovenia; DST/NRF, South Africa; MICINN, Spain; SRC and Wallenberg Foundation, Sweden; SERI, SNSF and Cantons of Bern and Geneva, Switzerland; MOST, Taiwan; TAEK, Turkey; STFC, United Kingdom; DOE and NSF, United States of America. In addition, individual groups and members have received support from BCKDF, CANARIE, Compute Canada, CRC and IVADO, Canada; Beijing Municipal Science & Technology Commission, China; COST, ERC, ERDF, Horizon 2020 and Marie Skłodowska-Curie Actions, European Union; Investissements d’Avenir Labex, Investissements d’Avenir Idex and ANR, France; DFG and AvH Foundation, Germany; Herakleitos, Thales and Aristeia programmes co-financed by EU-ESF and the Greek NSRF, Greece; BSF-NSF and GIF, Israel; La Caixa Banking Foundation, CERCA Programme Generalitat de Catalunya and PROMETEO and GenT Programmes Generalitat Valenciana, Spain; Göran Gustafssons Stiftelse, Sweden; The Royal Society and Leverhulme Trust, United Kingdom.

The crucial computing support from all WLCG partners is acknowledged gratefully, in particular from CERN, the ATLAS Tier-1 facilities at TRIUMF (Canada), NDGF (Denmark, Norway, Sweden), CC-IN2P3 (France), KIT/GridKA (Germany), INFN-CNAF (Italy), NL-T1 (Netherlands), PIC (Spain), ASGC (Taiwan), RAL (UK) and BNL (USA), the Tier-2 facilities worldwide and large non-WLCG resource providers. Major contributors of computing resources are listed in Ref. [85].

References

- [1] C. T. Hill and S. J. Parke, *Top quark production: Sensitivity to new physics*, *Phys. Rev. D* **49** (1994) 4454, arXiv: [hep-ph/9312324](#) [[hep-ph](#)].
- [2] C. T. Hill, *Topcolor assisted technicolor*, *Phys. Lett. B* **345** (1995) 483, arXiv: [hep-ph/9411426](#) [[hep-ph](#)].
- [3] R. M. Harris and S. Jain, *Cross sections for leptophobic topcolor Z' decaying to top-antitop*, *Eur. Phys. J. C* **72** (2012) 2072, arXiv: [1112.4928](#) [[hep-ph](#)].
- [4] G. C. Branco et al., *Theory and phenomenology of two-Higgs-doublet models*, *Phys. Rept.* **516** (2012) 1, arXiv: [1106.0034](#) [[hep-ph](#)].
- [5] L. Randall and R. Sundrum, *Large Mass Hierarchy from a Small Extra Dimension*, *Phys. Rev. Lett.* **83** (1999) 3370, arXiv: [hep-ph/9905221](#) [[hep-ph](#)].
- [6] B. Lillie, L. Randall and L.-T. Wang, *The Bulk RS KK-gluon at the LHC*, *JHEP* **09** (2007) 074, arXiv: [hep-ph/0701166](#) [[hep-ph](#)].

- [7] ATLAS Collaboration, *Search for heavy particles decaying into a top-quark pair in the fully hadronic final state in pp collisions at $\sqrt{s} = 13$ TeV with the ATLAS detector*, *Phys. Rev. D* **99** (2019) 092004, arXiv: [1902.10077 \[hep-ex\]](#).
- [8] CMS Collaboration, *Search for resonant $t\bar{t}$ production in proton–proton collisions at $\sqrt{s} = 13$ TeV*, *JHEP* **04** (2019) 031, arXiv: [1810.05905 \[hep-ex\]](#).
- [9] ATLAS Collaboration, *A search for $t\bar{t}$ resonances in lepton+jets events with highly boosted top quarks collected in pp collisions at $\sqrt{s} = 7$ TeV with the ATLAS detector*, *JHEP* **09** (2012) 041, arXiv: [1207.2409 \[hep-ex\]](#).
- [10] ATLAS Collaboration, *Search for $t\bar{t}$ resonances in the lepton plus jets final state with ATLAS using 4.7 fb^{-1} of pp collisions at $\sqrt{s} = 7$ TeV*, *Phys. Rev. D* **88** (2013) 012004, arXiv: [1305.2756 \[hep-ex\]](#).
- [11] CMS Collaboration, *Search for anomalous $t\bar{t}$ production in the highly-boosted all-hadronic final state*, *JHEP* **09** (2012) 029, arXiv: [1204.2488 \[hep-ex\]](#).
- [12] CMS Collaboration, *Search for Z' resonances decaying to $t\bar{t}$ in dilepton+jets final states in pp collisions at $\sqrt{s} = 7$ TeV*, *Phys. Rev. D* **87** (2013) 072002, arXiv: [1211.3338 \[hep-ex\]](#).
- [13] CMS Collaboration, *Search for resonant $t\bar{t}$ production in lepton+jets events in pp collisions at $\sqrt{s} = 7$ TeV*, *JHEP* **12** (2012) 015, arXiv: [1209.4397 \[hep-ex\]](#).
- [14] CMS Collaboration, *Searches for new physics using the $t\bar{t}$ invariant mass distribution in pp collisions at $\sqrt{s} = 8$ TeV*, *Phys. Rev. Lett.* **111** (2013) 211804, arXiv: [1309.2030 \[hep-ex\]](#).
- [15] ATLAS Collaboration, *A search for $t\bar{t}$ resonances using lepton-plus-jets events in proton–proton collisions at $\sqrt{s} = 8$ TeV with the ATLAS detector*, *JHEP* **08** (2015) 148, arXiv: [1505.07018 \[hep-ex\]](#).
- [16] CMS Collaboration, *Search for resonant $t\bar{t}$ production in proton–proton collisions at $\sqrt{s} = 8$ TeV*, *Phys. Rev. D* **93** (2016) 012001, arXiv: [1506.03062 \[hep-ex\]](#).
- [17] ATLAS Collaboration, *Search for Heavy Higgs Bosons A/H Decaying to a Top Quark Pair in pp Collisions at $\sqrt{s} = 8$ TeV with the ATLAS Detector*, *Phys. Rev. Lett.* **119** (2017) 191803, arXiv: [1707.06025 \[hep-ex\]](#).
- [18] ATLAS Collaboration, *Search for heavy particles decaying into top-quark pairs using lepton-plus-jets events in proton–proton collisions at $\sqrt{s} = 13$ TeV with the ATLAS detector*, *Eur. Phys. J. C* **78** (2018) 565, arXiv: [1804.10823 \[hep-ex\]](#).
- [19] CMS Collaboration, *Search for $t\bar{t}$ resonances in highly-boosted lepton+jets and fully hadronic final states in proton–proton collisions at $\sqrt{s} = 13$ TeV*, *JHEP* **07** (2017) 001, arXiv: [1704.03366 \[hep-ex\]](#).
- [20] R. M. Harris, C. T. Hill and S. J. Parke, *Cross Section for Topcolor Z'_t decaying to $t\bar{t}$* , (1999), arXiv: [hep-ph/9911288 \[hep-ph\]](#).
- [21] ATLAS Collaboration, *The ATLAS Experiment at the CERN Large Hadron Collider*, *JINST* **3** (2008) S08003.
- [22] ATLAS Collaboration, *ATLAS Insertable B-Layer Technical Design Report*, ATLAS-TDR-19, 2010, URL: <https://cds.cern.ch/record/1291633>, *ATLAS Insertable B-Layer Technical Design Report Addendum*, ATLAS-TDR-19-ADD-1, 2012, URL: <https://cds.cern.ch/record/1451888>.

- [23] B. Abbott et al., *Production and integration of the ATLAS Insertable B-Layer*, *JINST* **13** (2018) T05008, arXiv: [1803.00844 \[physics.ins-det\]](#).
- [24] ATLAS Collaboration, *Performance of the ATLAS trigger system in 2015*, *Eur. Phys. J. C* **77** (2017) 317, arXiv: [1611.09661 \[hep-ex\]](#).
- [25] P. Nason, *A new method for combining NLO QCD with shower Monte Carlo algorithms*, *JHEP* **11** (2004) 040, arXiv: [hep-ph/0409146 \[hep-ph\]](#).
- [26] S. Frixione, P. Nason and C. Oleari, *Matching NLO QCD computations with parton shower simulations: the POWHEG method*, *JHEP* **11** (2007) 070, arXiv: [0709.2092 \[hep-ph\]](#).
- [27] S. Alioli, P. Nason, C. Oleari and E. Re, *A general framework for implementing NLO calculations in shower Monte Carlo programs: the POWHEG BOX*, *JHEP* **06** (2010) 043, arXiv: [1002.2581 \[hep-ph\]](#).
- [28] R. D. Ball et al., *Parton distributions for the LHC run II*, *JHEP* **04** (2015) 040, arXiv: [1410.8849 \[hep-ph\]](#).
- [29] M. Cacciari, M. Czakon, M. Mangano, A. Mitov and P. Nason, *Top-pair production at hadron colliders with next-to-next-to-leading logarithmic soft-gluon resummation*, *Phys. Lett. B* **710** (2012) 612, arXiv: [1111.5869 \[hep-ph\]](#).
- [30] M. Beneke, P. Falgari, S. Klein and C. Schwinn, *Hadronic top-quark pair production with NNLL threshold resummation*, *Nucl. Phys. B* **855** (2012) 695, arXiv: [1109.1536 \[hep-ph\]](#).
- [31] P. Baernreuther, M. Czakon and A. Mitov, *Percent-Level-Precision Physics at the Tevatron: Next-to-Next-to-Leading Order QCD Corrections to $q\bar{q} \rightarrow t\bar{t} + X$* , *Phys. Rev. Lett.* **109** (2012) 132001, arXiv: [1204.5201 \[hep-ph\]](#).
- [32] M. Czakon and A. Mitov, *NNLO corrections to top-pair production at hadron colliders: the all-fermionic scattering channels*, *JHEP* **12** (2012) 054, arXiv: [1207.0236 \[hep-ph\]](#).
- [33] M. Czakon and A. Mitov, *NNLO corrections to top pair production at hadron colliders: the quark-gluon reaction*, *JHEP* **01** (2013) 080, arXiv: [1210.6832 \[hep-ph\]](#).
- [34] M. Czakon, P. Fiedler and A. Mitov, *Total Top-Quark Pair-Production Cross Section at Hadron Colliders Through $O(\alpha_S^4)$* , *Phys. Rev. Lett.* **110** (2013) 252004, arXiv: [1303.6254 \[hep-ph\]](#).
- [35] M. Czakon and A. Mitov, *Top++: A program for the calculation of the top-pair cross-section at hadron colliders*, *Comput. Phys. Commun.* **185** (2014) 2930, arXiv: [1112.5675 \[hep-ph\]](#).
- [36] T. Sjöstrand, S. Mrenna and P. Z. Skands, *A brief introduction to PYTHIA 8.1*, *Comput. Phys. Commun.* **178** (2008) 852, arXiv: [0710.3820 \[hep-ph\]](#).
- [37] R. D. Ball et al., *Parton distributions with LHC data*, *Nucl. Phys. B* **867** (2013) 244, arXiv: [1207.1303 \[hep-ph\]](#).
- [38] ATLAS Collaboration, *ATLAS Pythia 8 tunes to 7 TeV data*, ATL-PHYS-PUB-2014-021, 2014, URL: <https://cds.cern.ch/record/1966419>.
- [39] ATLAS Collaboration, *Studies on top-quark Monte Carlo modelling for Top2016*, ATL-PHYS-PUB-2016-020, 2016, URL: <https://cds.cern.ch/record/2216168>.
- [40] J. Kühn, A. Scharf and P. Uwer, *Weak interactions in top-quark pair production at hadron colliders: An update*, *Phys. Rev. D* **91** (2015) 014020, arXiv: [1305.5773 \[hep-ph\]](#).
- [41] R. Bonciani, T. Jezo, M. Klasen, F. Lyonnet and I. Schienbein, *Electroweak top-quark pair production at the LHC with Z' bosons to NLO QCD in POWHEG*, *JHEP* **02** (2016) 141, arXiv: [1511.08185 \[hep-ph\]](#).

- [42] D. J. Lange, *The EvtGen particle decay simulation package*, *Nucl. Instrum. Meth. A* **462** (2001) 152.
- [43] ATLAS Collaboration, *The ATLAS Simulation Infrastructure*, *Eur. Phys. J. C* **70** (2010) 823, arXiv: [1005.4568 \[physics.ins-det\]](#).
- [44] S. Agostinelli et al., *GEANT4—a simulation toolkit*, *Nucl. Instrum. Meth. A* **506** (2003) 250.
- [45] A. Martin, W. Stirling, R. Thorne and G. Watt, *Parton distributions for the LHC*, *Eur. Phys. J. C* **63** (2009) 189, arXiv: [0901.0002 \[hep-ph\]](#).
- [46] ATLAS Collaboration, *Summary of ATLAS Pythia 8 tunes*, ATL-PHYS-PUB-2012-003, 2012, URL: <https://cds.cern.ch/record/1474107>.
- [47] ATLAS Collaboration, *Topological cell clustering in the ATLAS calorimeters and its performance in LHC Run 1*, *Eur. Phys. J. C* **77** (2017) 490, arXiv: [1603.02934 \[hep-ex\]](#).
- [48] M. Cacciari, G. P. Salam and G. Soyez, *The anti- k_t jet clustering algorithm*, *JHEP* **04** (2008) 063, arXiv: [0802.1189 \[hep-ph\]](#).
- [49] D. Krohn, J. Thaler and L.-T. Wang, *Jet trimming*, *JHEP* **02** (2010) 084, arXiv: [0912.1342 \[hep-ph\]](#).
- [50] S. Catani, Y. L. Dokshitzer, M. Olsson, G. Turnock and B. Webber, *New clustering algorithm for multijet cross sections in e^+e^- annihilation*, *Phys. Lett. B* **269** (1991) 432.
- [51] S. D. Ellis and D. E. Soper, *Successive combination jet algorithm for hadron collisions*, *Phys. Rev. D* **48** (1993) 3160, arXiv: [hep-ph/9305266 \[hep-ph\]](#).
- [52] S. Catani, Y. L. Dokshitzer, M. Seymour and B. Webber, *Longitudinally-invariant k_{\perp} -clustering algorithms for hadron-hadron collisions*, *Nucl. Phys. B* **406** (1993) 187.
- [53] ATLAS Collaboration, *Performance of jet substructure techniques in early $\sqrt{s} = 13$ TeV pp collisions with the ATLAS detector*, ATLAS-CONF-2015-035, 2015, URL: <https://cds.cern.ch/record/2041462>.
- [54] ATLAS Collaboration, *Jet energy measurement with the ATLAS detector in proton–proton collisions at $\sqrt{s} = 7$ TeV*, *Eur. Phys. J. C* **73** (2013) 2304, arXiv: [1112.6426 \[hep-ex\]](#).
- [55] ATLAS Collaboration, *Jet energy measurement and its systematic uncertainty in proton–proton collisions at $\sqrt{s} = 7$ TeV with the ATLAS detector*, *Eur. Phys. J. C* **75** (2015) 17, arXiv: [1406.0076 \[hep-ex\]](#).
- [56] ATLAS Collaboration, *Jet mass reconstruction with the ATLAS Detector in early Run 2 data*, ATLAS-CONF-2016-035, 2016, URL: <https://cds.cern.ch/record/2200211>.
- [57] ATLAS Collaboration, *Performance of top-quark and W-boson tagging with ATLAS in Run 2 of the LHC*, *Eur. Phys. J. C* **79** (2019) 375, arXiv: [1808.07858 \[hep-ex\]](#).
- [58] J. Thaler and K. Van Tilburg, *Identifying boosted objects with N-subjettiness*, *JHEP* **03** (2011) 015, arXiv: [1011.2268 \[hep-ph\]](#).
- [59] J. Thaler and K. Van Tilburg, *Maximizing boosted top identification by minimizing N-subjettiness*, *JHEP* **02** (2012) 093, arXiv: [1108.2701 \[hep-ph\]](#).
- [60] J. Thaler and L.-T. Wang, *Strategies to Identify Boosted Tops*, *JHEP* **07** (2008) 092, arXiv: [0806.0023 \[hep-ph\]](#).
- [61] A. J. Larkoski, G. P. Salam and J. Thaler, *Energy correlation functions for jet substructure*, *JHEP* **06** (2013) 108, arXiv: [1305.0007 \[hep-ph\]](#).

- [62] A. J. Larkoski, I. Moult and D. Neill, *Power counting to better jet observables*, *JHEP* **12** (2014) 009, arXiv: [1409.6298 \[hep-ph\]](#).
- [63] M. Cacciari, G. P. Salam and G. Soyez, *The catchment area of jets*, *JHEP* **04** (2008) 005, arXiv: [0802.1188 \[hep-ph\]](#).
- [64] D. Krohn, J. Thaler and L.-T. Wang, *Jets with variable R*, *JHEP* **06** (2009) 059, arXiv: [0903.0392 \[hep-ph\]](#).
- [65] ATLAS Collaboration, *Variable Radius, Exclusive- k_T , and Center-of-Mass Subjet Reconstruction for Higgs($\rightarrow b\bar{b}$) Tagging in ATLAS*, ATL-PHYS-PUB-2017-010, 2017, URL: <https://cds.cern.ch/record/2268678>.
- [66] ATLAS Collaboration, *ATLAS b-jet identification performance and efficiency measurement with $t\bar{t}$ events in pp collisions at $\sqrt{s} = 13$ TeV*, *Eur. Phys. J. C* **79** (2019) 970, arXiv: [1907.05120 \[hep-ex\]](#).
- [67] ATLAS Collaboration, *Electron reconstruction and identification in the ATLAS experiment using the 2015 and 2016 LHC proton–proton collision data at $\sqrt{s} = 13$ TeV*, *Eur. Phys. J. C* **79** (2019) 639, arXiv: [1902.04655 \[hep-ex\]](#).
- [68] ATLAS Collaboration, *Electron and photon performance measurements with the ATLAS detector using the 2015–2017 LHC proton–proton collision data*, *JINST* **14** (2019) P12006, arXiv: [1908.00005 \[hep-ex\]](#).
- [69] ATLAS Collaboration, *Electron efficiency measurements with the ATLAS detector using the 2015 LHC proton–proton collision data*, ATLAS-CONF-2016-024, 2016, URL: <https://cds.cern.ch/record/2157687>.
- [70] ATLAS Collaboration, *Muon reconstruction performance of the ATLAS detector in proton–proton collision data at $\sqrt{s} = 13$ TeV*, *Eur. Phys. J. C* **76** (2016) 292, arXiv: [1603.05598 \[hep-ex\]](#).
- [71] ATLAS Collaboration, *Performance of pile-up mitigation techniques for jets in pp collisions at $\sqrt{s} = 8$ TeV using the ATLAS detector*, *Eur. Phys. J. C* **76** (2016) 581, arXiv: [1510.03823 \[hep-ex\]](#).
- [72] ATLAS Collaboration, *Search for resonances in the mass distribution of jet pairs with one or two jets identified as b-jets in proton–proton collisions at $\sqrt{s} = 13$ TeV with the ATLAS detector*, *Phys. Rev. D* **98** (2018) 032016, arXiv: [1805.09299 \[hep-ex\]](#).
- [73] G. Choudalakis, *On hypothesis testing, trials factor, hypertests and the BumpHunter*, (2011), arXiv: [1101.0390 \[physics.data-an\]](#).
- [74] S. S. Wilks, *The Large-Sample Distribution of the Likelihood Ratio for Testing Composite Hypotheses*, *Annals Math. Statist.* **9** (1938) 60.
- [75] ATLAS Collaboration, *Identification of high transverse momentum top quarks in pp collisions at $\sqrt{s} = 8$ TeV with the ATLAS detector*, *JHEP* **06** (2016) 093, arXiv: [1603.03127 \[hep-ex\]](#).
- [76] ATLAS Collaboration, *Jet energy resolution in proton–proton collisions at $\sqrt{s} = 7$ TeV recorded in 2010 with the ATLAS detector*, *Eur. Phys. J. C* **73** (2013) 2306, arXiv: [1210.6210 \[hep-ex\]](#).
- [77] ATLAS Collaboration, *Measurements of b-jet tagging efficiency with the ATLAS detector using $t\bar{t}$ events at $\sqrt{s} = 13$ TeV*, *JHEP* **08** (2018) 089, arXiv: [1805.01845 \[hep-ex\]](#).
- [78] ATLAS Collaboration, *Luminosity determination in pp collisions at $\sqrt{s} = 13$ TeV using the ATLAS detector at the LHC*, ATLAS-CONF-2019-021, 2019, URL: <https://cds.cern.ch/record/2677054>.

- [79] G. Avoni et al., *The new LUCID-2 detector for luminosity measurement and monitoring in ATLAS*, [JINST **13** \(2018\) P07017](#).
- [80] L. Lyons, *Open statistical issues in Particle Physics*, [Ann. Appl. Stat. **2** \(2008\) 887](#), arXiv: [0811.1663 \[Stat.AP\]](#).
- [81] E. Gross and O. Vitells, *Trial factors for the look elsewhere effect in high energy physics*, [Eur. Phys. J. C **70** \(2010\) 525](#), arXiv: [1005.1891 \[physics.data-an\]](#).
- [82] G. Cowan, K. Cranmer, E. Gross and O. Vitells, *Asymptotic formulae for likelihood-based tests of new physics*, [Eur. Phys. J. C **71** \(2011\) 1554](#), Erratum: [Eur. Phys. J. C **73** \(2013\) 2501](#), arXiv: [1007.1727 \[physics.data-an\]](#), Erratum: [Eur. Phys. J. C **73** \(2013\) 2501](#).
- [83] A.L. Read, *Presentation of search results: the CL_s technique*, [J. Phys. G **28** \(2002\) 2693](#).
- [84] *The Durham High-Energy Physics Database*, <https://www.hepdata.net>.
- [85] ATLAS Collaboration, *ATLAS Computing Acknowledgements*, ATL-SOFT-PUB-2020-001, URL: <https://cds.cern.ch/record/2717821>.

The ATLAS Collaboration

G. Aad¹⁰², B. Abbott¹²⁸, D.C. Abbott¹⁰³, A. Abed Abud³⁶, K. Abeling⁵³, D.K. Abhayasinghe⁹⁴, S.H. Abidi¹⁶⁷, O.S. AbouZeid⁴⁰, N.L. Abraham¹⁵⁶, H. Abramowicz¹⁶¹, H. Abreu¹⁶⁰, Y. Abulaiti⁶, B.S. Acharya^{67a,67b,n}, B. Achkar⁵³, L. Adam¹⁰⁰, C. Adam Bourdarios⁵, L. Adamczyk^{84a}, L. Adamek¹⁶⁷, J. Adelman¹²¹, M. Adersberger¹¹⁴, A. Adiguzel^{12c,ae}, S. Adorni⁵⁴, T. Adye¹⁴³, A.A. Affolder¹⁴⁵, Y. Afik¹⁶⁰, C. Agapopoulou⁶⁵, M.N. Agaras³⁸, A. Aggarwal¹¹⁹, C. Agheorghiesei^{27c}, J.A. Aguilar-Saavedra^{139f,139a,ad}, A. Ahmad³⁶, F. Ahmadov⁸⁰, W.S. Ahmed¹⁰⁴, X. Ai¹⁸, G. Aielli^{74a,74b}, S. Akatsuka⁸⁶, T.P.A. Åkesson⁹⁷, E. Akilli⁵⁴, A.V. Akimov¹¹¹, K. Al Houry⁶⁵, G.L. Alberghi^{23b,23a}, J. Albert¹⁷⁶, M.J. Alconada Verzini¹⁶¹, S. Alderweireldt³⁶, M. Aleksa³⁶, I.N. Aleksandrov⁸⁰, C. Alexa^{27b}, T. Alexopoulos¹⁰, A. Alfonsi¹²⁰, F. Alfonsi^{23b,23a}, M. Alhroob¹²⁸, B. Ali¹⁴¹, S. Ali¹⁵⁸, M. Aliev¹⁶⁶, G. Alimonti^{69a}, C. Allaire³⁶, B.M.M. Allbrooke¹⁵⁶, B.W. Allen¹³¹, P.P. Allport²¹, A. Aloisio^{70a,70b}, F. Alonso⁸⁹, C. Alpigiani¹⁴⁸, E. Alunno Camelia^{74a,74b}, M. Alvarez Estevez⁹⁹, M.G. Alvigi^{70a,70b}, Y. Amaral Coutinho^{81b}, A. Ambler¹⁰⁴, L. Ambroz¹³⁴, C. Amelung²⁶, D. Amidei¹⁰⁶, S.P. Amor Dos Santos^{139a}, S. Amoroso⁴⁶, C.S. Amrouche⁵⁴, F. An⁷⁹, C. Anastopoulos¹⁴⁹, N. Andari¹⁴⁴, T. Andeen¹¹, J.K. Anders²⁰, S.Y. Andreev^{45a,45b}, A. Andreatta^{69a,69b}, V. Andrei^{61a}, C.R. Anelli¹⁷⁶, S. Angelidakis⁹, A. Angerami³⁹, A.V. Anisenkov^{122b,122a}, A. Annovi^{72a}, C. Antel⁵⁴, M.T. Anthony¹⁴⁹, E. Antipov¹²⁹, M. Antonelli⁵¹, D.J.A. Antrim¹⁷¹, F. Anulli^{73a}, M. Aoki⁸², J.A. Aparisi Pozo¹⁷⁴, M.A. Aparo¹⁵⁶, L. Aperio Bella⁴⁶, N. Aranzabal³⁶, V. Araujo Ferraz^{81a}, R. Araujo Pereira^{81b}, C. Arcangeletti⁵¹, A.T.H. Arce⁴⁹, F.A. Arduh⁸⁹, J-F. Arguin¹¹⁰, S. Argyropoulos⁵², J.-H. Arling⁴⁶, A.J. Armbruster³⁶, A. Armstrong¹⁷¹, O. Arnaez¹⁶⁷, H. Arnold¹²⁰, Z.P. Arrubarrena Tame¹¹⁴, G. Artoni¹³⁴, K. Asai¹²⁶, S. Asai¹⁶³, T. Asawatavonvanich¹⁶⁵, N. Asbah⁵⁹, E.M. Asimakopoulou¹⁷², L. Asquith¹⁵⁶, J. Assahsah^{35e}, K. Assamagan²⁹, R. Astalos^{28a}, R.J. Atkin^{33a}, M. Atkinson¹⁷³, N.B. Atlay¹⁹, H. Atmani⁶⁵, K. Augsten¹⁴¹, V.A. Austrup¹⁸², G. Avolio³⁶, M.K. Ayoub^{15a}, G. Azuelos^{110,am}, H. Bachacou¹⁴⁴, K. Bachas¹⁶², M. Backes¹³⁴, F. Backman^{45a,45b}, P. Bagnaia^{73a,73b}, M. Bahmani⁸⁵, H. Bahrasemani¹⁵², A.J. Bailey¹⁷⁴, V.R. Bailey¹⁷³, J.T. Baines¹⁴³, C. Bakalis¹⁰, O.K. Baker¹⁸³, P.J. Bakker¹²⁰, E. Bakos¹⁶, D. Bakshi Gupta⁸, S. Balaji¹⁵⁷, E.M. Baldin^{122b,122a}, P. Balek¹⁸⁰, F. Balli¹⁴⁴, W.K. Balunas¹³⁴, J. Balz¹⁰⁰, E. Banas⁸⁵, M. Bandieramonte¹³⁸, A. Bandyopadhyay²⁴, Sw. Banerjee^{181,i}, L. Barak¹⁶¹, W.M. Barbe³⁸, E.L. Barberio¹⁰⁵, D. Barberis^{55b,55a}, M. Barbero¹⁰², G. Barbour⁹⁵, T. Barillari¹¹⁵, M-S. Barisits³⁶, J. Barkeloo¹³¹, T. Barklow¹⁵³, R. Barnea¹⁶⁰, B.M. Barnett¹⁴³, R.M. Barnett¹⁸, Z. Barnovska-Blenessy^{60a}, A. Baroncelli^{60a}, G. Barone²⁹, A.J. Barr¹³⁴, L. Barranco Navarro^{45a,45b}, F. Barreiro⁹⁹, J. Barreiro Guimarães da Costa^{15a}, U. Barron¹⁶¹, S. Barsov¹³⁷, F. Bartels^{61a}, R. Bartoldus¹⁵³, G. Bartolini¹⁰², A.E. Barton⁹⁰, P. Bartos^{28a}, A. Basalae⁴⁶, A. Basan¹⁰⁰, A. Bassalat^{65,aj}, M.J. Basso¹⁶⁷, R.L. Bates⁵⁷, S. Batlamous^{35f}, J.R. Batley³², B. Batool¹⁵¹, M. Battaglia¹⁴⁵, M. Bauce^{73a,73b}, F. Bauer^{144,*}, K.T. Bauer¹⁷¹, P. Bauer²⁴, H.S. Bawa³¹, A. Bayirli^{12c}, J.B. Beacham⁴⁹, T. Beau¹³⁵, P.H. Beauchemin¹⁷⁰, F. Becherer⁵², P. Bechtel²⁴, H.C. Beck⁵³, H.P. Beck^{20,p}, K. Becker¹⁷⁸, C. Becot⁴⁶, A. Beddall^{12d}, A.J. Beddall^{12a}, V.A. Bednyakov⁸⁰, M. Bedognetti¹²⁰, C.P. Bee¹⁵⁵, T.A. Beermann¹⁸², M. Begalli^{81b}, M. Begel²⁹, A. Behera¹⁵⁵, J.K. Behr⁴⁶, F. Beisiegel²⁴, M. Belfkir⁵, A.S. Bell⁹⁵, G. Bella¹⁶¹, L. Bellagamba^{23b}, A. Bellerive³⁴, P. Bellos⁹, K. Beloborodov^{122b,122a}, K. Belotskiy¹¹², N.L. Belyaev¹¹², D. Benchekroun^{35a}, N. Benekos¹⁰, Y. Benhammou¹⁶¹, D.P. Benjamin⁶, M. Benoit⁵⁴, J.R. Bensinger²⁶, S. Bentvelsen¹²⁰, L. Beresford¹³⁴, M. Beretta⁵¹, D. Berge¹⁹, E. Bergeaas Kuutmann¹⁷², N. Berger⁵, B. Bergmann¹⁴¹, L.J. Bergsten²⁶, J. Beringer¹⁸, S. Berlendis⁷, G. Bernardi¹³⁵, C. Bernius¹⁵³, F.U. Bernlochner²⁴, T. Berry⁹⁴, P. Berta¹⁰⁰, C. Bertella^{15a}, A. Berthold⁴⁸, I.A. Bertram⁹⁰, O. Bessidskaia Bylund¹⁸², N. Besson¹⁴⁴, A. Bethani¹⁰¹, S. Bethke¹¹⁵, A. Betti⁴², A.J. Bevan⁹³, J. Beyer¹¹⁵, D.S. Bhattacharya¹⁷⁷, P. Bhattarai²⁶, V.S. Bhopatkar⁶, R. Bi¹³⁸, R.M. Bianchi¹³⁸, O. Biebel¹¹⁴, D. Biedermann¹⁹, R. Bielski³⁶, K. Bierwagen¹⁰⁰, N.V. Biesuz^{72a,72b}, M. Biglietti^{75a}, T.R.V. Billoud¹¹⁰,

M. Bindi⁵³, A. Bingul^{12d}, C. Bini^{73a,73b}, S. Biondi^{23b,23a}, C.J. Birch-sykes¹⁰¹, M. Birman¹⁸⁰, T. Bisanz³⁶,
J.P. Biswal³, D. Biswas^{181,i}, A. Bitadze¹⁰¹, C. Bittrich⁴⁸, K. Bjørke¹³³, T. Blazek^{28a}, I. Bloch⁴⁶,
C. Blocker²⁶, A. Blue⁵⁷, U. Blumenschein⁹³, G.J. Bobbink¹²⁰, V.S. Bobrovnikov^{122b,122a}, S.S. Bocchetta⁹⁷,
D. Bogavac¹⁴, A.G. Bogdanchikov^{122b,122a}, C. Bohm^{45a}, V. Boisvert⁹⁴, P. Bokan⁵³, T. Bold^{84a},
A.E. Bolz^{61b}, M. Bomben¹³⁵, M. Bona⁹³, J.S. Bonilla¹³¹, M. Boonekamp¹⁴⁴, C.D. Booth⁹⁴,
H.M. Borecka-Bielska⁹¹, L.S. Borgna⁹⁵, A. Borisov¹²³, G. Borisso⁹⁰, J. Bortfeldt³⁶, D. Bortoletto¹³⁴,
D. Boscherini^{23b}, M. Bosman¹⁴, J.D. Bossio Sola¹⁰⁴, K. Bouaouda^{35a}, J. Boudreau¹³⁸,
E.V. Bouhova-Thacker⁹⁰, D. Boumediene³⁸, S.K. Boutle⁵⁷, A. Boveia¹²⁷, J. Boyd³⁶, D. Boye^{33c},
I.R. Boyko⁸⁰, A.J. Bozson⁹⁴, J. Bracinik²¹, N. Brahimi^{60d,60c}, G. Brandt¹⁸², O. Brandt³², F. Braren⁴⁶,
B. Brau¹⁰³, J.E. Brau¹³¹, W.D. Breaden Madden⁵⁷, K. Brendlinger⁴⁶, L. Brenner³⁶, R. Brenner¹⁷²,
S. Bressler¹⁸⁰, B. Brickwedde¹⁰⁰, D.L. Briglin²¹, D. Britton⁵⁷, D. Britzger¹¹⁵, I. Brock²⁴, R. Brock¹⁰⁷,
G. Brooijmans³⁹, W.K. Brooks^{146d}, E. Brost²⁹, P.A. Bruckman de Renstrom⁸⁵, B. Brüers⁴⁶, D. Bruncko^{28b},
A. Bruni^{23b}, G. Bruni^{23b}, L.S. Bruni¹²⁰, S. Bruno^{74a,74b}, M. Bruschi^{23b}, N. Brusino^{73a,73b},
L. Bryngemark¹⁵³, T. Buanes¹⁷, Q. Buat³⁶, P. Buchholz¹⁵¹, A.G. Buckley⁵⁷, I.A. Budagov⁸⁰,
M.K. Bugge¹³³, F. Bühner⁵², O. Bulekov¹¹², B.A. Bullard⁵⁹, T.J. Burch¹²¹, S. Burdin⁹¹, C.D. Burgard¹²⁰,
A.M. Burger¹²⁹, B. Burghgrave⁸, J.T.P. Burr⁴⁶, C.D. Burton¹¹, J.C. Burzynski¹⁰³, V. Büscher¹⁰⁰,
E. Buschmann⁵³, P.J. Bussey⁵⁷, J.M. Butler²⁵, C.M. Buttar⁵⁷, J.M. Butterworth⁹⁵, P. Butti³⁶,
W. Buttinger³⁶, C.J. Buxo Vazquez¹⁰⁷, A. Buzatu¹⁵⁸, A.R. Buzykaev^{122b,122a}, G. Cabras^{23b,23a},
S. Cabrera Urbán¹⁷⁴, D. Caforio⁵⁶, H. Cai¹³⁸, V.M.M. Cairo¹⁵³, O. Cakir^{4a}, N. Calace³⁶, P. Calafiura¹⁸,
G. Calderini¹³⁵, P. Calfayan⁶⁶, G. Callea⁵⁷, L.P. Caloba^{81b}, A. Caltabiano^{74a,74b}, S. Calvente Lopez⁹⁹,
D. Calvet³⁸, S. Calvet³⁸, T.P. Calvet¹⁰², M. Calvetti^{72a,72b}, R. Camacho Toro¹³⁵, S. Camarda³⁶,
D. Camarero Munoz⁹⁹, P. Camarri^{74a,74b}, M.T. Camerlingo^{75a,75b}, D. Cameron¹³³, C. Camincher³⁶,
S. Campana³⁶, M. Campanelli⁹⁵, A. Camplani⁴⁰, V. Canale^{70a,70b}, A. Canesse¹⁰⁴, M. Cano Bret⁷⁸,
J. Cantero¹²⁹, T. Cao¹⁶¹, Y. Cao¹⁷³, M.D.M. Capeans Garrido³⁶, M. Capua^{41b,41a}, R. Cardarelli^{74a},
F. Cardillo¹⁴⁹, G. Carducci^{41b,41a}, I. Carli¹⁴², T. Carli³⁶, G. Carlino^{70a}, B.T. Carlson¹³⁸,
E.M. Carlson^{176,168a}, L. Carminati^{69a,69b}, R.M.D. Carney¹⁵³, S. Caron¹¹⁹, E. Carquin^{146d}, S. Carrá⁴⁶,
G. Carratta^{23b,23a}, J.W.S. Carter¹⁶⁷, T.M. Carter⁵⁰, M.P. Casado^{14,f}, A.F. Casha¹⁶⁷, F.L. Castillo¹⁷⁴,
L. Castillo Garcia¹⁴, V. Castillo Gimenez¹⁷⁴, N.F. Castro^{139a,139e}, A. Catinaccio³⁶, J.R. Catmore¹³³,
A. Cattai³⁶, V. Cavaliere²⁹, V. Cavasinni^{72a,72b}, E. Celebi^{12b}, F. Celli¹³⁴, K. Cerny¹³⁰, A.S. Cerqueira^{81a},
A. Cerri¹⁵⁶, L. Cerrito^{74a,74b}, F. Cerutti¹⁸, A. Cervelli^{23b,23a}, S.A. Cetin^{12b}, Z. Chadi^{35a}, D. Chakraborty¹²¹,
J. Chan¹⁸¹, W.S. Chan¹²⁰, W.Y. Chan⁹¹, J.D. Chapman³², B. Chargeishvili^{159b}, D.G. Charlton²¹,
T.P. Charman⁹³, C.C. Chau³⁴, S. Che¹²⁷, S. Chekanov⁶, S.V. Chekulaev^{168a}, G.A. Chelkov^{80,ah}, B. Chen⁷⁹,
C. Chen^{60a}, C.H. Chen⁷⁹, H. Chen²⁹, J. Chen^{60a}, J. Chen³⁹, J. Chen²⁶, S. Chen¹³⁶, S.J. Chen^{15c},
X. Chen^{15b}, Y. Chen^{60a}, Y-H. Chen⁴⁶, H.C. Cheng^{63a}, H.J. Cheng^{15a}, A. Cheplakov⁸⁰,
E. Cheremushkina¹²³, R. Cherkaoui El Moursli^{35f}, E. Cheu⁷, K. Cheung⁶⁴, T.J.A. Chevalérias¹⁴⁴,
L. Chevalier¹⁴⁴, V. Chiarella⁵¹, G. Chiarelli^{72a}, G. Chiodini^{68a}, A.S. Chisholm²¹, A. Chitan^{27b}, I. Chiu¹⁶³,
Y.H. Chiu¹⁷⁶, M.V. Chizhov⁸⁰, K. Choi¹¹, A.R. Chomont^{73a,73b}, Y.S. Chow¹²⁰, L.D. Christopher^{33e},
M.C. Chu^{63a}, X. Chu^{15a,15d}, J. Chudoba¹⁴⁰, J.J. Chwastowski⁸⁵, L. Chytka¹³⁰, D. Cieri¹¹⁵, K.M. Ciesla⁸⁵,
D. Cinca⁴⁷, V. Cindro⁹², I.A. Cioară^{27b}, A. Ciocio¹⁸, F. Ciotto^{70a,70b}, Z.H. Citron^{180,j}, M. Citterio^{69a},
D.A. Ciubotaru^{27b}, B.M. Ciungu¹⁶⁷, A. Clark⁵⁴, M.R. Clark³⁹, P.J. Clark⁵⁰, S.E. Clawson¹⁰¹,
C. Clement^{45a,45b}, Y. Coadou¹⁰², M. Cobal^{167a,67c}, A. Coccaro^{55b}, J. Cochran⁷⁹, R. Coelho Lopes De Sa¹⁰³,
H. Cohen¹⁶¹, A.E.C. Coimbra³⁶, B. Cole³⁹, A.P. Colijn¹²⁰, J. Collot⁵⁸, P. Conde Muiño^{139a,139h},
S.H. Connell^{33c}, I.A. Connelly⁵⁷, S. Constantinescu^{27b}, F. Conventi^{70a,an}, A.M. Cooper-Sarkar¹³⁴,
F. Cormier¹⁷⁵, K.J.R. Cormier¹⁶⁷, L.D. Corpe⁹⁵, M. Corradi^{73a,73b}, E.E. Corrigan⁹⁷, F. Corriveau^{104,ab},
M.J. Costa¹⁷⁴, F. Costanza⁵, D. Costanzo¹⁴⁹, G. Cowan⁹⁴, J.W. Cowley³², J. Crane¹⁰¹, K. Cranmer¹²⁵,
R.A. Creager¹³⁶, S. Crépe-Renaudin⁵⁸, F. Crescioli¹³⁵, M. Cristinziani²⁴, V. Croft¹⁷⁰, G. Crosetti^{41b,41a},
A. Cueto⁵, T. Cuhadar Donszelmann¹⁷¹, H. Cui^{15a,15d}, A.R. Cukierman¹⁵³, W.R. Cunningham⁵⁷,

S. Czekerda⁸⁵, P. Czodrowski³⁶, M.M. Czurylo^{61b}, M.J. Da Cunha Sargedas De Sousa^{60b},
 J.V. Da Fonseca Pinto^{81b}, C. Da Via¹⁰¹, W. Dabrowski^{84a}, F. Dachs³⁶, T. Dado⁴⁷, S. Dahbi^{33e}, T. Dai¹⁰⁶,
 C. Dallapiccola¹⁰³, M. Dam⁴⁰, G. D'amen²⁹, V. D'Amico^{75a,75b}, J. Damp¹⁰⁰, J.R. Dandoy¹³⁶,
 M.F. Daneri³⁰, M. Danninger¹⁵², V. Dao³⁶, G. Darbo^{55b}, O. Dartsis⁵, A. Dattagupta¹³¹, T. Daubney⁴⁶,
 S. D'Auria^{69a,69b}, C. David^{168b}, T. Davidek¹⁴², D.R. Davis⁴⁹, I. Dawson¹⁴⁹, K. De⁸, R. De Asmundis^{70a},
 M. De Beurs¹²⁰, S. De Castro^{23b,23a}, N. De Groot¹¹⁹, P. de Jong¹²⁰, H. De la Torre¹⁰⁷, A. De Maria^{15c},
 D. De Pedis^{73a}, A. De Salvo^{73a}, U. De Sanctis^{74a,74b}, M. De Santis^{74a,74b}, A. De Santo¹⁵⁶,
 J.B. De Vivie De Regie⁶⁵, C. Debenedetti¹⁴⁵, D.V. Dedovich⁸⁰, A.M. Deiana⁴², J. Del Peso⁹⁹,
 Y. Delabat Diaz⁴⁶, D. Delgove⁶⁵, F. Deliot¹⁴⁴, C.M. Delitzsch⁷, M. Della Pietra^{70a,70b}, D. Della Volpe⁵⁴,
 A. Dell'Acqua³⁶, L. Dell'Asta^{74a,74b}, M. Delmastro⁵, C. Delporte⁶⁵, P.A. Delsart⁵⁸, D.A. DeMarco¹⁶⁷,
 S. Demers¹⁸³, M. Demichev⁸⁰, G. Demontigny¹¹⁰, S.P. Denisov¹²³, L. D'Eramo¹²¹, D. Derendarz⁸⁵,
 J.E. Derkaoui^{35e}, F. Derue¹³⁵, P. Dervan⁹¹, K. Desch²⁴, K. Dette¹⁶⁷, C. Deutsch²⁴, M.R. Devesa³⁰,
 P.O. Deviveiros³⁶, F.A. Di Bello^{73a,73b}, A. Di Ciaccio^{74a,74b}, L. Di Ciaccio⁵, W.K. Di Clemente¹³⁶,
 C. Di Donato^{70a,70b}, A. Di Girolamo³⁶, G. Di Gregorio^{72a,72b}, B. Di Micco^{75a,75b}, R. Di Nardo^{75a,75b},
 K.F. Di Petrillo⁵⁹, R. Di Sipio¹⁶⁷, C. Diaconu¹⁰², F.A. Dias⁴⁰, T. Dias Do Vale^{139a}, M.A. Diaz^{146a},
 F.G. Diaz Capriles²⁴, J. Dickinson¹⁸, M. Didenko¹⁶⁶, E.B. Diehl¹⁰⁶, J. Dietrich¹⁹, S. Díez Cornell⁴⁶,
 C. Diez Pardos¹⁵¹, A. Dimitrievska¹⁸, W. Ding^{15b}, J. Dingfelder²⁴, S.J. Dittmeier^{61b}, F. Dittus³⁶,
 F. Djama¹⁰², T. Djobava^{159b}, J.I. Djuvsland¹⁷, M.A.B. Do Vale¹⁴⁷, M. Dobre^{27b}, D. Dodsworth²⁶,
 C. Doglioni⁹⁷, J. Dolejsi¹⁴², Z. Dolezal¹⁴², M. Donadelli^{81c}, B. Dong^{60c}, J. Donini³⁸, A. D'onofrio^{15c},
 M. D'Onofrio⁹¹, J. Dopke¹⁴³, A. Doria^{70a}, M.T. Dova⁸⁹, A.T. Doyle⁵⁷, E. Drechsler¹⁵², E. Dreyer¹⁵²,
 T. Dreyer⁵³, A.S. Drobac¹⁷⁰, D. Du^{60b}, T.A. du Pree¹²⁰, Y. Duan^{60d}, F. Dubinin¹¹¹, M. Dubovsky^{28a},
 A. Dubreuil⁵⁴, E. Duchovni¹⁸⁰, G. Duckeck¹¹⁴, O.A. Ducu^{36,27b}, D. Duda¹¹⁵, A. Dudarev³⁶,
 A.C. Dudder¹⁰⁰, E.M. Duffield¹⁸, M. D'uffizi¹⁰¹, L. Duflot⁶⁵, M. Dührssen³⁶, C. Dülsen¹⁸²,
 M. Dumancic¹⁸⁰, A.E. Dumitriu^{27b}, M. Dunford^{61a}, A. Duperrin¹⁰², H. Duran Yildiz^{4a}, M. Düren⁵⁶,
 A. Durglishvili^{159b}, D. Duschinger⁴⁸, B. Dutta⁴⁶, D. Duvnjak¹, G.I. Dyckes¹³⁶, M. Dyndal³⁶, S. Dysch¹⁰¹,
 B.S. Dziedzic⁸⁵, M.G. Eggleston⁴⁹, T. Eifert⁸, G. Eigen¹⁷, K. Einsweiler¹⁸, T. Ekelof¹⁷², H. El Jarrari^{35f},
 V. Ellajosyula¹⁷², M. Ellert¹⁷², F. Ellinghaus¹⁸², A.A. Elliot⁹³, N. Ellis³⁶, J. Elmsheuser²⁹, M. Elsing³⁶,
 D. Emel'yanov¹⁴³, A. Emerman³⁹, Y. Enari¹⁶³, M.B. Epland⁴⁹, J. Erdmann⁴⁷, A. Ereditato²⁰,
 P.A. Erland⁸⁵, M. Errenst³⁶, M. Escalier⁶⁵, C. Escobar¹⁷⁴, O. Estrada Pastor¹⁷⁴, E. Etzion¹⁶¹, H. Evans⁶⁶,
 M.O. Evans¹⁵⁶, A. Ezhilov¹³⁷, F. Fabbri⁵⁷, L. Fabbri^{23b,23a}, V. Fabiani¹¹⁹, G. Facini¹⁷⁸,
 R.M. Fakhruddinov¹²³, S. Falciano^{73a}, P.J. Falke²⁴, S. Falke³⁶, J. Faltova¹⁴², Y. Fang^{15a}, Y. Fang^{15a},
 G. Fanourakis⁴⁴, M. Fanti^{69a,69b}, M. Faraj^{67a,67c,q}, A. Farbin⁸, A. Farilla^{75a}, E.M. Farina^{71a,71b},
 T. Farooque¹⁰⁷, S.M. Farrington⁵⁰, P. Farthouat³⁶, F. Fassi^{35f}, P. Fassnacht³⁶, D. Fassouliotis⁹,
 M. Fauci Giannelli⁵⁰, W.J. Fawcett³², L. Fayard⁶⁵, O.L. Fedin^{137,o}, W. Fedorko¹⁷⁵, A. Fehr²⁰,
 M. Feickert¹⁷³, L. Feligioni¹⁰², A. Fell¹⁴⁹, C. Feng^{60b}, M. Feng⁴⁹, M.J. Fenton¹⁷¹, A.B. Fenyuk¹²³,
 S.W. Ferguson⁴³, J. Ferrando⁴⁶, A. Ferrante¹⁷³, A. Ferrari¹⁷², P. Ferrari¹²⁰, R. Ferrari^{71a},
 D.E. Ferreira de Lima^{61b}, A. Ferrer¹⁷⁴, D. Ferrere⁵⁴, C. Ferretti¹⁰⁶, F. Fiedler¹⁰⁰, A. Filipčić⁹²,
 F. Filthaut¹¹⁹, K.D. Finelli²⁵, M.C.N. Fiolhais^{139a,139c,a}, L. Fiorini¹⁷⁴, F. Fischer¹¹⁴, J. Fischer¹⁰⁰,
 W.C. Fisher¹⁰⁷, T. Fitschen²¹, I. Fleck¹⁵¹, P. Fleischmann¹⁰⁶, T. Flick¹⁸², B.M. Flierl¹¹⁴, L. Flores¹³⁶,
 L.R. Flores Castillo^{63a}, F.M. Follega^{76a,76b}, N. Fomin¹⁷, J.H. Foo¹⁶⁷, G.T. Forcolin^{76a,76b}, B.C. Forland⁶⁶,
 A. Formica¹⁴⁴, F.A. Förster¹⁴, A.C. Forti¹⁰¹, E. Fortin¹⁰², M.G. Foti¹³⁴, D. Fournier⁶⁵, H. Fox⁹⁰,
 P. Francavilla^{72a,72b}, S. Francescato^{73a,73b}, M. Franchini^{23b,23a}, S. Franchino^{61a}, D. Francis³⁶, L. Franco⁵,
 L. Franconi²⁰, M. Franklin⁵⁹, G. Frattari^{73a,73b}, A.N. Fray⁹³, P.M. Freeman²¹, B. Freund¹¹⁰,
 W.S. Freund^{181b}, E.M. Freundlich⁴⁷, D.C. Frizzell¹²⁸, D. Froidevaux³⁶, J.A. Frost¹³⁴, M. Fujimoto¹²⁶,
 C. Fukunaga¹⁶⁴, E. Fullana Torregrosa¹⁷⁴, T. Fusayasu¹¹⁶, J. Fuster¹⁷⁴, A. Gabrielli^{23b,23a}, A. Gabrielli³⁶,
 S. Gadatsch⁵⁴, P. Gadow¹¹⁵, G. Gagliardi^{55b,55a}, L.G. Gagnon¹¹⁰, G.E. Gallardo¹³⁴, E.J. Gallas¹³⁴,
 B.J. Gallop¹⁴³, G. Galster⁴⁰, R. Gamboa Goni⁹³, K.K. Gan¹²⁷, S. Ganguly¹⁸⁰, J. Gao^{60a}, Y. Gao⁵⁰,

Y.S. Gao^{31,l}, F.M. Garay Walls^{146a}, C. García¹⁷⁴, J.E. García Navarro¹⁷⁴, J.A. García Pascual^{15a},
 C. Garcia-Argos⁵², M. Garcia-Sciveres¹⁸, R.W. Gardner³⁷, N. Garelli¹⁵³, S. Gargiulo⁵², C.A. Garner¹⁶⁷,
 V. Garonne¹³³, S.J. Gasiorowski¹⁴⁸, P. Gaspar^{81b}, A. Gaudiello^{55b,55a}, G. Gaudio^{71a}, I.L. Gavrilenko¹¹¹,
 A. Gavriluk¹²⁴, C. Gay¹⁷⁵, G. Gaycken⁴⁶, E.N. Gazis¹⁰, A.A. Geanta^{27b}, C.M. Gee¹⁴⁵, C.N.P. Gee¹⁴³,
 J. Geisen⁹⁷, M. Geisen¹⁰⁰, C. Gemme^{55b}, M.H. Genest⁵⁸, C. Geng¹⁰⁶, S. Gentile^{73a,73b}, S. George⁹⁴,
 T. Geralis⁴⁴, L.O. Gerlach⁵³, P. Gessinger-Befurt¹⁰⁰, G. Gessner⁴⁷, S. Ghasemi¹⁵¹,
 M. Ghasemi Bostanabad¹⁷⁶, M. Ghneimat¹⁵¹, A. Ghosh⁶⁵, A. Ghosh⁷⁸, B. Giacobbe^{23b}, S. Giagu^{73a,73b},
 N. Giangiacomi^{23b,23a}, P. Giannetti^{72a}, A. Giannini^{70a,70b}, G. Giannini¹⁴, S.M. Gibson⁹⁴, M. Gignac¹⁴⁵,
 D.T. Gil^{84b}, B.J. Gilbert³⁹, D. Gillberg³⁴, G. Gilles¹⁸², D.M. Gingrich^{3,am}, M.P. Giordani^{67a,67c},
 P.F. Giraud¹⁴⁴, G. Giugliarelli^{67a,67c}, D. Giugni^{69a}, F. Giuli^{74a,74b}, S. Gkaitatzis¹⁶², I. Gkialas^{9,g},
 E.L. Gkoukousis¹⁴, P. Gkoutoumis¹⁰, L.K. Gladilin¹¹³, C. Glasman⁹⁹, J. Glatzer¹⁴, P.C.F. Glaysher⁴⁶,
 A. Glazov⁴⁶, G.R. Gledhill¹³¹, I. Gnesi^{41b,b}, M. Goblirsch-Kolb²⁶, D. Godin¹¹⁰, S. Goldfarb¹⁰⁵,
 T. Golling⁵⁴, D. Golubkov¹²³, A. Gomes^{139a,139b}, R. Goncalves Gama⁵³, R. Gonçalo^{139a,139c},
 G. Gonella¹³¹, L. Gonella²¹, A. Gongadze⁸⁰, F. Gonnella²¹, J.L. Gonski³⁹, S. González de la Hoz¹⁷⁴,
 S. Gonzalez Fernandez¹⁴, R. Gonzalez Lopez⁹¹, C. Gonzalez Renteria¹⁸, R. Gonzalez Suarez¹⁷²,
 S. Gonzalez-Sevilla⁵⁴, G.R. Gonzalvo Rodriguez¹⁷⁴, L. Goossens³⁶, N.A. Gorasia²¹, P.A. Gorbounov¹²⁴,
 H.A. Gordon²⁹, B. Gorini³⁶, E. Gorini^{68a,68b}, A. Gorišek⁹², A.T. Goshaw⁴⁹, M.I. Gostkin⁸⁰,
 C.A. Gottardo¹¹⁹, M. Gouighri^{35b}, A.G. Goussiou¹⁴⁸, N. Govender^{33c}, C. Goy⁵, I. Grabowska-Bold^{84a},
 E.C. Graham⁹¹, J. Gramling¹⁷¹, E. Gramstad¹³³, S. Grancagnolo¹⁹, M. Grandi¹⁵⁶, V. Gratchev¹³⁷,
 P.M. Gravila^{27f}, F.G. Gravili^{68a,68b}, C. Gray⁵⁷, H.M. Gray¹⁸, C. Grefe²⁴, K. Gregersen⁹⁷, I.M. Gregor⁴⁶,
 P. Grenier¹⁵³, K. Grevtsov⁴⁶, C. Grieco¹⁴, N.A. Grieser¹²⁸, A.A. Grillo¹⁴⁵, K. Grimm^{31,k}, S. Grinstein^{14,w},
 J.-F. Grivaz⁶⁵, S. Groh¹⁰⁰, E. Gross¹⁸⁰, J. Grosse-Knetter⁵³, Z.J. Grout⁹⁵, C. Grud¹⁰⁶, A. Grummer¹¹⁸,
 J.C. Grundy¹³⁴, L. Guan¹⁰⁶, W. Guan¹⁸¹, C. Gubbels¹⁷⁵, J. Guenther³⁶, A. Guerguichon⁶⁵,
 J.G.R. Guerrero Rojas¹⁷⁴, F. Guescini¹¹⁵, D. Guest¹⁷¹, R. Gugel¹⁰⁰, T. Guillemin⁵, S. Guindon³⁶, U. Gul⁵⁷,
 J. Guo^{60c}, W. Guo¹⁰⁶, Y. Guo^{60a}, Z. Guo¹⁰², R. Gupta⁴⁶, S. Gurbuz^{12c}, G. Gustavino¹²⁸, M. Guth⁵²,
 P. Gutierrez¹²⁸, C. Gutschow⁹⁵, C. Guyot¹⁴⁴, C. Gwenlan¹³⁴, C.B. Gwilliam⁹¹, E.S. Haaland¹³³,
 A. Haas¹²⁵, C. Haber¹⁸, H.K. Hadavand⁸, A. Hader^{60a}, M. Haleem¹⁷⁷, J. Haley¹²⁹, J.J. Hall¹⁴⁹,
 G. Halladjian¹⁰⁷, G.D. Hallewell¹⁰², K. Hamano¹⁷⁶, H. Hamdaoui^{35f}, M. Hamer²⁴, G.N. Hamity⁵⁰,
 K. Han^{60a,v}, L. Han^{60a}, S. Han¹⁸, Y.F. Han¹⁶⁷, K. Hanagaki^{82,t}, M. Hance¹⁴⁵, D.M. Handl¹¹⁴,
 M.D. Hank³⁷, R. Hankache¹³⁵, E. Hansen⁹⁷, J.B. Hansen⁴⁰, J.D. Hansen⁴⁰, M.C. Hansen²⁴, P.H. Hansen⁴⁰,
 E.C. Hanson¹⁰¹, K. Hara¹⁶⁹, T. Harenberg¹⁸², S. Harkusha¹⁰⁸, P.F. Harrison¹⁷⁸, N.M. Hartman¹⁵³,
 N.M. Hartmann¹¹⁴, Y. Hasegawa¹⁵⁰, A. Hasib⁵⁰, S. Hassani¹⁴⁴, S. Haug²⁰, R. Hauser¹⁰⁷, L.B. Havener³⁹,
 M. Havranek¹⁴¹, C.M. Hawkes²¹, R.J. Hawkings³⁶, S. Hayashida¹¹⁷, D. Hayden¹⁰⁷, C. Hayes¹⁰⁶,
 R.L. Hayes¹⁷⁵, C.P. Hays¹³⁴, J.M. Hays⁹³, H.S. Hayward⁹¹, S.J. Haywood¹⁴³, F. He^{60a}, Y. He¹⁶⁵,
 M.P. Heath⁵⁰, V. Hedberg⁹⁷, S. Heer²⁴, A.L. Heggelund¹³³, C. Heidegger⁵², K.K. Heidegger⁵²,
 W.D. Heidorn⁷⁹, J. Heilman³⁴, S. Heim⁴⁶, T. Heim¹⁸, B. Heinemann^{46,ak}, J.G. Heinlein¹³⁶, J.J. Heinrich¹³¹,
 L. Heinrich³⁶, J. Hejbal¹⁴⁰, L. Helary⁴⁶, A. Held¹²⁵, S. Hellesund¹³³, C.M. Helling¹⁴⁵, S. Hellman^{45a,45b},
 C. Hensens³⁶, R.C.W. Henderson⁹⁰, Y. Heng¹⁸¹, L. Henkelmann³², A.M. Henriques Correia³⁶, H. Herde²⁶,
 Y. Hernández Jiménez^{33e}, H. Herr¹⁰⁰, M.G. Herrmann¹¹⁴, T. Herrmann⁴⁸, G. Herten⁵², R. Hertenberger¹¹⁴,
 L. Hervas³⁶, T.C. Herwig¹³⁶, G.G. Hesketh⁹⁵, N.P. Hessey^{168a}, H. Hibi⁸³, A. Higashida¹⁶³, S. Higashino⁸²,
 E. Higón-Rodríguez¹⁷⁴, K. Hildebrand³⁷, J.C. Hill³², K.K. Hill²⁹, K.H. Hiller⁴⁶, S.J. Hillier²¹, M. Hils⁴⁸,
 I. Hinchliffe¹⁸, F. Hinterkeuser²⁴, M. Hirose¹³², S. Hirose⁵², D. Hirschbuehl¹⁸², B. Hiti⁹², O. Hladik¹⁴⁰,
 D.R. Hlaluku^{33e}, J. Hobbs¹⁵⁵, N. Hod¹⁸⁰, M.C. Hodgkinson¹⁴⁹, A. Hoecker³⁶, D. Hohn⁵², D. Hohov⁶⁵,
 T. Holm²⁴, T.R. Holmes³⁷, M. Holzbock¹¹⁴, L.B.A.H. Hommels³², T.M. Hong¹³⁸, J.C. Honig⁵²,
 A. Hönle¹¹⁵, B.H. Hooberman¹⁷³, W.H. Hopkins⁶, Y. Horii¹¹⁷, P. Horn⁴⁸, L.A. Horyn³⁷, S. Hou¹⁵⁸,
 A. Hoummada^{35a}, J. Howarth⁵⁷, J. Hoya⁸⁹, M. Hrabovsky¹³⁰, J. Hrdinka⁷⁷, J. Hrivnac⁶⁵, A. Hrynevich¹⁰⁹,
 T. Hryn'ova⁵, P.J. Hsu⁶⁴, S.-C. Hsu¹⁴⁸, Q. Hu²⁹, S. Hu^{60c}, Y.F. Hu^{15a,15d,ao}, D.P. Huang⁹⁵, Y. Huang^{60a},

Y. Huang^{15a}, Z. Hubacek¹⁴¹, F. Hubaut¹⁰², M. Huebner²⁴, F. Huegging²⁴, T.B. Huffman¹³⁴, M. Huhtinen³⁶,
 R. Hulskens⁵⁸, R.F.H. Hunter³⁴, P. Huo¹⁵⁵, N. Huseynov^{80,ac}, J. Huston¹⁰⁷, J. Huth⁵⁹, R. Hyneman¹⁰⁶,
 S. Hyrych^{28a}, G. Iacobucci⁵⁴, G. Iakovidis²⁹, I. Ibragimov¹⁵¹, L. Iconomidou-Fayard⁶⁵, P. Iengo³⁶,
 R. Ignazzi⁴⁰, O. Igonkina^{120,y,*}, R. Iguchi¹⁶³, T. Iizawa⁵⁴, Y. Ikegami⁸², M. Ikeno⁸², D. Iliadis¹⁶²,
 N. Ilic^{119,167,ab}, F. Iltzsche⁴⁸, H. Imam^{35a}, G. Introzzi^{71a,71b}, M. Iodice^{75a}, K. Iordanidou^{168a},
 V. Ippolito^{73a,73b}, M.F. Isacson¹⁷², M. Ishino¹⁶³, W. Islam¹²⁹, C. Issever^{19,46}, S. Istin¹⁶⁰, F. Ito¹⁶⁹,
 J.M. Iturbe Ponce^{63a}, R. Iuppa^{76a,76b}, A. Ivina¹⁸⁰, H. Iwasaki⁸², J.M. Izen⁴³, V. Izzo^{70a}, P. Jacka¹⁴⁰,
 P. Jackson¹, R.M. Jacobs⁴⁶, B.P. Jaeger¹⁵², V. Jain², G. Jäkel¹⁸², K.B. Jakobi¹⁰⁰, K. Jakobs⁵²,
 T. Jakoubek¹⁸⁰, J. Jamieson⁵⁷, K.W. Janas^{84a}, R. Jansky⁵⁴, M. Janus⁵³, P.A. Janus^{84a}, G. Jarlskog⁹⁷,
 A.E. Jaspan⁹¹, N. Javadov^{80,ac}, T. Javůrek³⁶, M. Javurkova¹⁰³, F. Jeanneau¹⁴⁴, L. Jeanty¹³¹, J. Jejelava^{159a},
 P. Jenni^{52,c}, N. Jeong⁴⁶, S. Jézéquel⁵, H. Ji¹⁸¹, J. Jia¹⁵⁵, H. Jiang⁷⁹, Y. Jiang^{60a}, Z. Jiang¹⁵³, S. Jiggins⁵²,
 F.A. Jimenez Morales³⁸, J. Jimenez Pena¹¹⁵, S. Jin^{15c}, A. Jinaru^{27b}, O. Jinnouchi¹⁶⁵, H. Jivan^{33e},
 P. Johansson¹⁴⁹, K.A. Johns⁷, C.A. Johnson⁶⁶, R.W.L. Jones⁹⁰, S.D. Jones¹⁵⁶, T.J. Jones⁹¹,
 J. Jongmanns^{61a}, J. Jovicevic³⁶, X. Ju¹⁸, J.J. Junggeburth¹¹⁵, A. Juste Rozas^{14,w}, A. Kaczmarzka⁸⁵,
 M. Kado^{73a,73b}, H. Kagan¹²⁷, M. Kagan¹⁵³, A. Kahn³⁹, C. Kahra¹⁰⁰, T. Kaji¹⁷⁹, E. Kajomovitz¹⁶⁰,
 C.W. Kalderon²⁹, A. Kaluza¹⁰⁰, A. Kamenshchikov¹²³, M. Kaneda¹⁶³, N.J. Kang¹⁴⁵, S. Kang⁷⁹,
 Y. Kano¹¹⁷, J. Kanzaki⁸², L.S. Kaplan¹⁸¹, D. Kar^{33e}, K. Karava¹³⁴, M.J. Kareem^{168b}, I. Karkanas¹⁶²,
 S.N. Karpov⁸⁰, Z.M. Karpova⁸⁰, V. Kartvelishvili⁹⁰, A.N. Karyukhin¹²³, E. Kasimi¹⁶², A. Kastanas^{45a,45b},
 C. Kato^{60d,60c}, J. Katzy⁴⁶, K. Kawade¹⁵⁰, K. Kawagoe⁸⁸, T. Kawaguchi¹¹⁷, T. Kawamoto¹⁴⁴,
 G. Kawamura⁵³, E.F. Kay¹⁷⁶, S. Kazakos¹⁴, V.F. Kazanin^{122b,122a}, R. Keeler¹⁷⁶, R. Kehoe⁴², J.S. Keller³⁴,
 E. Kellermann⁹⁷, D. Kelsey¹⁵⁶, J.J. Kempster²¹, J. Kendrick²¹, K.E. Kennedy³⁹, O. Kepka¹⁴⁰,
 S. Kersten¹⁸², B.P. Kerševan⁹², S. Ketabchi Haghighat¹⁶⁷, M. Khader¹⁷³, F. Khalil-Zada¹³,
 M. Khandoga¹⁴⁴, A. Khanov¹²⁹, A.G. Kharlamov^{122b,122a}, T. Kharlamova^{122b,122a}, E.E. Khoda¹⁷⁵,
 A. Khodinov¹⁶⁶, T.J. Khoo⁵⁴, G. Khorauli¹⁷⁷, E. Khramov⁸⁰, J. Khubua^{159b}, S. Kido⁸³, M. Kiehn⁵⁴,
 C.R. Kilby⁹⁴, E. Kim¹⁶⁵, Y.K. Kim³⁷, N. Kimura⁹⁵, A. Kirchhoff⁵³, D. Kirchmeier⁴⁸, J. Kirk¹⁴³,
 A.E. Kiryunin¹¹⁵, T. Kishimoto¹⁶³, D.P. Kisliuk¹⁶⁷, V. Kitali⁴⁶, C. Kitsaki¹⁰, O. Kivernyk²⁴,
 T. Klapdor-Kleingrothaus⁵², M. Klassen^{61a}, C. Klein³⁴, M.H. Klein¹⁰⁶, M. Klein⁹¹, U. Klein⁹¹,
 K. Kleinknecht¹⁰⁰, P. Klimek¹²¹, A. Klimentov²⁹, T. Klingl²⁴, T. Klioutchnikova³⁶, F.F. Klitzner¹¹⁴,
 P. Kluit¹²⁰, S. Kluth¹¹⁵, E. Kneringer⁷⁷, E.B.F.G. Knoops¹⁰², A. Knue⁵², D. Kobayashi⁸⁸, M. Kobel⁴⁸,
 M. Kocian¹⁵³, T. Kodama¹⁶³, P. Kodys¹⁴², D.M. Koeck¹⁵⁶, P.T. Koenig²⁴, T. Koffas³⁴, N.M. Köhler³⁶,
 M. Kolb¹⁴⁴, I. Koletsou⁵, T. Komarek¹³⁰, T. Kondo⁸², K. Köneke⁵², A.X.Y. Kong¹, A.C. König¹¹⁹,
 T. Kono¹²⁶, V. Konstantinides⁹⁵, N. Konstantinidis⁹⁵, B. Konya⁹⁷, R. Kopeliansky⁶⁶, S. Koperny^{84a},
 K. Korcyl⁸⁵, K. Kordas¹⁶², G. Koren¹⁶¹, A. Korn⁹⁵, I. Korolkov¹⁴, E.V. Korolkova¹⁴⁹, N. Korotkova¹¹³,
 O. Kortner¹¹⁵, S. Kortner¹¹⁵, V.V. Kostyukhin^{149,166}, A. Kotskechagia⁶⁵, A. Kotwal⁴⁹, A. Koulouris¹⁰,
 A. Kourkoumeli-Charalampidi^{71a,71b}, C. Kourkoumelis⁹, E. Kourlitis⁶, V. Kouskoura²⁹, R. Kowalewski¹⁷⁶,
 W. Kozanecki¹⁰¹, A.S. Kozhin¹²³, V.A. Kramarenko¹¹³, G. Kramberger⁹², D. Krasnopevtsev^{60a},
 M.W. Krasny¹³⁵, A. Krasznahorkay³⁶, D. Krauss¹¹⁵, J.A. Kremer¹⁰⁰, J. Kretzschmar⁹¹, P. Krieger¹⁶⁷,
 F. Krieter¹¹⁴, A. Krishnan^{61b}, M. Krivos¹⁴², K. Krizka¹⁸, K. Kroeninger⁴⁷, H. Kroha¹¹⁵, J. Kroll¹⁴⁰,
 J. Kroll¹³⁶, K.S. Krowpman¹⁰⁷, U. Kruchonak⁸⁰, H. Krüger²⁴, N. Krumnack⁷⁹, M.C. Kruse⁴⁹,
 J.A. Krzysiak⁸⁵, O. Kuchinskaia¹⁶⁶, S. Kuday^{4b}, D. Kuechler⁴⁶, J.T. Kuechler⁴⁶, S. Kuehn³⁶, T. Kuhl⁴⁶,
 V. Kukhtin⁸⁰, Y. Kulchitsky^{108,af}, S. Kuleshov^{146b}, Y.P. Kulinich¹⁷³, M. Kuna⁵⁸, T. Kunigo⁸⁶, A. Kupco¹⁴⁰,
 T. Kupfer⁴⁷, O. Kuprash⁵², H. Kurashige⁸³, L.L. Kurchaninov^{168a}, Y.A. Kurochkin¹⁰⁸, A. Kurova¹¹²,
 M.G. Kurth^{15a,15d}, E.S. Kuwertz³⁶, M. Kuze¹⁶⁵, A.K. Kvam¹⁴⁸, J. Kvita¹³⁰, T. Kwan¹⁰⁴, F. La Ruffa^{41b,41a},
 C. Lacasta¹⁷⁴, F. Lacava^{73a,73b}, D.P.J. Lack¹⁰¹, H. Lacker¹⁹, D. Lacour¹³⁵, E. Ladygin⁸⁰, R. Lafaye⁵,
 B. Laforge¹³⁵, T. Lagouri^{146b}, S. Lai⁵³, I.K. Lakomic^{84a}, J.E. Lambert¹²⁸, S. Lammers⁶⁶, W. Lampl⁷,
 C. Lampoudis¹⁶², E. Lançon²⁹, U. Landgraf⁵², M.P.J. Landon⁹³, M.C. Lanfermann⁵⁴, V.S. Lang⁵²,
 J.C. Lange⁵³, R.J. Langenberg¹⁰³, A.J. Lankford¹⁷¹, F. Lanni²⁹, K. Lantzsich²⁴, A. Lanza^{71a},

A. Lapertosa^{55b,55a}, S. Laplace¹³⁵, J.F. Laporte¹⁴⁴, T. Lari^{69a}, F. Lasagni Manghi^{23b,23a}, M. Lassnig³⁶,
 T.S. Lau^{63a}, A. Laudrain⁶⁵, A. Laurier³⁴, M. Lavorgna^{70a,70b}, S.D. Lawlor⁹⁴, M. Lazzaroni^{69a,69b}, B. Le¹⁰¹,
 E. Le Guirriec¹⁰², A. Lebedev⁷⁹, M. LeBlanc⁷, T. LeCompte⁶, F. Ledroit-Guillon⁵⁸, A.C.A. Lee⁹⁵,
 C.A. Lee²⁹, G.R. Lee¹⁷, L. Lee⁵⁹, S.C. Lee¹⁵⁸, S. Lee⁷⁹, B. Lefebvre^{168a}, H.P. Lefebvre⁹⁴, M. Lefebvre¹⁷⁶,
 C. Leggett¹⁸, K. Lehmann¹⁵², N. Lehmann²⁰, G. Lehmann Miotto³⁶, W.A. Leight⁴⁶, A. Leisos^{162,u},
 M.A.L. Leite^{81c}, C.E. Leitgeb¹¹⁴, R. Leitner¹⁴², D. Lellouch^{180,*}, K.J.C. Leney⁴², T. Lenz²⁴, S. Leone^{72a},
 C. Leonidopoulos⁵⁰, A. Leopold¹³⁵, C. Leroy¹¹⁰, R. Les¹⁰⁷, C.G. Lester³², M. Levchenko¹³⁷, J. Levêque⁵,
 D. Levin¹⁰⁶, L.J. Levinson¹⁸⁰, D.J. Lewis²¹, B. Li^{15b}, B. Li¹⁰⁶, C-Q. Li^{60a}, F. Li^{60c}, H. Li^{60a}, H. Li^{60b},
 J. Li^{60c}, K. Li¹⁴⁸, L. Li^{60c}, M. Li^{15a,15d}, Q. Li^{15a,15d}, Q.Y. Li^{60a}, S. Li^{60d,60c}, X. Li⁴⁶, Y. Li⁴⁶, Z. Li^{60b},
 Z. Li¹³⁴, Z. Li¹⁰⁴, Z. Liang^{15a}, M. Liberatore⁴⁶, B. Liberti^{74a}, A. Liblong¹⁶⁷, K. Lie^{63c}, S. Lim²⁹,
 C.Y. Lin³², K. Lin¹⁰⁷, R.A. Linck⁶⁶, R.E. Lindley⁷, J.H. Lindon²¹, A. Linss⁴⁶, A.L. Lioni⁵⁴, E. Lipeles¹³⁶,
 A. Lipniacka¹⁷, T.M. Liss^{173,al}, A. Lister¹⁷⁵, J.D. Little⁸, B. Liu⁷⁹, B.X. Liu⁶, H.B. Liu²⁹, J.B. Liu^{60a},
 J.K.K. Liu³⁷, K. Liu^{60d,60c}, M. Liu^{60a}, P. Liu^{15a}, Y. Liu⁴⁶, Y. Liu^{15a,15d}, Y.L. Liu¹⁰⁶, Y.W. Liu^{60a},
 M. Livan^{71a,71b}, A. Lleres⁵⁸, J. Llorente Merino¹⁵², S.L. Lloyd⁹³, C.Y. Lo^{63b}, E.M. Lobodzinska⁴⁶,
 P. Loch⁷, S. Loffredo^{74a,74b}, T. Lohse¹⁹, K. Lohwasser¹⁴⁹, M. Lokajicek¹⁴⁰, J.D. Long¹⁷³, R.E. Long⁹⁰,
 I. Longarini^{73a,73b}, L. Longo³⁶, K.A. Looper¹²⁷, I. Lopez Paz¹⁰¹, A. Lopez Solis¹⁴⁹, J. Lorenz¹¹⁴,
 N. Lorenzo Martinez⁵, A.M. Lory¹¹⁴, P.J. Lösel¹¹⁴, A. Lösle⁵², X. Lou⁴⁶, X. Lou^{15a}, A. Lounis⁶⁵, J. Love⁶,
 P.A. Love⁹⁰, J.J. Lozano Bahilo¹⁷⁴, M. Lu^{60a}, Y.J. Lu⁶⁴, H.J. Lubatti¹⁴⁸, C. Luci^{73a,73b}, F.L. Lucio Alves^{15c},
 A. Lucotte⁵⁸, F. Luehring⁶⁶, I. Luise¹³⁵, L. Luminari^{73a}, B. Lund-Jensen¹⁵⁴, M.S. Lutz¹⁶¹, D. Lynn²⁹,
 H. Lyons⁹¹, R. Lysak¹⁴⁰, E. Lytken⁹⁷, F. Lyu^{15a}, V. Lyubushkin⁸⁰, T. Lyubushkina⁸⁰, H. Ma²⁹, L.L. Ma^{60b},
 Y. Ma⁹⁵, D.M. Mac Donell¹⁷⁶, G. Maccarrone⁵¹, A. Macchiolo¹¹⁵, C.M. Macdonald¹⁴⁹,
 J.C. MacDonald¹⁴⁹, J. Machado Miguens¹³⁶, D. Madaffari¹⁷⁴, R. Madar³⁸, W.F. Mader⁴⁸,
 M. Madugoda Ralalage Don¹²⁹, N. Madysa⁴⁸, J. Maeda⁸³, T. Maeno²⁹, M. Maerker⁴⁸, V. Magerl⁵²,
 N. Magini⁷⁹, J. Magro^{67a,67c,q}, D.J. Mahon³⁹, C. Maidantchik^{81b}, T. Maier¹¹⁴, A. Maio^{139a,139b,139d},
 K. Maj^{84a}, O. Majersky^{28a}, S. Majewski¹³¹, Y. Makida⁸², N. Makovec⁶⁵, B. Malaescu¹³⁵, Pa. Malecki⁸⁵,
 V.P. Maleev¹³⁷, F. Malek⁵⁸, D. Malito^{41b,41a}, U. Mallik⁷⁸, D. Malon⁶, C. Malone³², S. Maltezos¹⁰,
 S. Malyukov⁸⁰, J. Mamuzic¹⁷⁴, G. Mancini^{70a,70b}, I. Mandić⁹², L. Manhaes de Andrade Filho^{81a},
 I.M. Maniatis¹⁶², J. Manjarres Ramos⁴⁸, K.H. Mankinen⁹⁷, A. Mann¹¹⁴, A. Manousos⁷⁷, B. Mansoulie¹⁴⁴,
 I. Manthos¹⁶², S. Manzoni¹²⁰, A. Marantis¹⁶², G. Marceca³⁰, L. Marchese¹³⁴, G. Marchiori¹³⁵,
 M. Marcisovsky¹⁴⁰, L. Marcoccia^{74a,74b}, C. Marcon⁹⁷, C.A. Marin Tobon³⁶, M. Marjanovic¹²⁸,
 Z. Marshall¹⁸, M.U.F. Martensson¹⁷², S. Marti-Garcia¹⁷⁴, C.B. Martin¹²⁷, T.A. Martin¹⁷⁸, V.J. Martin⁵⁰,
 B. Martin dit Latour¹⁷, L. Martinelli^{75a,75b}, M. Martinez^{14,w}, P. Martinez Agullo¹⁷⁴,
 V.I. Martinez Outschoorn¹⁰³, S. Martin-Haugh¹⁴³, V.S. Martoiu^{27b}, A.C. Martyniuk⁹⁵, A. Marzin³⁶,
 S.R. Maschek¹¹⁵, L. Masetti¹⁰⁰, T. Mashimo¹⁶³, R. Mashinistov¹¹¹, J. Masik¹⁰¹, A.L. Maslennikov^{122b,122a},
 L. Massa^{23b,23a}, P. Massarotti^{70a,70b}, P. Mastrandrea^{72a,72b}, A. Mastroberardino^{41b,41a}, T. Masubuchi¹⁶³,
 D. Matakias²⁹, A. Matic¹¹⁴, N. Matsuzawa¹⁶³, P. Mättig²⁴, J. Maurer^{27b}, B. Maček⁹²,
 D.A. Maximov^{122b,122a}, R. Mazini¹⁵⁸, I. Maznas¹⁶², S.M. Mazza¹⁴⁵, J.P. Mc Gowan¹⁰⁴, S.P. Mc Kee¹⁰⁶,
 T.G. McCarthy¹¹⁵, W.P. McCormack¹⁸, E.F. McDonald¹⁰⁵, J.A. Mcfayden³⁶, G. Mchedlidze^{159b},
 M.A. McKay⁴², K.D. McLean¹⁷⁶, S.J. McMahan¹⁴³, P.C. McNamara¹⁰⁵, C.J. McNicol¹⁷⁸,
 R.A. McPherson^{176,ab}, J.E. Mdhluli^{33e}, Z.A. Meadows¹⁰³, S. Meehan³⁶, T. Megy³⁸, S. Mehlhase¹¹⁴,
 A. Mehta⁹¹, B. Meirose⁴³, D. Melini¹⁶⁰, B.R. Mellado Garcia^{33e}, J.D. Mellenthin⁵³, M. Melo^{28a},
 F. Meloni⁴⁶, A. Melzer²⁴, E.D. Mendes Gouveia^{139a,139e}, L. Meng³⁶, X.T. Meng¹⁰⁶, S. Menke¹¹⁵,
 E. Meoni^{41b,41a}, S. Mergelmeyer¹⁹, S.A.M. Merkt¹³⁸, C. Merlassino¹³⁴, P. Mermod⁵⁴, L. Merola^{70a,70b},
 C. Meroni^{69a}, G. Merz¹⁰⁶, O. Meshkov^{113,111}, J.K.R. Meshreki¹⁵¹, J. Metcalfe⁶, A.S. Mete⁶, C. Meyer⁶⁶,
 J-P. Meyer¹⁴⁴, M. Michetti¹⁹, R.P. Middleton¹⁴³, L. Mijović⁵⁰, G. Mikenberg¹⁸⁰, M. Mikesikova¹⁴⁰,
 M. Mikuž⁹², H. Mildner¹⁴⁹, A. Milic¹⁶⁷, C.D. Milke⁴², D.W. Miller³⁷, A. Milov¹⁸⁰, D.A. Milstead^{45a,45b},
 R.A. Mina¹⁵³, A.A. Minaenko¹²³, I.A. Minashvili^{159b}, A.I. Mincer¹²⁵, B. Mindur^{84a}, M. Mineev⁸⁰,

Y. Minegishi¹⁶³, L.M. Mir¹⁴, M. Mironova¹³⁴, A. Mirto^{68a,68b}, K.P. Mistry¹³⁶, T. Mitani¹⁷⁹,
 J. Mitrevski¹¹⁴, V.A. Mitsou¹⁷⁴, M. Mittal^{60c}, O. Miu¹⁶⁷, A. Miucci²⁰, P.S. Miyagawa⁹³, A. Mizukami⁸²,
 J.U. Mjörnmark⁹⁷, T. Mkrtchyan^{61a}, M. Mlynarikova¹⁴², T. Moa^{45a,45b}, S. Mobius⁵³, K. Mochizuki¹¹⁰,
 P. Mogg¹¹⁴, S. Mohapatra³⁹, R. Moles-Valls²⁴, K. Mönig⁴⁶, E. Monnier¹⁰², A. Montalbano¹⁵²,
 J. Montejo Berlingen³⁶, M. Montella⁹⁵, F. Monticelli⁸⁹, S. Monzani^{69a}, N. Morange⁶⁵,
 A.L. Moreira De Carvalho^{139a}, D. Moreno^{22a}, M. Moreno Llácer¹⁷⁴, C. Moreno Martinez¹⁴,
 P. Morettini^{55b}, M. Morgenstern¹⁶⁰, S. Morgenstern⁴⁸, D. Mori¹⁵², M. Morii⁵⁹, M. Morinaga¹⁷⁹,
 V. Morisbak¹³³, A.K. Morley³⁶, G. Mornacchi³⁶, A.P. Morris⁹⁵, L. Morvaj¹⁵⁵, P. Moschovakos³⁶,
 B. Moser¹²⁰, M. Mosidze^{159b}, T. Moskalets¹⁴⁴, J. Moss^{31,m}, E.J.W. Moyse¹⁰³, S. Muanza¹⁰², J. Mueller¹³⁸,
 R.S.P. Mueller¹¹⁴, D. Muenstermann⁹⁰, G.A. Mullier⁹⁷, D.P. Mungo^{69a,69b}, J.L. Munoz Martinez¹⁴,
 F.J. Munoz Sanchez¹⁰¹, P. Murin^{28b}, W.J. Murray^{178,143}, A. Murrone^{69a,69b}, J.M. Muse¹²⁸, M. Muškinja¹⁸,
 C. Mwewa^{33a}, A.G. Myagkov^{123,ah}, A.A. Myers¹³⁸, J. Myers¹³¹, M. Myska¹⁴¹, B.P. Nachman¹⁸,
 O. Nackenhorst⁴⁷, A. Nag Nag⁴⁸, K. Nagai¹³⁴, K. Nagano⁸², Y. Nagasaka⁶², J.L. Nagle²⁹, E. Nagy¹⁰²,
 A.M. Nairz³⁶, Y. Nakahama¹¹⁷, K. Nakamura⁸², T. Nakamura¹⁶³, H. Nanjo¹³², F. Napolitano^{61a},
 R.F. Naranjo Garcia⁴⁶, R. Narayan⁴², I. Naryshkin¹³⁷, T. Naumann⁴⁶, G. Navarro^{22a}, P.Y. Nechaeva¹¹¹,
 F. Nechansky⁴⁶, T.J. Neep²¹, A. Negri^{71a,71b}, M. Negrini^{23b}, C. Nellist¹¹⁹, C. Nelson¹⁰⁴,
 M.E. Nelson^{45a,45b}, S. Nemecek¹⁴⁰, M. Nessi^{36,e}, M.S. Neubauer¹⁷³, F. Neuhaus¹⁰⁰, M. Neumann¹⁸²,
 R. Newhouse¹⁷⁵, P.R. Newman²¹, C.W. Ng¹³⁸, Y.S. Ng¹⁹, Y.W.Y. Ng¹⁷¹, B. Ngair^{35f}, H.D.N. Nguyen¹⁰²,
 T. Nguyen Manh¹¹⁰, E. Nibigira³⁸, R.B. Nickerson¹³⁴, R. Nicolaidou¹⁴⁴, D.S. Nielsen⁴⁰, J. Nielsen¹⁴⁵,
 M. Niemeyer⁵³, N. Nikipforou¹¹, V. Nikolaenko^{123,ah}, I. Nikolic-Audit¹³⁵, K. Nikolopoulos²¹, P. Nilsson²⁹,
 H.R. Nindhito⁵⁴, Y. Ninomiya⁸², A. Nisati^{73a}, N. Nishu^{60c}, R. Nisius¹¹⁵, I. Nitsche⁴⁷, T. Nitta¹⁷⁹,
 T. Nobe¹⁶³, D.L. Noel³², Y. Noguchi⁸⁶, I. Nomidis¹³⁵, M.A. Nomura²⁹, M. Nordberg³⁶, J. Novak⁹²,
 T. Novak⁹², O. Novgorodova⁴⁸, R. Novotny¹⁴¹, L. Nozka¹³⁰, K. Ntekas¹⁷¹, E. Nurse⁹⁵, F.G. Oakham^{34,am},
 H. Oberlack¹¹⁵, J. Ocariz¹³⁵, A. Ochi⁸³, I. Ochoa³⁹, J.P. Ochoa-Ricoux^{146a}, K. O'Connor²⁶, S. Oda⁸⁸,
 S. Odaka⁸², S. Oerdek⁵³, A. Ogrodnik^{84a}, A. Oh¹⁰¹, S.H. Oh⁴⁹, C.C. Ohm¹⁵⁴, H. Oide¹⁶⁵, M.L. Ojeda¹⁶⁷,
 H. Okawa¹⁶⁹, Y. Okazaki⁸⁶, M.W. O'Keefe⁹¹, Y. Okumura¹⁶³, T. Okuyama⁸², A. Olariu^{27b},
 L.F. Oleiro Seabra^{139a}, S.A. Olivares Pino^{146a}, D. Oliveira Damazio²⁹, J.L. Oliver¹, M.J.R. Olsson¹⁷¹,
 A. Olszewski⁸⁵, J. Olszowska⁸⁵, Ö.O. Öncel²⁴, D.C. O'Neil¹⁵², A.P. O'Neill¹³⁴, A. Onofre^{139a,139e},
 P.U.E. Onyisi¹¹, H. Oppen¹³³, R.G. Oreamuno Madriz¹²¹, M.J. Oreglia³⁷, G.E. Orellana⁸⁹,
 D. Orestano^{75a,75b}, N. Orlando¹⁴, R.S. Orr¹⁶⁷, V. O'Shea⁵⁷, R. Ospanov^{60a}, G. Otero y Garzon³⁰,
 H. Otono⁸⁸, P.S. Ott^{61a}, G.J. Ottino¹⁸, T. Ou³⁷, M. Ouchrif^{35e}, J. Ouellette²⁹, F. Ould-Saada¹³³,
 A. Ouraou^{144,*}, Q. Ouyang^{15a}, M. Owen⁵⁷, R.E. Owen¹⁴³, V.E. Ozcan^{12c}, N. Ozturk⁸, J. Pacalt¹³⁰,
 H.A. Pacey³², K. Pachal⁴⁹, A. Pacheco Pages¹⁴, C. Padilla Aranda¹⁴, S. Pagan Griso¹⁸, G. Palacino⁶⁶,
 S. Palazzo⁵⁰, S. Palestini³⁶, M. Palka^{84b}, P. Palmi^{84a}, C.E. Pandini⁵⁴, J.G. Panduro Vazquez⁹⁴, P. Pani⁴⁶,
 G. Panizzo^{67a,67c}, L. Paolozzi⁵⁴, C. Papadatos¹¹⁰, K. Papageorgiou^{9,g}, S. Parajuli⁴², A. Paramonov⁶,
 C. Paraskevopoulos¹⁰, D. Paredes Hernandez^{63b}, S.R. Paredes Saenz¹³⁴, B. Parida¹⁸⁰, T.H. Park¹⁶⁷,
 A.J. Parker³¹, M.A. Parker³², F. Parodi^{55b,55a}, E.W. Parrish¹²¹, J.A. Parsons³⁹, U. Parzefall⁵²,
 L. Pascual Dominguez¹³⁵, V.R. Pascuzzi¹⁸, J.M.P. Pasner¹⁴⁵, F. Pasquali¹²⁰, E. Pasqualucci^{73a},
 S. Passaggio^{55b}, F. Pastore⁹⁴, P. Pasuwan^{45a,45b}, S. Patariaia¹⁰⁰, J.R. Pater¹⁰¹, A. Pathak^{181,i}, J. Patton⁹¹,
 T. Pauly³⁶, J. Pearkes¹⁵³, B. Pearson¹¹⁵, M. Pedersen¹³³, L. Pedraza Diaz¹¹⁹, R. Pedro^{139a}, T. Peiffer⁵³,
 S.V. Peleganchuk^{122b,122a}, O. Penc¹⁴⁰, H. Peng^{60a}, B.S. Peralva^{81a}, M.M. Perego⁶⁵, A.P. Pereira Peixoto^{139a},
 L. Pereira Sanchez^{45a,45b}, D.V. Perepelitsa²⁹, E. Perez Codina^{168a}, F. Peri¹⁹, L. Perini^{69a,69b},
 H. Pernegger³⁶, S. Perrella³⁶, A. Perrevoort¹²⁰, K. Peters⁴⁶, R.F.Y. Peters¹⁰¹, B.A. Petersen³⁶,
 T.C. Petersen⁴⁰, E. Petit¹⁰², V. Petousis¹⁴¹, A. Petridis¹, C. Petridou¹⁶², F. Petrucci^{75a,75b}, M. Pettee¹⁸³,
 N.E. Pettersson¹⁰³, K. Petukhova¹⁴², A. Peyaud¹⁴⁴, R. Pezoa^{146d}, L. Pezzotti^{71a,71b}, T. Pham¹⁰⁵,
 F.H. Phillips¹⁰⁷, P.W. Phillips¹⁴³, M.W. Phipps¹⁷³, G. Piacquadio¹⁵⁵, E. Pianori¹⁸, A. Picazio¹⁰³,
 R.H. Pickles¹⁰¹, R. Piegai³⁰, D. Pietreanu^{27b}, J.E. Pilcher³⁷, A.D. Pilkington¹⁰¹, M. Pinamonti^{67a,67c},

J.L. Pinfold³, C. Pitman Donaldson⁹⁵, M. Pitt¹⁶¹, L. Pizzimento^{74a,74b}, M.-A. Pleier²⁹, V. Pleskot¹⁴², E. Plotnikova⁸⁰, P. Podberzko^{122b,122a}, R. Poettgen⁹⁷, R. Poggi⁵⁴, L. Poggioli¹³⁵, I. Pogrebnyak¹⁰⁷, D. Pohl²⁴, I. Pokharel⁵³, G. Polesello^{71a}, A. Poley^{152,168a}, A. Policicchio^{73a,73b}, R. Polifka¹⁴², A. Polini^{23b}, C.S. Pollard⁴⁶, V. Polychronakos²⁹, D. Ponomarenko¹¹², L. Pontecorvo³⁶, S. Popa^{27a}, G.A. Popeneciu^{27d}, L. Portales⁵, D.M. Portillo Quintero⁵⁸, S. Pospisil¹⁴¹, K. Potamianos⁴⁶, I.N. Potrap⁸⁰, C.J. Potter³², H. Potti¹¹, T. Poulsen⁹⁷, J. Poveda¹⁷⁴, T.D. Powell¹⁴⁹, G. Pownall⁴⁶, M.E. Pozo Astigarraga³⁶, P. Pralavorio¹⁰², S. Prell⁷⁹, D. Price¹⁰¹, M. Primavera^{68a}, M.L. Proffitt¹⁴⁸, N. Proklova¹¹², K. Prokofiev^{63c}, F. Prokoshin⁸⁰, S. Protopopescu²⁹, J. Proudfoot⁶, M. Przybycien^{84a}, D. Pudzha¹³⁷, A. Puri¹⁷³, P. Puzo⁶⁵, D. Pyatiizbyantseva¹¹², J. Qian¹⁰⁶, Y. Qin¹⁰¹, A. Quadri⁵³, M. Queitsch-Maitland³⁶, A. Qureshi¹, M. Racko^{28a}, F. Ragusa^{69a,69b}, G. Rahal⁹⁸, J.A. Raine⁵⁴, S. Rajagopalan²⁹, A. Ramirez Morales⁹³, K. Ran^{15a,15d}, D.M. Rauch⁴⁶, F. Rauscher¹¹⁴, S. Rave¹⁰⁰, B. Ravina¹⁴⁹, I. Ravinovich¹⁸⁰, J.H. Rawling¹⁰¹, M. Raymond³⁶, A.L. Read¹³³, N.P. Readioff¹⁴⁹, M. Reale^{68a,68b}, D.M. Rebutzi^{71a,71b}, G. Redlinger²⁹, K. Reeves⁴³, J. Reichert¹³⁶, D. Reikher¹⁶¹, A. Reiss¹⁰⁰, A. Rej¹⁵¹, C. Rembser³⁶, A. Renardi⁴⁶, M. Renda^{27b}, M.B. Rendel¹¹⁵, S. Resconi^{69a}, E.D. Resseguie¹⁸, S. Rettie⁹⁵, B. Reynolds¹²⁷, E. Reynolds²¹, O.L. Rezanova^{122b,122a}, P. Reznicek¹⁴², E. Ricci^{76a,76b}, R. Richter¹¹⁵, S. Richter⁴⁶, E. Richter-Was^{84b}, M. Ridel¹³⁵, P. Rieck¹¹⁵, O. Rifki⁴⁶, M. Rijssenbeek¹⁵⁵, A. Rimoldi^{71a,71b}, M. Rimoldi⁴⁶, L. Rinaldi^{23b}, T.T. Rinn¹⁷³, G. Ripellino¹⁵⁴, I. Riu¹⁴, P. Rivadeneira⁴⁶, J.C. Rivera Vergara¹⁷⁶, F. Rizatdinova¹²⁹, E. Rizvi⁹³, C. Rizzi³⁶, S.H. Robertson^{104.ab}, M. Robin⁴⁶, D. Robinson³², C.M. Robles Gajardo^{146d}, M. Robles Manzano¹⁰⁰, A. Robson⁵⁷, A. Rocchi^{74a,74b}, E. Rocco¹⁰⁰, C. Roda^{72a,72b}, S. Rodriguez Bosca¹⁷⁴, A.M. Rodríguez Vera^{168b}, S. Roe³⁶, J. Roggel¹⁸², O. Røhne¹³³, R. Röhrig¹¹⁵, R.A. Rojas^{146d}, B. Roland⁵², C.P.A. Roland⁶⁶, J. Roloff²⁹, A. Romaniouk¹¹², M. Romano^{23b,23a}, N. Rompotis⁹¹, M. Ronzani¹²⁵, L. Roos¹³⁵, S. Rosati^{73a}, G. Rosin¹⁰³, B.J. Rosser¹³⁶, E. Rossi⁴⁶, E. Rossi^{75a,75b}, E. Rossi^{70a,70b}, L.P. Rossi^{55b}, L. Rossini^{69a,69b}, R. Rosten¹⁴, M. Rotaru^{27b}, B. Rottler⁵², D. Rousseau⁶⁵, G. Rovelli^{71a,71b}, A. Roy¹¹, D. Roy^{33e}, A. Rozanov¹⁰², Y. Rozen¹⁶⁰, X. Ruan^{33e}, F. Rühr⁵², A. Ruiz-Martinez¹⁷⁴, A. Rummler³⁶, Z. Rurikova⁵², N.A. Rusakovich⁸⁰, H.L. Russell¹⁰⁴, L. Rustige^{38,47}, J.P. Rutherford⁷, E.M. Rüttinger¹⁴⁹, M. Rybar³⁹, G. Rybkin⁶⁵, E.B. Rye¹³³, A. Ryzhov¹²³, J.A. Sabater Iglesias⁴⁶, P. Sabatini⁵³, L. Sabetta^{73a,73b}, S. Sacerdoti⁶⁵, H.F.W. Sadrozinski¹⁴⁵, R. Sadykov⁸⁰, F. Safai Tehrani^{73a}, B. Safarzadeh Samani¹⁵⁶, M. Safdari¹⁵³, P. Saha¹²¹, S. Saha¹⁰⁴, M. Sahinsoy¹¹⁵, A. Sahu¹⁸², M. Saimpert³⁶, M. Saito¹⁶³, T. Saito¹⁶³, H. Sakamoto¹⁶³, D. Salamani⁵⁴, G. Salamanna^{75a,75b}, A. Salnikov¹⁵³, J. Salt¹⁷⁴, A. Salvador Salas¹⁴, D. Salvatore^{41b,41a}, F. Salvatore¹⁵⁶, A. Salvucci^{63a,63b,63c}, A. Salzburger³⁶, J. Samarati³⁶, D. Sammel⁵², D. Sampsonidis¹⁶², D. Sampsonidou¹⁶², J. Sánchez¹⁷⁴, A. Sanchez Pineda^{67a,36,67c}, H. Sandaker¹³³, C.O. Sander⁴⁶, I.G. Sanderswood⁹⁰, M. Sandhoff¹⁸², C. Sandoval^{22a}, D.P.C. Sankey¹⁴³, M. Sannino^{55b,55a}, Y. Sano¹¹⁷, A. Sansoni⁵¹, C. Santoni³⁸, H. Santos^{139a,139b}, S.N. Santpur¹⁸, A. Santra¹⁷⁴, K.A. Saoucha¹⁴⁹, A. Sapronov⁸⁰, J.G. Saraiva^{139a,139d}, O. Sasaki⁸², K. Sato¹⁶⁹, F. Sauerburger⁵², E. Sauvan⁵, P. Savard^{167.am}, R. Sawada¹⁶³, C. Sawyer¹⁴³, L. Sawyer^{96.ag}, I. Sayago Galvan¹⁷⁴, C. Sbarra^{23b}, A. Sbrizzi^{67a,67c}, T. Scanlon⁹⁵, J. Schaarschmidt¹⁴⁸, P. Schacht¹¹⁵, D. Schaefer³⁷, L. Schaefer¹³⁶, S. Schaepe³⁶, U. Schäfer¹⁰⁰, A.C. Schaffer⁶⁵, D. Schaile¹¹⁴, R.D. Schamberger¹⁵⁵, E. Schanet¹¹⁴, C. Scharf¹⁹, N. Scharmberg¹⁰¹, V.A. Schegelsky¹³⁷, D. Scheirich¹⁴², F. Schenck¹⁹, M. Schernau¹⁷¹, C. Schiavi^{55b,55a}, L.K. Schildgen²⁴, Z.M. Schillaci²⁶, E.J. Schioppa^{68a,68b}, M. Schioppa^{41b,41a}, K.E. Schleicher⁵², S. Schlenker³⁶, K.R. Schmidt-Sommerfeld¹¹⁵, K. Schmieden³⁶, C. Schmitt¹⁰⁰, S. Schmitt⁴⁶, J.C. Schmoeckel⁴⁶, L. Schoeffel¹⁴⁴, A. Schoening^{61b}, P.G. Scholer⁵², E. Schopf¹³⁴, M. Schott¹⁰⁰, J.F.P. Schouwenberg¹¹⁹, J. Schovancova³⁶, S. Schramm⁵⁴, F. Schroeder¹⁸², A. Schulte¹⁰⁰, H.-C. Schultz-Coulon^{61a}, M. Schumacher⁵², B.A. Schumm¹⁴⁵, Ph. Schune¹⁴⁴, A. Schwartzman¹⁵³, T.A. Schwarz¹⁰⁶, Ph. Schwemling¹⁴⁴, R. Schwienhorst¹⁰⁷, A. Sciandra¹⁴⁵, G. Sciolla²⁶, M. Scornajenghi^{41b,41a}, F. Scuri^{72a}, F. Scutti¹⁰⁵, L.M. Scyboz¹¹⁵, C.D. Sebastiani⁹¹, P. Seema¹⁹, S.C. Seidel¹¹⁸, A. Seiden¹⁴⁵, B.D. Seidlitz²⁹, T. Seiss³⁷, C. Seitz⁴⁶, J.M. Seixas^{81b}, G. Sekhniaidze^{70a}, S.J. Sekula⁴², N. Semprini-Cesari^{23b,23a}, S. Sen⁴⁹, C. Serfon²⁹, L. Serin⁶⁵,

L. Serkin^{67a,67b}, M. Sessa^{60a}, H. Severini¹²⁸, S. Sevova¹⁵³, F. Sforza^{55b,55a}, A. Sfyrla⁵⁴, E. Shabalina⁵³, J.D. Shahinian¹⁴⁵, N.W. Shaikh^{45a,45b}, D. Shaked Renous¹⁸⁰, L.Y. Shan^{15a}, M. Shapiro¹⁸, A. Sharma¹³⁴, A.S. Sharma¹, P.B. Shatalov¹²⁴, K. Shaw¹⁵⁶, S.M. Shaw¹⁰¹, M. Shehade¹⁸⁰, Y. Shen¹²⁸, A.D. Sherman²⁵, P. Sherwood⁹⁵, L. Shi⁹⁵, S. Shimizu⁸², C.O. Shimmin¹⁸³, Y. Shimogama¹⁷⁹, M. Shimojima¹¹⁶, I.P.J. Shipsey¹³⁴, S. Shirabe¹⁶⁵, M. Shiyakova^{80,z}, J. Shlomi¹⁸⁰, A. Shmeleva¹¹¹, M.J. Shochet³⁷, J. Shojaii¹⁰⁵, D.R. Shope¹⁵⁴, S. Shrestha¹²⁷, E.M. Shrif^{33e}, E. Shulga¹⁸⁰, P. Sicho¹⁴⁰, A.M. Sickles¹⁷³, E. Sideras Haddad^{33e}, O. Sidiropoulou³⁶, A. Sidoti^{23b,23a}, F. Siegert⁴⁸, Dj. Sijacki¹⁶, M.Jr. Silva¹⁸¹, M.V. Silva Oliveira³⁶, S.B. Silverstein^{45a}, S. Simion⁶⁵, R. Simoniello¹⁰⁰, C.J. Simpson-allso²¹, S. Simsek^{12b}, P. Sinervo¹⁶⁷, V. Sinetckii¹¹³, S. Singh¹⁵², M. Sioli^{23b,23a}, I. Siral¹³¹, S.Yu. Sivoklov¹¹³, J. Sjölin^{45a,45b}, A. Skaf⁵³, E. Skorda⁹⁷, P. Skubic¹²⁸, M. Slawinska⁸⁵, K. Sliwa¹⁷⁰, R. Slovak¹⁴², V. Smakhtin¹⁸⁰, B.H. Smart¹⁴³, J. Smiesko^{28b}, N. Smirnov¹¹², S.Yu. Smirnov¹¹², Y. Smirnov¹¹², L.N. Smirnova^{113,r}, O. Smirnova⁹⁷, H.A. Smith¹³⁴, M. Smizanska⁹⁰, K. Smolek¹⁴¹, A. Smykiewicz⁸⁵, A.A. Snesarev¹¹¹, H.L. Snoek¹²⁰, I.M. Snyder¹³¹, S. Snyder²⁹, R. Sobie^{176,ab}, A. Soffer¹⁶¹, A. Søggaard⁵⁰, F. Sohns⁵³, C.A. Solans Sanchez³⁶, E.Yu. Soldatov¹¹², U. Soldevila¹⁷⁴, A.A. Solodkov¹²³, A. Soloshenko⁸⁰, O.V. Solovyanov¹²³, V. Solovyev¹³⁷, P. Sommer¹⁴⁹, H. Son¹⁷⁰, W. Song¹⁴³, W.Y. Song^{168b}, A. Sopczak¹⁴¹, A.L. Sopio⁹⁵, F. Sopkova^{28b}, S. Sottocornola^{71a,71b}, R. Soualah^{67a,67c}, A.M. Soukharev^{122b,122a}, D. South⁴⁶, S. Spagnolo^{68a,68b}, M. Spalla¹¹⁵, M. Spangenberg¹⁷⁸, F. Spanò⁹⁴, D. Sperlich⁵², T.M. Spieker^{61a}, G. Spigo³⁶, M. Spina¹⁵⁶, D.P. Spiteri⁵⁷, M. Spousta¹⁴², A. Stabile^{69a,69b}, B.L. Stamas¹²¹, R. Stamen^{61a}, M. Stamenkovic¹²⁰, E. Stanecka⁸⁵, B. Stanislaus¹³⁴, M.M. Stanitzki⁴⁶, M. Stankaityte¹³⁴, B. Stapf¹²⁰, E.A. Starchenko¹²³, G.H. Stark¹⁴⁵, J. Stark⁵⁸, P. Staroba¹⁴⁰, P. Starovoitov^{61a}, S. Stärz¹⁰⁴, R. Staszewski⁸⁵, G. Stavropoulos⁴⁴, M. Stegler⁴⁶, P. Steinberg²⁹, A.L. Steinhebel¹³¹, B. Stelzer^{152,168a}, H.J. Stelzer¹³⁸, O. Stelzer-Chilton^{168a}, H. Stenzel⁵⁶, T.J. Stevenson¹⁵⁶, G.A. Stewart³⁶, M.C. Stockton³⁶, G. Stoicea^{27b}, M. Stolarski^{139a}, S. Stonjek¹¹⁵, A. Straessner⁴⁸, J. Strandberg¹⁵⁴, S. Strandberg^{45a,45b}, M. Strauss¹²⁸, T. Streblor¹⁰², P. Strizenec^{28b}, R. Ströhmer¹⁷⁷, D.M. Strom¹³¹, R. Stroynowski⁴², A. Strubig⁵⁰, S.A. Stucci²⁹, B. Stugu¹⁷, J. Stupak¹²⁸, N.A. Styles⁴⁶, D. Su¹⁵³, W. Su^{60c,148}, S. Suchek^{61a}, V.V. Sulin¹¹¹, M.J. Sullivan⁹¹, D.M.S. Sultan⁵⁴, S. Sultansoy^{4c}, T. Sumida⁸⁶, S. Sun¹⁰⁶, X. Sun¹⁰¹, K. Suruliz¹⁵⁶, C.J.E. Suster¹⁵⁷, M.R. Sutton¹⁵⁶, S. Suzuki⁸², M. Svatos¹⁴⁰, M. Swiatlowski^{168a}, S.P. Swift², T. Swirski¹⁷⁷, A. Sydorenko¹⁰⁰, I. Sykora^{28a}, M. Sykora¹⁴², T. Sykora¹⁴², D. Ta¹⁰⁰, K. Tackmann^{46,x}, J. Taenzer¹⁶¹, A. Taffard¹⁷¹, R. Tafirout^{168a}, E. Tagiev¹²³, R. Takashima⁸⁷, K. Takeda⁸³, T. Takeshita¹⁵⁰, E.P. Takeva⁵⁰, Y. Takubo⁸², M. Talby¹⁰², A.A. Talyshev^{122b,122a}, K.C. Tam^{63b}, N.M. Tamir¹⁶¹, J. Tanaka¹⁶³, R. Tanaka⁶⁵, S. Tapia Araya¹⁷³, S. Tapprogge¹⁰⁰, A. Tarek Abouelfadl Mohamed¹⁰⁷, S. Tarem¹⁶⁰, K. Tariq^{60b}, G. Tarna^{27b,d}, G.F. Tartarelli^{69a}, P. Tas¹⁴², M. Tasevsky¹⁴⁰, T. Tashiro⁸⁶, E. Tassi^{41b,41a}, A. Tavares Delgado^{139a}, Y. Tayalati^{35f}, A.J. Taylor⁵⁰, G.N. Taylor¹⁰⁵, W. Taylor^{168b}, H. Teagle⁹¹, A.S. Tee⁹⁰, R. Teixeira De Lima¹⁵³, P. Teixeira-Dias⁹⁴, H. Ten Kate³⁶, J.J. Teoh¹²⁰, S. Terada⁸², K. Terashi¹⁶³, J. Terron⁹⁹, S. Terzo¹⁴, M. Testa⁵¹, R.J. Teuscher^{167,ab}, S.J. Thais¹⁸³, N. Themistokleous⁵⁰, T. Thevenaux-Pelzer⁴⁶, F. Thiele⁴⁰, D.W. Thomas⁹⁴, J.O. Thomas⁴², J.P. Thomas²¹, E.A. Thompson⁴⁶, P.D. Thompson²¹, E. Thomson¹³⁶, E.J. Thorpe⁹³, R.E. Ticse Torres⁵³, V.O. Tikhomirov^{111,ai}, Yu.A. Tikhonov^{122b,122a}, S. Timoshenko¹¹², P. Tipton¹⁸³, S. Tisserant¹⁰², K. Todome^{23b,23a}, S. Todorova-Nova¹⁴², S. Todt⁴⁸, J. Tojo⁸⁸, S. Tokár^{28a}, K. Tokushuku⁸², E. Tolley¹²⁷, R. Tombs³², K.G. Tomiwa^{33e}, M. Tomoto¹¹⁷, L. Tompkins¹⁵³, P. Tornambe¹⁰³, E. Torrence¹³¹, H. Torres⁴⁸, E. Torró Pastor¹⁴⁸, C. Toscirì¹³⁴, J. Toth^{102,aa}, D.R. Tovey¹⁴⁹, A. Traet¹⁷, C.J. Treado¹²⁵, T. Trefzger¹⁷⁷, F. Tresoldi¹⁵⁶, A. Tricoli²⁹, I.M. Trigger^{168a}, S. Trincaz-Duvold¹³⁵, D.A. Trischuk¹⁷⁵, W. Trischuk¹⁶⁷, B. Trocme⁵⁸, A. Trofymov⁶⁵, C. Troncon^{69a}, F. Trovato¹⁵⁶, L. Truong^{33c}, M. Trzebinski⁸⁵, A. Trzupek⁸⁵, F. Tsai⁴⁶, J.C-L. Tseng¹³⁴, P.V. Tsiarshka^{108,af}, A. Tsirigotis^{162,u}, V. Tsiskaridze¹⁵⁵, E.G. Tskhadadze^{159a}, M. Tsopoulou¹⁶², I.I. Tsukerman¹²⁴, V. Tsulaia¹⁸, S. Tsuno⁸², D. Tsybychev¹⁵⁵, Y. Tu^{63b}, A. Tudorache^{27b}, V. Tudorache^{27b}, T.T. Tulbure^{27a}, A.N. Tuna⁵⁹, S. Turchikhin⁸⁰, D. Turgeman¹⁸⁰, I. Turk Cakir^{4b,s},

R.J. Turner²¹, R. Turra^{69a}, P.M. Tuts³⁹, S. Tzamarias¹⁶², E. Tzovara¹⁰⁰, K. Uchida¹⁶³, F. Ukegawa¹⁶⁹, G. Unal³⁶, M. Unal¹¹, A. Undrus²⁹, G. Unel¹⁷¹, F.C. Ungaro¹⁰⁵, Y. Unno⁸², K. Uno¹⁶³, J. Urban^{28b}, P. Urquijo¹⁰⁵, G. Usai⁸, Z. Uysal^{12d}, V. Vacek¹⁴¹, B. Vachon¹⁰⁴, K.O.H. Vadla¹³³, T. Vafeiadis³⁶, A. Vaidya⁹⁵, C. Valderanis¹¹⁴, E. Valdes Santurio^{45a,45b}, M. Valente⁵⁴, S. Valentinetti^{23b,23a}, A. Valero¹⁷⁴, L. Valéry⁴⁶, R.A. Vallance²¹, A. Vallier³⁶, J.A. Valls Ferrer¹⁷⁴, T.R. Van Daalen¹⁴, P. Van Gemmeren⁶, S. Van Stroud⁹⁵, I. Van Vulpen¹²⁰, M. Vanadia^{74a,74b}, W. Vandelli³⁶, M. Vandenbroucke¹⁴⁴, E.R. Vandewall¹²⁹, A. Vaniachine¹⁶⁶, D. Vannicola^{73a,73b}, R. Vari^{73a}, E.W. Varnes⁷, C. Varni^{55b,55a}, T. Varol¹⁵⁸, D. Varouchas⁶⁵, K.E. Varvell¹⁵⁷, M.E. Vasile^{27b}, G.A. Vasquez¹⁷⁶, F. Vazeille³⁸, D. Vazquez Furelos¹⁴, T. Vazquez Schroeder³⁶, J. Veatch⁵³, V. Vecchio¹⁰¹, M.J. Veen¹²⁰, L.M. Veloce¹⁶⁷, F. Veloso^{139a,139c}, S. Veneziano^{73a}, A. Ventura^{68a,68b}, A. Verbytskyi¹¹⁵, V. Vercesi^{71a}, M. Verducci^{72a,72b}, C.M. Vergel Infante⁷⁹, C. Vergis²⁴, W. Verkerke¹²⁰, A.T. Vermeulen¹²⁰, J.C. Vermeulen¹²⁰, C. Vernieri¹⁵³, M.C. Vetterli^{152,am}, N. Viaux Maira^{146d}, T. Vickey¹⁴⁹, O.E. Vickey Boeriu¹⁴⁹, G.H.A. Viehhauser¹³⁴, L. Vignani^{61b}, M. Villa^{23b,23a}, M. Villaplana Perez³, E.M. Villhauer⁵⁰, E. Vilucchi⁵¹, M.G. Vincter³⁴, G.S. Virdee²¹, A. Vishwakarma⁵⁰, C. Vittori^{23b,23a}, I. Vivarelli¹⁵⁶, M. Vogel¹⁸², P. Vokac¹⁴¹, S.E. von Buddenbrock^{33e}, E. Von Toerne²⁴, V. Vorobel¹⁴², K. Vorobev¹¹², M. Vos¹⁷⁴, J.H. Vosseveld⁹¹, M. Vozak¹⁰¹, N. Vranjes¹⁶, M. Vranjes Milosavljevic¹⁶, V. Vrba^{141,*}, M. Vreeswijk¹²⁰, R. Vuillermet³⁶, I. Vukotic³⁷, S. Wada¹⁶⁹, P. Wagner²⁴, W. Wagner¹⁸², J. Wagner-Kuhr¹¹⁴, S. Wahdan¹⁸², H. Wahlberg⁸⁹, R. Wakasa¹⁶⁹, V.M. Walbrecht¹¹⁵, J. Walder¹⁴³, R. Walker¹¹⁴, S.D. Walker⁹⁴, W. Walkowiak¹⁵¹, V. Wallangen^{45a,45b}, A.M. Wang⁵⁹, A.Z. Wang¹⁸¹, C. Wang^{60a}, C. Wang^{60c}, F. Wang¹⁸¹, H. Wang¹⁸, H. Wang³, J. Wang^{63a}, P. Wang⁴², Q. Wang¹²⁸, R.-J. Wang¹⁰⁰, R. Wang^{60a}, R. Wang⁶, S.M. Wang¹⁵⁸, W.T. Wang^{60a}, W. Wang^{15c}, W.X. Wang^{60a}, Y. Wang^{60a}, Z. Wang¹⁰⁶, C. Wanotayaroj⁴⁶, A. Warburton¹⁰⁴, C.P. Ward³², D.R. Wardrope⁹⁵, N. Warrack⁵⁷, A.T. Watson²¹, M.F. Watson²¹, G. Watts¹⁴⁸, B.M. Waugh⁹⁵, A.F. Webb¹¹, C. Weber²⁹, M.S. Weber²⁰, S.A. Weber³⁴, S.M. Weber^{61a}, A.R. Weidberg¹³⁴, J. Weingarten⁴⁷, M. Weirich¹⁰⁰, C. Weiser⁵², P.S. Wells³⁶, T. Wenaus²⁹, B. Wendland⁴⁷, T. Wengler³⁶, S. Wenig³⁶, N. Wermes²⁴, M. Wessels^{61a}, T.D. Weston²⁰, K. Whalen¹³¹, N.L. Whallon¹⁴⁸, A.M. Wharton⁹⁰, A.S. White¹⁰⁶, A. White⁸, M.J. White¹, D. Whiteson¹⁷¹, B.W. Whitmore⁹⁰, W. Wiedenmann¹⁸¹, C. Wiel⁴⁸, M. Wielers¹⁴³, N. Wieseotte¹⁰⁰, C. Wiglesworth⁴⁰, L.A.M. Wiik-Fuchs⁵², H.G. Wilkens³⁶, L.J. Wilkins⁹⁴, H.H. Williams¹³⁶, S. Williams³², S. Willocq¹⁰³, P.J. Windischhofer¹³⁴, I. Wingerter-Seez⁵, E. Winkels¹⁵⁶, F. Winklmeier¹³¹, B.T. Winter⁵², M. Wittgen¹⁵³, M. Wobisch⁹⁶, A. Wolf¹⁰⁰, R. Wölker¹³⁴, J. Wollrath⁵², M.W. Wolter⁸⁵, H. Wolters^{139a,139c}, V.W.S. Wong¹⁷⁵, N.L. Woods¹⁴⁵, S.D. Worm⁴⁶, B.K. Wosiek⁸⁵, K.W. Woźniak⁸⁵, K. Wraight⁵⁷, S.L. Wu¹⁸¹, X. Wu⁵⁴, Y. Wu^{60a}, J. Wuerzinger¹³⁴, T.R. Wyatt¹⁰¹, B.M. Wynne⁵⁰, S. Xella⁴⁰, J. Xiang^{63c}, X. Xiao¹⁰⁶, X. Xie^{60a}, I. Xiotidis¹⁵⁶, D. Xu^{15a}, H. Xu^{60a}, H. Xu^{60a}, L. Xu²⁹, T. Xu¹⁴⁴, W. Xu¹⁰⁶, Z. Xu^{60b}, Z. Xu¹⁵³, B. Yabsley¹⁵⁷, S. Yacoob^{33a}, K. Yajima¹³², D.P. Yallup⁹⁵, N. Yamaguchi⁸⁸, Y. Yamaguchi¹⁶⁵, A. Yamamoto⁸², M. Yamatani¹⁶³, T. Yamazaki¹⁶³, Y. Yamazaki⁸³, J. Yan^{60c}, Z. Yan²⁵, H.J. Yang^{60c,60d}, H.T. Yang¹⁸, S. Yang^{60a}, T. Yang^{63c}, X. Yang^{60b,58}, Y. Yang¹⁶³, Z. Yang^{60a}, W.-M. Yao¹⁸, Y.C. Yap⁴⁶, Y. Yasu⁸², E. Yatsenko^{60c}, H. Ye^{15c}, J. Ye⁴², S. Ye²⁹, I. Yeletsikh⁸⁰, M.R. Yexley⁹⁰, E. Yigitbasi²⁵, P. Yin³⁹, K. Yorita¹⁷⁹, K. Yoshihara⁷⁹, C.J.S. Young³⁶, C. Young¹⁵³, J. Yu⁷⁹, R. Yuan^{60b,h}, X. Yue^{61a}, M. Zaazoua^{35f}, B. Zabinski⁸⁵, G. Zacharis¹⁰, E. Zaffaroni⁵⁴, J. Zahreddine¹³⁵, A.M. Zaitsev^{123,ah}, T. Zakareishvili^{159b}, N. Zakharchuk³⁴, S. Zambito³⁶, D. Zanzi³⁶, D.R. Zaripovas⁵⁷, S.V. Zeißner⁴⁷, C. Zeitnitz¹⁸², G. Zemaityte¹³⁴, J.C. Zeng¹⁷³, O. Zenin¹²³, T. Ženiš^{28a}, D. Zerwas⁶⁵, M. Zgubić¹³⁴, B. Zhang^{15c}, D.F. Zhang^{15b}, G. Zhang^{15b}, J. Zhang⁶, K. Zhang^{15a}, L. Zhang^{15c}, L. Zhang^{60a}, M. Zhang¹⁷³, R. Zhang¹⁸¹, S. Zhang¹⁰⁶, X. Zhang^{60c}, X. Zhang^{60b}, Y. Zhang^{15a,15d}, Z. Zhang^{63a}, Z. Zhang⁶⁵, P. Zhao⁴⁹, Z. Zhao^{60a}, A. Zhemchugov⁸⁰, Z. Zheng¹⁰⁶, D. Zhong¹⁷³, B. Zhou¹⁰⁶, C. Zhou¹⁸¹, H. Zhou⁷, M.S. Zhou^{15a,15d}, M. Zhou¹⁵⁵, N. Zhou^{60c}, Y. Zhou⁷, C.G. Zhu^{60b}, C. Zhu^{15a,15d}, H.L. Zhu^{60a}, H. Zhu^{15a}, J. Zhu¹⁰⁶, Y. Zhu^{60a}, X. Zhuang^{15a}, K. Zhukov¹¹¹, V. Zhulanov^{122b,122a}, D. Ziemska⁶⁶, N.I. Zimine⁸⁰, S. Zimmermann^{52,*}, Z. Zinonos¹¹⁵, M. Ziolkowski¹⁵¹, L. Živković¹⁶, G. Zobernig¹⁸¹, A. Zoccoli^{23b,23a},

K. Zoch⁵³, T.G. Zorbas¹⁴⁹, R. Zou³⁷, L. Zwalinski³⁶.

¹Department of Physics, University of Adelaide, Adelaide; Australia.

²Physics Department, SUNY Albany, Albany NY; United States of America.

³Department of Physics, University of Alberta, Edmonton AB; Canada.

⁴(^a)Department of Physics, Ankara University, Ankara; (^b)Istanbul Aydin University, Application and Research Center for Advanced Studies, Istanbul; (^c)Division of Physics, TOBB University of Economics and Technology, Ankara; Turkey.

⁵LAPP, Université Grenoble Alpes, Université Savoie Mont Blanc, CNRS/IN2P3, Annecy; France.

⁶High Energy Physics Division, Argonne National Laboratory, Argonne IL; United States of America.

⁷Department of Physics, University of Arizona, Tucson AZ; United States of America.

⁸Department of Physics, University of Texas at Arlington, Arlington TX; United States of America.

⁹Physics Department, National and Kapodistrian University of Athens, Athens; Greece.

¹⁰Physics Department, National Technical University of Athens, Zografou; Greece.

¹¹Department of Physics, University of Texas at Austin, Austin TX; United States of America.

¹²(^a)Bahcesehir University, Faculty of Engineering and Natural Sciences, Istanbul; (^b)Istanbul Bilgi University, Faculty of Engineering and Natural Sciences, Istanbul; (^c)Department of Physics, Bogazici University, Istanbul; (^d)Department of Physics Engineering, Gaziantep University, Gaziantep; Turkey.

¹³Institute of Physics, Azerbaijan Academy of Sciences, Baku; Azerbaijan.

¹⁴Institut de Física d'Altes Energies (IFAE), Barcelona Institute of Science and Technology, Barcelona; Spain.

¹⁵(^a)Institute of High Energy Physics, Chinese Academy of Sciences, Beijing; (^b)Physics Department, Tsinghua University, Beijing; (^c)Department of Physics, Nanjing University, Nanjing; (^d)University of Chinese Academy of Science (UCAS), Beijing; China.

¹⁶Institute of Physics, University of Belgrade, Belgrade; Serbia.

¹⁷Department for Physics and Technology, University of Bergen, Bergen; Norway.

¹⁸Physics Division, Lawrence Berkeley National Laboratory and University of California, Berkeley CA; United States of America.

¹⁹Institut für Physik, Humboldt Universität zu Berlin, Berlin; Germany.

²⁰Albert Einstein Center for Fundamental Physics and Laboratory for High Energy Physics, University of Bern, Bern; Switzerland.

²¹School of Physics and Astronomy, University of Birmingham, Birmingham; United Kingdom.

²²(^a)Facultad de Ciencias y Centro de Investigaciones, Universidad Antonio Nariño, Bogotá; (^b)Departamento de Física, Universidad Nacional de Colombia, Bogotá, Colombia; Colombia.

²³(^a)INFN Bologna and Università di Bologna, Dipartimento di Fisica; (^b)INFN Sezione di Bologna; Italy.

²⁴Physikalisches Institut, Universität Bonn, Bonn; Germany.

²⁵Department of Physics, Boston University, Boston MA; United States of America.

²⁶Department of Physics, Brandeis University, Waltham MA; United States of America.

²⁷(^a)Transilvania University of Brasov, Brasov; (^b)Horia Hulubei National Institute of Physics and Nuclear Engineering, Bucharest; (^c)Department of Physics, Alexandru Ioan Cuza University of Iasi, Iasi; (^d)National Institute for Research and Development of Isotopic and Molecular Technologies, Physics Department, Cluj-Napoca; (^e)University Politehnica Bucharest, Bucharest; (^f)West University in Timisoara, Timisoara; Romania.

²⁸(^a)Faculty of Mathematics, Physics and Informatics, Comenius University, Bratislava; (^b)Department of Subnuclear Physics, Institute of Experimental Physics of the Slovak Academy of Sciences, Kosice; Slovak Republic.

²⁹Physics Department, Brookhaven National Laboratory, Upton NY; United States of America.

- ³⁰Departamento de Física, Universidad de Buenos Aires, Buenos Aires; Argentina.
- ³¹California State University, CA; United States of America.
- ³²Cavendish Laboratory, University of Cambridge, Cambridge; United Kingdom.
- ³³(^a)Department of Physics, University of Cape Town, Cape Town; (^b)iThemba Labs, Western Cape; (^c)Department of Mechanical Engineering Science, University of Johannesburg, Johannesburg; (^d)University of South Africa, Department of Physics, Pretoria; (^e)School of Physics, University of the Witwatersrand, Johannesburg; South Africa.
- ³⁴Department of Physics, Carleton University, Ottawa ON; Canada.
- ³⁵(^a)Faculté des Sciences Ain Chock, Réseau Universitaire de Physique des Hautes Energies - Université Hassan II, Casablanca; (^b)Faculté des Sciences, Université Ibn-Tofail, Kénitra; (^c)Faculté des Sciences Semlalia, Université Cadi Ayyad, LPHEA-Marrakech; (^d)Moroccan Foundation for Advanced Science Innovation and Research (MAScIR), Rabat; (^e)Faculté des Sciences, Université Mohamed Premier and LPTPM, Oujda; (^f)Faculté des sciences, Université Mohammed V, Rabat; Morocco.
- ³⁶CERN, Geneva; Switzerland.
- ³⁷Enrico Fermi Institute, University of Chicago, Chicago IL; United States of America.
- ³⁸LPC, Université Clermont Auvergne, CNRS/IN2P3, Clermont-Ferrand; France.
- ³⁹Nevis Laboratory, Columbia University, Irvington NY; United States of America.
- ⁴⁰Niels Bohr Institute, University of Copenhagen, Copenhagen; Denmark.
- ⁴¹(^a)Dipartimento di Fisica, Università della Calabria, Rende; (^b)INFN Gruppo Collegato di Cosenza, Laboratori Nazionali di Frascati; Italy.
- ⁴²Physics Department, Southern Methodist University, Dallas TX; United States of America.
- ⁴³Physics Department, University of Texas at Dallas, Richardson TX; United States of America.
- ⁴⁴National Centre for Scientific Research "Demokritos", Agia Paraskevi; Greece.
- ⁴⁵(^a)Department of Physics, Stockholm University; (^b)Oskar Klein Centre, Stockholm; Sweden.
- ⁴⁶Deutsches Elektronen-Synchrotron DESY, Hamburg and Zeuthen; Germany.
- ⁴⁷Lehrstuhl für Experimentelle Physik IV, Technische Universität Dortmund, Dortmund; Germany.
- ⁴⁸Institut für Kern- und Teilchenphysik, Technische Universität Dresden, Dresden; Germany.
- ⁴⁹Department of Physics, Duke University, Durham NC; United States of America.
- ⁵⁰SUPA - School of Physics and Astronomy, University of Edinburgh, Edinburgh; United Kingdom.
- ⁵¹INFN e Laboratori Nazionali di Frascati, Frascati; Italy.
- ⁵²Physikalisches Institut, Albert-Ludwigs-Universität Freiburg, Freiburg; Germany.
- ⁵³II. Physikalisches Institut, Georg-August-Universität Göttingen, Göttingen; Germany.
- ⁵⁴Département de Physique Nucléaire et Corpusculaire, Université de Genève, Genève; Switzerland.
- ⁵⁵(^a)Dipartimento di Fisica, Università di Genova, Genova; (^b)INFN Sezione di Genova; Italy.
- ⁵⁶II. Physikalisches Institut, Justus-Liebig-Universität Giessen, Giessen; Germany.
- ⁵⁷SUPA - School of Physics and Astronomy, University of Glasgow, Glasgow; United Kingdom.
- ⁵⁸LPSC, Université Grenoble Alpes, CNRS/IN2P3, Grenoble INP, Grenoble; France.
- ⁵⁹Laboratory for Particle Physics and Cosmology, Harvard University, Cambridge MA; United States of America.
- ⁶⁰(^a)Department of Modern Physics and State Key Laboratory of Particle Detection and Electronics, University of Science and Technology of China, Hefei; (^b)Institute of Frontier and Interdisciplinary Science and Key Laboratory of Particle Physics and Particle Irradiation (MOE), Shandong University, Qingdao; (^c)School of Physics and Astronomy, Shanghai Jiao Tong University, KLPPAC-MoE, SKLPPC, Shanghai; (^d)Tsung-Dao Lee Institute, Shanghai; China.
- ⁶¹(^a)Kirchhoff-Institut für Physik, Ruprecht-Karls-Universität Heidelberg, Heidelberg; (^b)Physikalisches Institut, Ruprecht-Karls-Universität Heidelberg, Heidelberg; Germany.
- ⁶²Faculty of Applied Information Science, Hiroshima Institute of Technology, Hiroshima; Japan.

- ⁶³(^a)Department of Physics, Chinese University of Hong Kong, Shatin, N.T., Hong Kong; (^b)Department of Physics, University of Hong Kong, Hong Kong; (^c)Department of Physics and Institute for Advanced Study, Hong Kong University of Science and Technology, Clear Water Bay, Kowloon, Hong Kong; China.
- ⁶⁴Department of Physics, National Tsing Hua University, Hsinchu; Taiwan.
- ⁶⁵IJCLab, Université Paris-Saclay, CNRS/IN2P3, 91405, Orsay; France.
- ⁶⁶Department of Physics, Indiana University, Bloomington IN; United States of America.
- ⁶⁷(^a)INFN Gruppo Collegato di Udine, Sezione di Trieste, Udine; (^b)ICTP, Trieste; (^c)Dipartimento Politecnico di Ingegneria e Architettura, Università di Udine, Udine; Italy.
- ⁶⁸(^a)INFN Sezione di Lecce; (^b)Dipartimento di Matematica e Fisica, Università del Salento, Lecce; Italy.
- ⁶⁹(^a)INFN Sezione di Milano; (^b)Dipartimento di Fisica, Università di Milano, Milano; Italy.
- ⁷⁰(^a)INFN Sezione di Napoli; (^b)Dipartimento di Fisica, Università di Napoli, Napoli; Italy.
- ⁷¹(^a)INFN Sezione di Pavia; (^b)Dipartimento di Fisica, Università di Pavia, Pavia; Italy.
- ⁷²(^a)INFN Sezione di Pisa; (^b)Dipartimento di Fisica E. Fermi, Università di Pisa, Pisa; Italy.
- ⁷³(^a)INFN Sezione di Roma; (^b)Dipartimento di Fisica, Sapienza Università di Roma, Roma; Italy.
- ⁷⁴(^a)INFN Sezione di Roma Tor Vergata; (^b)Dipartimento di Fisica, Università di Roma Tor Vergata, Roma; Italy.
- ⁷⁵(^a)INFN Sezione di Roma Tre; (^b)Dipartimento di Matematica e Fisica, Università Roma Tre, Roma; Italy.
- ⁷⁶(^a)INFN-TIFPA; (^b)Università degli Studi di Trento, Trento; Italy.
- ⁷⁷Institut für Astro- und Teilchenphysik, Leopold-Franzens-Universität, Innsbruck; Austria.
- ⁷⁸University of Iowa, Iowa City IA; United States of America.
- ⁷⁹Department of Physics and Astronomy, Iowa State University, Ames IA; United States of America.
- ⁸⁰Joint Institute for Nuclear Research, Dubna; Russia.
- ⁸¹(^a)Departamento de Engenharia Elétrica, Universidade Federal de Juiz de Fora (UFJF), Juiz de Fora; (^b)Universidade Federal do Rio De Janeiro COPPE/EE/IF, Rio de Janeiro; (^c)Instituto de Física, Universidade de São Paulo, São Paulo; Brazil.
- ⁸²KEK, High Energy Accelerator Research Organization, Tsukuba; Japan.
- ⁸³Graduate School of Science, Kobe University, Kobe; Japan.
- ⁸⁴(^a)AGH University of Science and Technology, Faculty of Physics and Applied Computer Science, Krakow; (^b)Marian Smoluchowski Institute of Physics, Jagiellonian University, Krakow; Poland.
- ⁸⁵Institute of Nuclear Physics Polish Academy of Sciences, Krakow; Poland.
- ⁸⁶Faculty of Science, Kyoto University, Kyoto; Japan.
- ⁸⁷Kyoto University of Education, Kyoto; Japan.
- ⁸⁸Research Center for Advanced Particle Physics and Department of Physics, Kyushu University, Fukuoka ; Japan.
- ⁸⁹Instituto de Física La Plata, Universidad Nacional de La Plata and CONICET, La Plata; Argentina.
- ⁹⁰Physics Department, Lancaster University, Lancaster; United Kingdom.
- ⁹¹Oliver Lodge Laboratory, University of Liverpool, Liverpool; United Kingdom.
- ⁹²Department of Experimental Particle Physics, Jožef Stefan Institute and Department of Physics, University of Ljubljana, Ljubljana; Slovenia.
- ⁹³School of Physics and Astronomy, Queen Mary University of London, London; United Kingdom.
- ⁹⁴Department of Physics, Royal Holloway University of London, Egham; United Kingdom.
- ⁹⁵Department of Physics and Astronomy, University College London, London; United Kingdom.
- ⁹⁶Louisiana Tech University, Ruston LA; United States of America.
- ⁹⁷Fysiska institutionen, Lunds universitet, Lund; Sweden.
- ⁹⁸Centre de Calcul de l'Institut National de Physique Nucléaire et de Physique des Particules (IN2P3), Villeurbanne; France.

- ⁹⁹Departamento de Física Teórica C-15 and CIAFF, Universidad Autónoma de Madrid, Madrid; Spain.
- ¹⁰⁰Institut für Physik, Universität Mainz, Mainz; Germany.
- ¹⁰¹School of Physics and Astronomy, University of Manchester, Manchester; United Kingdom.
- ¹⁰²CPPM, Aix-Marseille Université, CNRS/IN2P3, Marseille; France.
- ¹⁰³Department of Physics, University of Massachusetts, Amherst MA; United States of America.
- ¹⁰⁴Department of Physics, McGill University, Montreal QC; Canada.
- ¹⁰⁵School of Physics, University of Melbourne, Victoria; Australia.
- ¹⁰⁶Department of Physics, University of Michigan, Ann Arbor MI; United States of America.
- ¹⁰⁷Department of Physics and Astronomy, Michigan State University, East Lansing MI; United States of America.
- ¹⁰⁸B.I. Stepanov Institute of Physics, National Academy of Sciences of Belarus, Minsk; Belarus.
- ¹⁰⁹Research Institute for Nuclear Problems of Byelorussian State University, Minsk; Belarus.
- ¹¹⁰Group of Particle Physics, University of Montreal, Montreal QC; Canada.
- ¹¹¹P.N. Lebedev Physical Institute of the Russian Academy of Sciences, Moscow; Russia.
- ¹¹²National Research Nuclear University MEPhI, Moscow; Russia.
- ¹¹³D.V. Skobeltsyn Institute of Nuclear Physics, M.V. Lomonosov Moscow State University, Moscow; Russia.
- ¹¹⁴Fakultät für Physik, Ludwig-Maximilians-Universität München, München; Germany.
- ¹¹⁵Max-Planck-Institut für Physik (Werner-Heisenberg-Institut), München; Germany.
- ¹¹⁶Nagasaki Institute of Applied Science, Nagasaki; Japan.
- ¹¹⁷Graduate School of Science and Kobayashi-Maskawa Institute, Nagoya University, Nagoya; Japan.
- ¹¹⁸Department of Physics and Astronomy, University of New Mexico, Albuquerque NM; United States of America.
- ¹¹⁹Institute for Mathematics, Astrophysics and Particle Physics, Radboud University/Nikhef, Nijmegen; Netherlands.
- ¹²⁰Nikhef National Institute for Subatomic Physics and University of Amsterdam, Amsterdam; Netherlands.
- ¹²¹Department of Physics, Northern Illinois University, DeKalb IL; United States of America.
- ¹²²(^a) Budker Institute of Nuclear Physics and NSU, SB RAS, Novosibirsk; (^b) Novosibirsk State University Novosibirsk; Russia.
- ¹²³Institute for High Energy Physics of the National Research Centre Kurchatov Institute, Protvino; Russia.
- ¹²⁴Institute for Theoretical and Experimental Physics named by A.I. Alikhanov of National Research Centre "Kurchatov Institute", Moscow; Russia.
- ¹²⁵Department of Physics, New York University, New York NY; United States of America.
- ¹²⁶Ochanomizu University, Otsuka, Bunkyo-ku, Tokyo; Japan.
- ¹²⁷Ohio State University, Columbus OH; United States of America.
- ¹²⁸Homer L. Dodge Department of Physics and Astronomy, University of Oklahoma, Norman OK; United States of America.
- ¹²⁹Department of Physics, Oklahoma State University, Stillwater OK; United States of America.
- ¹³⁰Palacký University, RCPTM, Joint Laboratory of Optics, Olomouc; Czech Republic.
- ¹³¹Institute for Fundamental Science, University of Oregon, Eugene, OR; United States of America.
- ¹³²Graduate School of Science, Osaka University, Osaka; Japan.
- ¹³³Department of Physics, University of Oslo, Oslo; Norway.
- ¹³⁴Department of Physics, Oxford University, Oxford; United Kingdom.
- ¹³⁵LPNHE, Sorbonne Université, Université de Paris, CNRS/IN2P3, Paris; France.
- ¹³⁶Department of Physics, University of Pennsylvania, Philadelphia PA; United States of America.
- ¹³⁷Konstantinov Nuclear Physics Institute of National Research Centre "Kurchatov Institute", PNPI, St.

Petersburg; Russia.

¹³⁸Department of Physics and Astronomy, University of Pittsburgh, Pittsburgh PA; United States of America.

¹³⁹(^a)Laboratório de Instrumentação e Física Experimental de Partículas - LIP, Lisboa; (^b)Departamento de Física, Faculdade de Ciências, Universidade de Lisboa, Lisboa; (^c)Departamento de Física, Universidade de Coimbra, Coimbra; (^d)Centro de Física Nuclear da Universidade de Lisboa, Lisboa; (^e)Departamento de Física, Universidade do Minho, Braga; (^f)Departamento de Física Teórica y del Cosmos, Universidad de Granada, Granada (Spain); (^g)Dep Física and CEFITEC of Faculdade de Ciências e Tecnologia, Universidade Nova de Lisboa, Caparica; (^h)Instituto Superior Técnico, Universidade de Lisboa, Lisboa; Portugal.

¹⁴⁰Institute of Physics of the Czech Academy of Sciences, Prague; Czech Republic.

¹⁴¹Czech Technical University in Prague, Prague; Czech Republic.

¹⁴²Charles University, Faculty of Mathematics and Physics, Prague; Czech Republic.

¹⁴³Particle Physics Department, Rutherford Appleton Laboratory, Didcot; United Kingdom.

¹⁴⁴IRFU, CEA, Université Paris-Saclay, Gif-sur-Yvette; France.

¹⁴⁵Santa Cruz Institute for Particle Physics, University of California Santa Cruz, Santa Cruz CA; United States of America.

¹⁴⁶(^a)Departamento de Física, Pontificia Universidad Católica de Chile, Santiago; (^b)Universidad Andres Bello, Department of Physics, Santiago; (^c)Instituto de Alta Investigación, Universidad de Tarapacá; (^d)Departamento de Física, Universidad Técnica Federico Santa María, Valparaíso; Chile.

¹⁴⁷Universidade Federal de São João del Rei (UFSJ), São João del Rei; Brazil.

¹⁴⁸Department of Physics, University of Washington, Seattle WA; United States of America.

¹⁴⁹Department of Physics and Astronomy, University of Sheffield, Sheffield; United Kingdom.

¹⁵⁰Department of Physics, Shinshu University, Nagano; Japan.

¹⁵¹Department Physik, Universität Siegen, Siegen; Germany.

¹⁵²Department of Physics, Simon Fraser University, Burnaby BC; Canada.

¹⁵³SLAC National Accelerator Laboratory, Stanford CA; United States of America.

¹⁵⁴Physics Department, Royal Institute of Technology, Stockholm; Sweden.

¹⁵⁵Departments of Physics and Astronomy, Stony Brook University, Stony Brook NY; United States of America.

¹⁵⁶Department of Physics and Astronomy, University of Sussex, Brighton; United Kingdom.

¹⁵⁷School of Physics, University of Sydney, Sydney; Australia.

¹⁵⁸Institute of Physics, Academia Sinica, Taipei; Taiwan.

¹⁵⁹(^a)E. Andronikashvili Institute of Physics, Iv. Javakhishvili Tbilisi State University, Tbilisi; (^b)High Energy Physics Institute, Tbilisi State University, Tbilisi; Georgia.

¹⁶⁰Department of Physics, Technion, Israel Institute of Technology, Haifa; Israel.

¹⁶¹Raymond and Beverly Sackler School of Physics and Astronomy, Tel Aviv University, Tel Aviv; Israel.

¹⁶²Department of Physics, Aristotle University of Thessaloniki, Thessaloniki; Greece.

¹⁶³International Center for Elementary Particle Physics and Department of Physics, University of Tokyo, Tokyo; Japan.

¹⁶⁴Graduate School of Science and Technology, Tokyo Metropolitan University, Tokyo; Japan.

¹⁶⁵Department of Physics, Tokyo Institute of Technology, Tokyo; Japan.

¹⁶⁶Tomsk State University, Tomsk; Russia.

¹⁶⁷Department of Physics, University of Toronto, Toronto ON; Canada.

¹⁶⁸(^a)TRIUMF, Vancouver BC; (^b)Department of Physics and Astronomy, York University, Toronto ON; Canada.

¹⁶⁹Division of Physics and Tomonaga Center for the History of the Universe, Faculty of Pure and Applied

Sciences, University of Tsukuba, Tsukuba; Japan.

¹⁷⁰Department of Physics and Astronomy, Tufts University, Medford MA; United States of America.

¹⁷¹Department of Physics and Astronomy, University of California Irvine, Irvine CA; United States of America.

¹⁷²Department of Physics and Astronomy, University of Uppsala, Uppsala; Sweden.

¹⁷³Department of Physics, University of Illinois, Urbana IL; United States of America.

¹⁷⁴Instituto de Física Corpuscular (IFIC), Centro Mixto Universidad de Valencia - CSIC, Valencia; Spain.

¹⁷⁵Department of Physics, University of British Columbia, Vancouver BC; Canada.

¹⁷⁶Department of Physics and Astronomy, University of Victoria, Victoria BC; Canada.

¹⁷⁷Fakultät für Physik und Astronomie, Julius-Maximilians-Universität Würzburg, Würzburg; Germany.

¹⁷⁸Department of Physics, University of Warwick, Coventry; United Kingdom.

¹⁷⁹Waseda University, Tokyo; Japan.

¹⁸⁰Department of Particle Physics and Astrophysics, Weizmann Institute of Science, Rehovot; Israel.

¹⁸¹Department of Physics, University of Wisconsin, Madison WI; United States of America.

¹⁸²Fakultät für Mathematik und Naturwissenschaften, Fachgruppe Physik, Bergische Universität Wuppertal, Wuppertal; Germany.

¹⁸³Department of Physics, Yale University, New Haven CT; United States of America.

^a Also at Borough of Manhattan Community College, City University of New York, New York NY; United States of America.

^b Also at Centro Studi e Ricerche Enrico Fermi; Italy.

^c Also at CERN, Geneva; Switzerland.

^d Also at CPPM, Aix-Marseille Université, CNRS/IN2P3, Marseille; France.

^e Also at Département de Physique Nucléaire et Corpusculaire, Université de Genève, Genève; Switzerland.

^f Also at Departament de Física de la Universitat Autònoma de Barcelona, Barcelona; Spain.

^g Also at Department of Financial and Management Engineering, University of the Aegean, Chios; Greece.

^h Also at Department of Physics and Astronomy, Michigan State University, East Lansing MI; United States of America.

ⁱ Also at Department of Physics and Astronomy, University of Louisville, Louisville, KY; United States of America.

^j Also at Department of Physics, Ben Gurion University of the Negev, Beer Sheva; Israel.

^k Also at Department of Physics, California State University, East Bay; United States of America.

^l Also at Department of Physics, California State University, Fresno; United States of America.

^m Also at Department of Physics, California State University, Sacramento; United States of America.

ⁿ Also at Department of Physics, King's College London, London; United Kingdom.

^o Also at Department of Physics, St. Petersburg State Polytechnical University, St. Petersburg; Russia.

^p Also at Department of Physics, University of Fribourg, Fribourg; Switzerland.

^q Also at Dipartimento di Matematica, Informatica e Fisica, Università di Udine, Udine; Italy.

^r Also at Faculty of Physics, M.V. Lomonosov Moscow State University, Moscow; Russia.

^s Also at Giresun University, Faculty of Engineering, Giresun; Turkey.

^t Also at Graduate School of Science, Osaka University, Osaka; Japan.

^u Also at Hellenic Open University, Patras; Greece.

^v Also at IJCLab, Université Paris-Saclay, CNRS/IN2P3, 91405, Orsay; France.

^w Also at Institutio Catalana de Recerca i Estudis Avancats, ICREA, Barcelona; Spain.

^x Also at Institut für Experimentalphysik, Universität Hamburg, Hamburg; Germany.

^y Also at Institute for Mathematics, Astrophysics and Particle Physics, Radboud University/Nikhef, Nijmegen; Netherlands.

^z Also at Institute for Nuclear Research and Nuclear Energy (INRNE) of the Bulgarian Academy of Sciences, Sofia; Bulgaria.

^{aa} Also at Institute for Particle and Nuclear Physics, Wigner Research Centre for Physics, Budapest; Hungary.

^{ab} Also at Institute of Particle Physics (IPP); Canada.

^{ac} Also at Institute of Physics, Azerbaijan Academy of Sciences, Baku; Azerbaijan.

^{ad} Also at Instituto de Fisica Teorica, IFT-UAM/CSIC, Madrid; Spain.

^{ae} Also at Istanbul University, Dept. of Physics, Istanbul; Turkey.

^{af} Also at Joint Institute for Nuclear Research, Dubna; Russia.

^{ag} Also at Louisiana Tech University, Ruston LA; United States of America.

^{ah} Also at Moscow Institute of Physics and Technology State University, Dolgoprudny; Russia.

^{ai} Also at National Research Nuclear University MEPhI, Moscow; Russia.

^{aj} Also at Physics Department, An-Najah National University, Nablus; Palestine.

^{ak} Also at Physikalisches Institut, Albert-Ludwigs-Universität Freiburg, Freiburg; Germany.

^{al} Also at The City College of New York, New York NY; United States of America.

^{am} Also at TRIUMF, Vancouver BC; Canada.

^{an} Also at Università di Napoli Parthenope, Napoli; Italy.

^{ao} Also at University of Chinese Academy of Sciences (UCAS), Beijing; China.

* Deceased